AGT

Algebraic & Geometric Topology

Volume 25 (2025)

Unbounded $\mathfrak{sl}_3$-laminations and their shear coordinates

Tsukasa Ishibashi
Shunsuke Kano

msp

msp

Algebraic & Geometric Topology **25**:3 (2025) 1433–1500
DOI: 10.2140/agt.2025.25.1433
Published: 20 June 2025

Unbounded $\mathfrak{sl}_3$-laminations and their shear coordinates

TSUKASA ISHIBASHI
SHUNSUKE KANO

Generalizing the work of Fock and Goncharov on rational unbounded laminations, we give a geometric model of the tropical points of the cluster variety $\mathcal{X}_{\mathfrak{sl}_3,\Sigma}$, which we call *unbounded* $\mathfrak{sl}_3$*-laminations*, based on Kuperberg's $\mathfrak{sl}_3$-webs. We introduce their tropical cluster coordinates as an $\mathfrak{sl}_3$-analogue of Thurston's shear coordinates associated with any ideal triangulation. As a tropical analogue of gluing morphisms among the moduli spaces $\mathcal{P}_{\mathrm{PGL}_3,\Sigma}$ of Goncharov and Shen, we describe a geometric gluing procedure of unbounded $\mathfrak{sl}_3$-laminations with pinnings via "shearings". We also investigate a relation to the graphical basis of the $\mathfrak{sl}_3$-skein algebra of Ishibashi and Yuasa (2023), which conjecturally leads to a quantum duality map.

13F60, 57K20, 57K31

1 Introduction

1.1 Background

The notion of measured geodesic laminations (or its equivalent, measured foliations) on a surface was first introduced by W Thurston [43], as a powerful geometric tool to study the mapping class groups and the large-scale geometry of the Teichmüller space. After a couple of decades, Fock and Goncharov [11] studied Thurston's *shear coordinates* on the space $\widehat{\mathcal{ML}}(\Sigma)$ of (enhanced) measured geodesic laminations on a marked surface Σ, which gives a global coordinate system parametrized by the interior edges of an ideal triangulation $\triangle$ of Σ: $\widehat{\mathcal{ML}}(\Sigma) \xrightarrow{\sim} \mathbb{R}^{e_{\mathrm{int}}(\triangle)}$. Moreover, they observed that these coordinates can be viewed as a "tropical analogue" of the cross-ratio coordinates[1] on the enhanced Teichmüller space $\widehat{\mathcal{T}}(\Sigma) \xrightarrow{\sim} \mathbb{R}_{>0}^{e_{\mathrm{int}}(\triangle)}$ studied by Fock and Chekhov [8], as their coordinate transformation rule is exactly the tropical analogue of that for the latter. These facts indicate that there would be a universal algebraic object behind the Teichmüller and lamination spaces: this idea leads to the theory of *cluster varieties* developed by Fock and Goncharov [13]. In their terms, there is a cluster $\mathcal{X}$-variety[2] $\mathcal{X}_\Sigma^{\mathrm{uf}}$ associated with Σ such that the spaces $\widehat{\mathcal{T}}(\Sigma)$ and $\widehat{\mathcal{ML}}(\Sigma)$ are naturally identified with the spaces $\mathcal{X}_\Sigma^{\mathrm{uf}}(\mathbb{R}_{>0})$, $\mathcal{X}_\Sigma^{\mathrm{uf}}(\mathbb{R}^T)$ of positive real points and the real tropical points, respectively. We call the latter space $\mathcal{X}_\Sigma^{\mathrm{uf}}(\mathbb{R}^T)$ the *tropical cluster* $\mathcal{X}$*-variety* for short.

[1] The cross-ratio coordinate is an exponential version of the shear coordinate on the Teichmüller space. In this paper, we always use the term "shear coordinates" for those on the lamination spaces.

[2] Here, the superscript "uf" just indicates that it has only unfrozen coordinates. It corresponds to the situation where the shear/cross-ratio coordinates are defined only for internal edges $e_{\mathrm{int}}(\triangle)$ of an ideal triangulation $\triangle$.

In general, cluster varieties are schemes constructed from combinatorial data s (such as quivers) equipped with a birational atlas whose coordinate changes are given by specific rational transformations, called cluster transformations (see the appendix for a short review of this theory). They always come in a dual pair $(\mathcal{A}_\mathsf{s}, \mathcal{X}_\mathsf{s})$, forming a *cluster ensemble*. The *duality conjecture* is a profound conjecture of Fock and Goncharov [13] that asks for a construction of "duality maps"

$$\mathbb{I}_\mathcal{X}\colon \mathcal{X}_\mathsf{s}(\mathbb{Z}^T) \to \mathcal{O}(\mathcal{A}_{\mathsf{s}^\vee}) \quad (\text{resp. } \mathbb{I}_\mathcal{A}\colon \mathcal{A}_\mathsf{s}(\mathbb{Z}^T) \to \mathcal{O}(\mathcal{X}_{\mathsf{s}^\vee}))$$

which parametrizes a linear basis of the function ring $\mathcal{O}(\mathcal{A}_{\mathsf{s}^\vee})$ (resp. $\mathcal{O}(\mathcal{X}_{\mathsf{s}^\vee})$) of the dual cluster variety by the space $\mathcal{X}_\mathsf{s}(\mathbb{Z}^T) \subset \mathcal{X}_\mathsf{s}(\mathbb{R}^T)$ (resp. $\mathcal{A}_\mathsf{s}(\mathbb{Z}^T) \subset \mathcal{A}_\mathsf{s}(\mathbb{R}^T)$) of integral tropical points, satisfying certain strong axioms such as the positivity of structure constants.

In the surface case, the spaces $\mathcal{A}_\Sigma(\mathbb{R}_{>0})$ and $\mathcal{A}_\Sigma(\mathbb{R}^T)$ are identified with the decorated Teichmüller and lamination spaces — see Papadopoulos and Penner [39; 40] — via the λ-length and intersection coordinates [11]. The geometric realization of the tropical spaces $\mathcal{A}_\Sigma(\mathbb{Z}^T)$ $\mathcal{X}^{\mathrm{uf}}_\Sigma(\mathbb{Z}^T)$ by integral laminations [11] leads to a topological construction of the duality maps $\mathbb{I}_\mathcal{X}$ and $\mathbb{I}_\mathcal{A}$, and their required properties were proved recently by Mandel and Qin [37] based on a comparison with the *theta basis* of Gross, Hacking, Keel and Kontsevich [22]. These duality maps are two kinds of generalizations of the trace function basis for the function ring of the SL_2-character variety of a closed surface, parametrized by loops.

Strongly expected are "higher rank" generalizations of the above picture. The cluster varieties $\mathcal{X}^{\mathrm{uf}}_\Sigma$ and $\mathcal{A}_\Sigma$ are birationally isomorphic to certain generalizations of the PGL_2- and SL_2-character varieties; see Fock and Goncharov [10]. As a generalization for higher rank algebraic groups, there are cluster varieties $\mathcal{X}^{\mathrm{uf}}_{\mathfrak{g},\Sigma}$ and $\mathcal{A}_{\mathfrak{g},\Sigma}$ which are birationally isomorphic to the same kind of generalizations $\mathcal{X}_{G',\Sigma}$ and $\mathcal{A}_{G,\Sigma}$ of character varieties — see Fock, Goncharov and Shen [10; 21] and Le [35] — where the defining combinatorial data for these cluster varieties only depend on the surface Σ and a semisimple Lie algebra $\mathfrak{g}$. In particular, $\mathcal{X}^{\mathrm{uf}}_{\mathfrak{sl}_2,\Sigma} = \mathcal{X}^{\mathrm{uf}}_\Sigma$ and $\mathcal{A}_{\mathfrak{sl}_2,\Sigma} = \mathcal{A}_\Sigma$ correspond to the case mentioned above. Goncharov and Shen [21] introduced a cluster variety $\mathcal{X}_{\mathfrak{g},\Sigma}$ with frozen coordinates, which is birational to some extension $\mathcal{P}_{G',\Sigma}$ of $\mathcal{X}_{G',\Sigma}$. Hereupon, we have combinatorially defined tropical spaces $\mathcal{A}_{\mathfrak{g},\Sigma}(\mathbb{R}^T)$ and $\mathcal{X}_{\mathfrak{g},\Sigma}(\mathbb{R}^T)$, which should parametrize linear bases of the function rings of the dual varieties with good properties by the duality conjecture. The spaces $\mathcal{A}_{\mathfrak{g},\Sigma}(\mathbb{R}^T)$ and $\mathcal{X}_{\mathfrak{g},\Sigma}(\mathbb{R}^T)$ are widely expected to be certain spaces of $\mathfrak{g}$-webs on Σ, so that the duality maps are built from the web functions on the character variety. However, such a web description is still missing in general. We remark here that Le [34] gave a description of these spaces in terms of certain configurations in the affine buildings, which should be ultimately related to $\mathfrak{g}$-webs based on the geometric Satake correspondence (see, for instance, Fontaine, Kamnitzer and Kuperberg [18]).

For the first nontrivial case $\mathfrak{g} = \mathfrak{sl}_3$, major progress on the space $\mathcal{A}_{\mathfrak{sl}_3,\Sigma}(\mathbb{Z}^T)$ has been made by Douglas and Sun [6; 7] and Kim [32]. They describe this space as an appropriate space of Kuperberg's $\mathfrak{sl}_3$-webs [33] by introducing an $\mathfrak{sl}_3$-version of the intersection coordinates with an ideal triangulation. Their coordinates can also be extended to the space $\mathcal{A}_{\mathfrak{sl}_3,\Sigma}(\mathbb{Q}^T)$ by scaling equivariance.

1.2 Geometric model for the tropical space $\mathcal{X}^{\mathrm{uf}}_{\mathfrak{sl}_3,\Sigma}(\mathbb{Q}^T)$

Our aim in this paper is to describe the tropical cluster variety $\mathcal{X}_{\mathfrak{sl}_3,\Sigma}(\mathbb{Q}^T)$ on the dual side as a space of $\mathfrak{sl}_3$-webs with a different type of boundary conditions and some additional structures at punctures. We introduce the space $\mathcal{L}^x_{\mathfrak{sl}_3}(\Sigma,\mathbb{Q})$ of rational unbounded $\mathfrak{sl}_3$-laminations on Σ, which are certain equivalence classes of nonelliptic *signed* $\mathfrak{sl}_3$*-webs* with positive rational weights (see Section 2.2). Then we define an $\mathfrak{sl}_3$-version of the shear coordinates of these objects with respect to an ideal triangulation $\triangle$. As in the $\mathfrak{sl}_2$-case, we need to perturb the ends incident at punctures (and thus make them spiraling) so that they intersect with $\triangle$ transversely. The spiraling directions are controlled by the signs assigned to each end of the $\mathfrak{sl}_3$-web, and this procedure leads to the notion of *spiraling diagrams* (Definition 3.8) associated with signed $\mathfrak{sl}_3$-webs. After a careful study on the "good positions" of a spiraling diagram, we obtain well-defined shear coordinates.

Theorem 1 (Theorem 3.20) *For any marked surface Σ satisfying conditions* (S1)–(S4) *in Section 2.1 and its ideal triangulation $\triangle$ without self-folded triangles, we have a bijection*

$$\mathrm{x}^{\mathrm{uf}}_{\triangle}\colon \mathcal{L}^x_{\mathfrak{sl}_3}(\Sigma,\mathbb{Q}) \xrightarrow{\sim} \mathbb{Q}^{I_{\mathrm{uf}}(\triangle)}, \tag{1-1}$$

which we call the shear coordinate system associated with $\triangle$. Moreover, for any another ideal triangulation $\triangle'$ of Σ, the coordinate transformation $\mathrm{x}_{\triangle'}\circ\mathrm{x}_{\triangle}^{-1}$ is a composite of tropical cluster $\mathcal{X}$-transformations.

As a consequence, the shear coordinates combine to give an $\mathrm{MC}(\Sigma)$-equivariant bijection

$$\mathrm{x}^{\mathrm{uf}}_{\bullet}\colon \mathcal{L}^x_{\mathfrak{sl}_3}(\Sigma,\mathbb{Q}) \xrightarrow{\sim} \mathcal{X}^{\mathrm{uf}}_{\mathfrak{sl}_3,\Sigma}(\mathbb{Q}^T). \tag{1-2}$$

Therefore, our space $\mathcal{L}^x_{\mathfrak{sl}_3}(\Sigma,\mathbb{Q})$ of unbounded $\mathfrak{sl}_3$-laminations gives a geometric model for the tropical cluster $\mathcal{X}$-variety $\mathcal{X}^{\mathrm{uf}}_{\mathfrak{sl}_3,\Sigma}(\mathbb{Q}^T)$. In other words, the space $\mathcal{L}^x_{\mathfrak{sl}_3}(\Sigma,\mathbb{Q})$ can be viewed as a tropical analogue of the moduli space $\mathcal{X}_{\mathrm{PGL}_3,\Sigma}$ of framed PGL_3-local systems [10].

In Section 3.4, we give an explicit inverse map of $\mathrm{x}^{\mathrm{uf}}_{\triangle}$ by gluing local building blocks according to the shear coordinates, in the same spirit as Fock and Goncharov. The coordinate transformation formula could be obtained by case-by-case as in [7] for the $\mathcal{A}$-side. However, in order to reduce the length of computation, we choose to derive it from the computation on the $\mathcal{A}$-side performed by Douglas and Sun after investigating their relation in detail (see Theorem 2 below). So the second statement in Theorem 1 follows from Theorem 2.

1.3 Unbounded $\mathfrak{sl}_3$-laminations with pinnings and their gluing

In order to supply the frozen coordinates, we further introduce a larger space $\mathcal{L}^p_{\mathfrak{sl}_3}(\Sigma,\mathbb{Q})$ of unbounded $\mathfrak{sl}_3$-laminations *with pinnings* by attaching additional data on boundary intervals, in the same spirit as

Goncharov and Shen's construction of the moduli space $\mathcal{P}_{G',\Sigma}$ [21]. As in their work, these additional data allow us to glue the $\mathfrak{sl}_3$-laminations along boundary intervals, which leads to the *gluing map*

$$q_{E_L,E_R}\colon \mathcal{L}^p_{\mathfrak{sl}_3}(\Sigma,\mathbb{Q}) \to \mathcal{L}^p_{\mathfrak{sl}_3}(\Sigma',\mathbb{Q}) \tag{1-3}$$

where Σ' is the marked surface obtained from Σ by gluing two boundary intervals E_L and E_R.

The space $\mathcal{L}^p_{\mathfrak{sl}_3}(\Sigma,\mathbb{Q})$ is also suited for the comparison with the works of Douglas and Sun [6; 7] and Kim [32]. Let $\mathcal{L}^a_{\mathfrak{sl}_3}(\Sigma,\mathbb{Q})$ denote the space of rational bounded $\mathfrak{sl}_3$-laminations, which essentially appears in these works. See Remark 2.10. Then we define a *geometric ensemble map*

$$\tilde{p}\colon \mathcal{L}^a_{\mathfrak{sl}_3}(\Sigma,\mathbb{Q}) \to \mathcal{L}^p_{\mathfrak{sl}_3}(\Sigma,\mathbb{Q}) \tag{1-4}$$

by forgetting the peripheral components, and assigning pinnings in a certain way. When Σ has no punctures, $\tilde{p}$ gives a bijection. For these structures, we obtain the following:

Theorem 2 (Theorems 4.7 and 4.11 and Proposition 4.10) *Under the same assumption as in Theorem 1, we have a bijection*

$$\times_\Delta\colon \mathcal{L}^p_{\mathfrak{sl}_3}(\Sigma,\mathbb{Q}) \xrightarrow{\sim} \mathbb{Q}^{I(\Delta)}, \tag{1-5}$$

whose coordinate transformations are given by tropical cluster $\mathcal{X}$-transformations (including frozen coordinates). Via these coordinate systems:

(1) *The gluing map q_{E_L,E_R} coincides with the tropicalization of the amalgamation map* [9].

(2) *The geometric ensemble map $\tilde{p}$ coincides with the tropicalization of the Goncharov–Shen extension of the ensemble map* (A-6).

We will also see in Section 4.4 that the shear coordinates are equivariant under the Dynkin involution $*$, which generates $\mathrm{Out}(\mathrm{SL}_3)$. In particular, we have an $\mathrm{MC}(\Sigma)\times\mathrm{Out}(\mathrm{SL}_3)$-equivariant bijection

$$\times_\Delta\colon \mathcal{L}^p_{\mathfrak{sl}_3}(\Sigma,\mathbb{Q}) \xrightarrow{\sim} \mathcal{X}_{\mathfrak{sl}_3,\Sigma}(\mathbb{Q}^T). \tag{1-6}$$

In other words, the space $\mathcal{L}^p_{\mathfrak{sl}_3}(\Sigma,\mathbb{Q})$ can be viewed as a tropical analogue of the Goncharov and Shen's moduli space $\mathcal{P}_{\mathrm{PGL}_3,\Sigma}$ [21].

Property (1) allows one to reduce the computation of coordinate transformations to those for smaller surfaces. For a surface without punctures, the map $\tilde{p}$ is a bijection and property (2) shows that this map intertwines the two types of cluster transformations. This is our strategy to obtain the coordinate transformation formula for (1-5).

In our sequel paper [28], we will investigate the unbounded $\mathfrak{sl}_3$-laminations around punctures in detail, and study the tropicalizations of the cluster exact sequence of Fock and Goncharov [13] and the Weyl group actions at punctures introduced by Goncharov and Shen [20] in terms of $\mathfrak{sl}_3$-laminations. In the end, the bijections (1-2) and (1-6) turn out to be equivariant under the natural action of the group $(\mathrm{MC}(\Sigma)\times\mathrm{Out}(\mathrm{SL}_3))\ltimes W(\mathfrak{sl}_3)^{\mathbb{M}_\circ}$.

1.4 Relation to the graphical basis of the skein algebra $\mathcal{S}^{q}_{\mathfrak{sl}_3,\Sigma}$

As mentioned in the beginning, our space $\mathcal{L}^{p}_{\mathfrak{sl}_3}(\Sigma,\mathbb{Z}) \cong \mathcal{X}_{\mathfrak{sl}_3,\Sigma}(\mathbb{Z}^T)$ is expected to parametrize a linear basis of the function ring $\mathcal{O}(\mathcal{A}_{\mathfrak{sl}_3,\Sigma})$. When the marked surface has no punctures (hence the exchange matrix has full-rank), it is also expected to parametrize a linear basis of the *quantum upper cluster algebra* $\mathcal{O}_q(\mathcal{A}_{\mathfrak{sl}_3,\Sigma})$ of Berenstein and Zelevinsky [3]. On the other hand, a skein model for $\mathcal{O}_q(\mathcal{A}_{\mathfrak{sl}_3,\Sigma})$ is investigated in [30] by the first named author and W Yuasa. They study a skein algebra $\mathcal{S}^{q}_{\mathfrak{sl}_3,\Sigma}$ with appropriate "clasped" skein relations at marked points, and constructed an inclusion of its boundary-localization $\mathcal{S}^{q}_{\mathfrak{sl}_3,\Sigma}[\partial^{-1}]$ into the quantum cluster algebra (and hence into $\mathcal{O}_q(\mathcal{A}_{\mathfrak{sl}_3,\Sigma})$). Conjecturally these algebras coincide with each other. They give a $\mathbb{Z}_q$-basis $\mathsf{BWeb}_{\mathfrak{sl}_3,\Sigma}$ of the skein algebra $\mathcal{S}^{q}_{\mathfrak{sl}_3,\Sigma}$ consisting of flat trivalent graphs. In this paper, we relate our integral $\mathfrak{sl}_3$-laminations with pinnings to the basis webs:

Theorem 3 (Theorem 5.2) *Assume that Σ has no punctures. Then we have an $\mathrm{MC}(\Sigma)\times\mathrm{Out}(\mathrm{SL}_3)$-equivariant bijection*

$$\mathbb{I}^{q}_{\mathcal{X}}\colon \mathcal{L}^{p}_{\mathfrak{sl}_3}(\Sigma,\mathbb{Z})_+ \xrightarrow{\sim} \mathsf{BWeb}_{\mathfrak{sl}_3,\Sigma} \subset \mathcal{S}^{q}_{\mathfrak{sl}_3,\Sigma},$$

where $\mathcal{L}^{p}_{\mathfrak{sl}_3}(\Sigma,\mathbb{Z})_+ \subset \mathcal{L}^{p}_{\mathfrak{sl}_3}(\Sigma,\mathbb{Z})$ denotes the subspace of dominant integral $\mathfrak{sl}_3$-laminations. Moreover, it is extended to a map $\mathbb{I}^{q}_{\mathcal{X}}\colon \mathcal{L}^{p}_{\mathfrak{sl}_3}(\Sigma,\mathbb{Z}) \hookrightarrow \mathcal{S}^{q}_{\mathfrak{sl}_3,\Sigma}[\partial^{-1}]$, whose image gives a $\mathbb{Z}_q$-basis of $\mathcal{S}^{q}_{\mathfrak{sl}_3,\Sigma}[\partial^{-1}]$.

The latter correspondence should be a basic ingredient for a construction of the *quantum duality map* [13] (see Qin [41, Conjecture 4.14] for a finer formulation as well as Davison and Mandel [5]). See Section 5 for a detailed discussion. Our general expectation is the following:

Conjecture 4 *The basis $\mathbb{I}^{q}_{\mathcal{X}}(\mathcal{L}^{p}_{\mathfrak{sl}_3}(\Sigma,\mathbb{Z}))$ is **parametrized by tropical points** in the sense of* [41, Definition 4.13]. *Namely, for any integral $\mathfrak{sl}_3$-lamination $\widehat{L} \in \mathcal{L}^{p}_{\mathfrak{sl}_3}(\Sigma,\mathbb{Z})$, the quantum Laurent expression of $\mathbb{I}^{q}_{\mathcal{X}}(\widehat{L}) \in \mathcal{A}^{q}_{\mathfrak{sl}_3,\Sigma}$ in the quantum cluster $\{A_i\}_{i\in I}$ associated with a vertex $\omega \in \mathbb{E}\mathrm{xch}_{\mathfrak{sl}_3,\Sigma}$ has the leading term $\big[\prod_{i\in I} A_i^{\mathsf{x}_i(\widehat{L})}\big]$ with respect to the dominance order* [41, Definition 4.6], *where $\mathsf{x}^{(\omega)} = (\mathsf{x}_i)_{i\in I}$ is the shear coordinate system associated with ω.*

Currently we do not know if it gives a basis with positivity (of Laurent expressions and/or structure constants), or it requires a modification by using an $\mathfrak{sl}_3$-version of *bracelets*; see D Thurston [42]. See also Allegretti and Kim [1; 2] and Cho, Kim, Kim and Oh [4] for the progress on the positivity problem for the $\mathfrak{sl}_2$-case.

1.5 Future directions: real unbounded $\mathfrak{sl}_3$-laminations

Let $\mathcal{L}^{x}_{\mathfrak{sl}_3}(\Sigma,\mathbb{R})$ be the completion of the space $\mathcal{L}^{x}_{\mathfrak{sl}_3}(\Sigma,\mathbb{Q})$ such that each shear coordinate system (1-1) extends to a homeomorphism $\mathsf{x}^{\mathrm{uf}}_{\Delta}\colon \mathcal{L}^{x}_{\mathfrak{sl}_3}(\Sigma,\mathbb{R}) \xrightarrow{\sim} \mathbb{R}^{I_{\mathrm{uf}}(\Delta)}$. It is well defined since the cluster $\mathcal{X}$-transformations are Lipschitz continuous with respect to the Euclidean metrics on $\mathbb{Q}^{I_{\mathrm{uf}}(\Delta)}$. We call an

element of $\mathcal{L}^x_{\mathfrak{sl}_3}(\Sigma,\mathbb{R})$ a *real unbounded* $\mathfrak{sl}_3$*-lamination*, which is represented by a Cauchy sequence in $\mathcal{L}^x_{\mathfrak{sl}_3}(\Sigma,\mathbb{Q})$ with respect to shear coordinates. The space $\mathcal{L}^x_{\mathfrak{sl}_3}(\Sigma,\mathbb{R})$ has a natural PL structure, and is considered to be an $\mathfrak{sl}_3$-analogue of the space $\widehat{\mathcal{ML}}(\Sigma)$ of measured geodesic laminations. Recall that in the Teichmüller–Thurston theory, the latter PL manifold plays the following roles (among others):

Boundary at infinity of the Teichmüller space The *Thurston compactification* is a compactification of the Teichmüller space into a topological disk obtained by attaching the projectivization of $\widehat{\mathcal{ML}}(\Sigma)$, so that the mapping class group action is continuously extended. The measured geodesic laminations encode the "rate" of degenerations of geodesics in a divergent sequence in the Teichmüller space. The Thurston compactification is identified with the *Fock–Goncharov compactification* [14; 24; 34] $\overline{\mathcal{X}_\Sigma(\mathbb{R}_{>0})}=\mathcal{X}_\Sigma(\mathbb{R}_{>0})\cup\mathbb{S}\mathcal{X}_\Sigma(\mathbb{R}^T)$, which is defined for any cluster $\mathcal{X}$-variety.

Place for analyzing the pseudo-Anosov dynamics The PL action of the mapping class group on $\widehat{\mathcal{ML}}(\Sigma)$ provides us rich information on the dynamics of pseudo-Anosov mapping classes. In particular, each pseudo-Anosov mapping class has the north-south dynamics on the projectivized space, and its unique attracting/repelling points are represented by a transverse pair of measured geodesic laminations. A generalization of these specific properties for elements of a general cluster modular group is proposed in [25; 26; 27], which we call the *sign stability*. The equivalence between the "uniform" sign stability and the pseudo-Anosov property is discussed in [25], based on the identification $\widehat{\mathcal{ML}}(\Sigma)\cong\mathcal{X}^{\mathrm{uf}}_\Sigma(\mathbb{R}^T)$.

It is natural to expect that the space $\mathcal{L}^x_{\mathfrak{sl}_3}(\Sigma,\mathbb{R})$ plays the same role in the $\mathfrak{sl}_3$-case. Since the positive real part $\mathcal{X}^{\mathrm{uf}}_{\mathfrak{sl}_3,\Sigma}(\mathbb{R}_{>0})$ has been identified with the moduli space of convex $\mathbb{RP}^2$-structures on Σ, the real unbounded $\mathfrak{sl}_3$-laminations are expected to encode their degenerations. The PL action of a pseudo-Anosov mapping class on the space $\mathcal{L}^x_{\mathfrak{sl}_3}(\Sigma,\mathbb{R})$ is expected to provide more rich information, which may possibly lead to a finer classification of pseudo-Anosov mapping classes. Although a concrete description of a real unbounded $\mathfrak{sl}_3$-lamination as a certain geometric object (rather than a sequence) is still missing, the cluster algebraic interpretation of Thurston's train tracks studied in [31] will be a useful tool.

Generalizations of Thurston's earthquake maps and the Hubbard–Masur theorem that relates measured foliations with quadratic differentials will be also interesting topics. A study on a cluster algebraic analogue of these theories is in progress by the authors with Takeru Asaka.

Organization of the paper

Main part (Sections 2–4) In Section 2, we introduce rational unbounded $\mathfrak{sl}_3$-laminations and briefly discuss the relation to the works of Douglas and Sun [6; 7] and Kim [32]. We study the associated spiraling diagrams and define the shear coordinates in Section 3. The bijectivity of the shear coordinate systems (1-1) is proved. In Section 4, we introduce pinnings for rational unbounded $\mathfrak{sl}_3$-laminations and discuss their gluing and the extended ensemble map. Theorem 2 is proved, and hence the proof of Theorem 1 is completed.

Relation to skein theory (Section 5) We investigate the relation to the skein algebra and quantum duality map in Section 5. Theorem 3 is proved here.

Proofs for the technical statements (Section 6) The proofs of Theorems 3.10 and 3.19 are placed in Section 6. Logically they do not depend on the contents after the places where the statements are written.

Basic terminology on the cluster varieties and the known results we need for the $\mathfrak{sl}_3$-case are collected in the appendix.

Acknowledgements

The authors thank Hyun Kyu Kim for illuminating discussion on quantum duality maps. They also appreciate the referee's careful reading and suggestions. Ishibashi is grateful to Wataru Yuasa for a valuable discussion on $\mathfrak{sl}_3$-skein algebras in the early stage of this work. He is also grateful to Zhe Sun for explaining his works on the $\mathcal{A}$-side, and giving valuable comments on this work at several stages. Kano appreciates the support by Wataru Yuasa for his visit to Kyoto University in the spring of 2021. The main part of this work was done during this visit. Ishibashi is partially supported by JSPS KAKENHI (20K22304). Kano is partially supported by scientific research support of Research Alliance Center for Mathematical Sciences, Tohoku University.

2 Unbounded $\mathfrak{sl}_3$-laminations and their shear coordinates

2.1 Marked surfaces and their triangulations

A marked surface $(\Sigma, \mathbb{M})$ is a compact oriented surface Σ together with a fixed nonempty finite set $\mathbb{M} \subset \Sigma$ of *marked points*. When the choice of $\mathbb{M}$ is clear from the context, we simply denote a marked surface by Σ. A marked point is called a *puncture* if it lies in the interior of Σ, and a *special point* otherwise. Let $\mathbb{M}_\circ = \mathbb{M}_\circ(\Sigma)$ (resp. $\mathbb{M}_\partial = \mathbb{M}_\partial(\Sigma)$) denote the set of punctures (resp. special points), so that $\mathbb{M} = \mathbb{M}_\circ \sqcup \mathbb{M}_\partial$. Let $\Sigma^* := \Sigma \setminus \mathbb{M}_\circ$. We always assume the following conditions:

(S1) Each boundary component (if exists) has at least one marked point.

(S2) $-2\chi(\Sigma^*) + |\mathbb{M}_\partial| > 0$.

(S3) $(\Sigma, \mathbb{M})$ is not a once-punctured disk with a single special point on the boundary.

We call a connected component of the punctured boundary $\partial^*\Sigma := \partial\Sigma \setminus \mathbb{M}_\partial$ a *boundary interval*. The set of boundary intervals is denoted by $\mathbb{B} = \mathbb{B}(\Sigma)$. We always endow each boundary interval with the orientation induced from $\partial\Sigma$. Then we have $|\mathbb{M}_\partial| = |\mathbb{B}|$.

Unless otherwise stated, an *isotopy* in a marked surface $(\Sigma, \mathbb{M})$ means an ambient isotopy in Σ relative to $\mathbb{M}$, which preserves each boundary interval setwise. An *ideal arc* in $(\Sigma, \mathbb{M})$ is an immersed arc in Σ with endpoints in $\mathbb{M}$ which has no self-intersection except possibly at its endpoints, and not isotopic to one point.

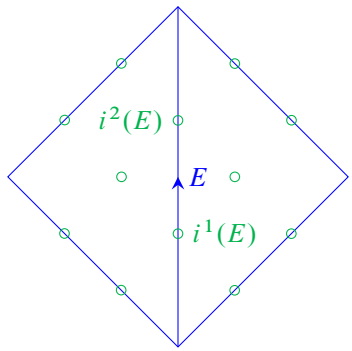

Figure 1: The set $I(\triangle)$ of distinguished points.

An *ideal triangulation* is a triangulation $\triangle$ of Σ whose set of 0-cells (vertices) coincides with $\mathbb{M}$. Conditions (S1) and (S2) ensure the existence of such an ideal triangulation, and the positive integer in (S2) gives the number of 2-cells (triangles). The 1-cells (edges) are necessarily ideal arcs. In this paper, we always consider an ideal triangulation without *self-folded triangles* of the form

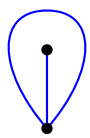

Such an ideal triangulation exists by condition (S3). See, for instance, [15, Lemma 2.13]. For an ideal triangulation $\triangle$, denote the set of edges (resp. interior edges, triangles) of $\triangle$ by $e(\triangle)$ (resp. $e_{\mathrm{int}}(\triangle)$, $t(\triangle)$). Since the boundary intervals belong to any ideal triangulation, $e(\triangle) = e_{\mathrm{int}}(\triangle) \sqcup \mathbb{B}$. By a computation on the Euler characteristics, we get

$$|e(\triangle)| = -3\chi(\Sigma^*) + 2|\mathbb{M}_\partial|, \quad |e_{\mathrm{int}}(\triangle)| = -3\chi(\Sigma^*) + |\mathbb{M}_\partial|, \quad |t(\triangle)| = -2\chi(\Sigma^*) + |\mathbb{M}_\partial|.$$

It is useful to equip $\triangle$ with two distinguished points on the interior of each edge and one point in the interior of each triangle, as shown in Figure 1. The set of such points is denoted by $I(\triangle) = I_{\mathfrak{sl}_3}(\triangle)$. This set will give the vertex set of the quiver $Q^\triangle$ associated with $\triangle$; see Section A.3. Let $I^{\mathrm{edge}}(\triangle)$ (resp. $I^{\mathrm{tri}}(\triangle)$) denote the set of points on edges (resp. faces of triangles) so that $I(\triangle) = I^{\mathrm{edge}}(\triangle) \sqcup I^{\mathrm{tri}}(\triangle)$, where we have a canonical bijection

$$t(\triangle) \xrightarrow{\sim} I^{\mathrm{tri}}(\triangle), \quad T \mapsto i(T).$$

When we need to label the two vertices on an edge $E \in e(\triangle)$, we endow E with an orientation. Then let $i^1(E) \in I(\triangle)$ (resp. $i^2(E) \in I(\triangle)$) denote the vertex closer to the initial (resp. terminal) endpoint of E. Let $I(\triangle)_{\mathrm{f}} \subset I^{\mathrm{edge}}(\triangle)$ ("frozen") be the subset consisting of the points on the boundary, and let $I(\triangle)_{\mathrm{uf}} := I(\triangle) \setminus I(\triangle)_{\mathrm{f}}$ ("unfrozen"). The numbers

$$|I(\triangle)| = 2|e(\triangle)| + |t(\triangle)| = -8\chi(\Sigma^*) + 5|\mathbb{M}_\partial|,$$
$$|I(\triangle)_{\mathrm{uf}}| = 2|e_{\mathrm{int}}(\triangle)| + |t(\triangle)| = -8\chi(\Sigma^*) + 3|\mathbb{M}_\partial|$$

will give the dimensions of the PL manifolds $\mathcal{L}^p_{\mathfrak{sl}_3}(\Sigma, \mathbb{R})$ and $\mathcal{L}^x_{\mathfrak{sl}_3}(\Sigma, \mathbb{R})$ respectively.

2.2 Unbounded $\mathfrak{sl}_3$-laminations

Recall that a *uni-trivalent* graph is a (possibly disconnected and/or infinite) graph whose vertices have valency either one or three. It is allowed to have a loop component (ie a connected component without vertices). An *orientation* of a uni-trivalent graph is an assignment of an orientation on each edge and loop such that any trivalent vertex is either a *sink* or a *source*, respectively:

An $\mathfrak{sl}_3$-web (or simply a *web*) on a marked surface Σ is an immersed oriented uni-trivalent graph W on Σ such that each univalent vertex lie in $\mathbb{M}_\circ \cup \partial^*\Sigma$, and the other part is embedded into $\operatorname{int}\Sigma^*$. It is said to be *nonelliptic* if it has none of the following *elliptic faces*:

(2-1)

(2-2)

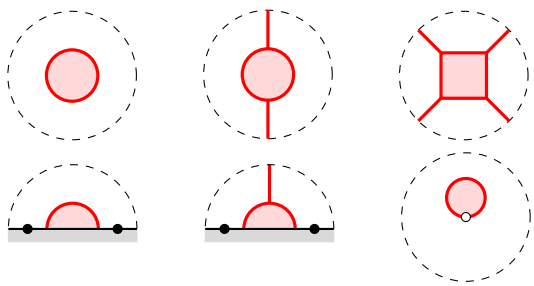

A web is said to be *bounded* if none of its univalent vertices lie in $\mathbb{M}_\circ$.

We will mostly deal with finite webs, while infinite ones appear when (and only when) we discuss spiraling diagrams (Definition 3.8), which are still locally finite except possibly around punctures. When we simply say an ($\mathfrak{sl}_3$-)web below, it will mean a finite web. When the web in consideration can be infinite, we will say a "possibly infinite web".

Remark 2.1 The exclusion of the internal faces in (2-1) is usual in literature. Indeed, a web containing these faces can be written as a linear combination of nonelliptic webs in the skein algebra (see Section 5), and hence not needed as a basis element. The first two faces in (2-2) are excluded as variants of boundary skein relations [30]. It is also related to the *weakly reduced* condition in [19]. The third one can be regarded as a variant for a boundary component without marked points.

Example 2.2 (honeycomb webs) Let $T \subset \operatorname{int}\Sigma^*$ be an embedded triangle. For each positive integer n, the incoming (resp. outgoing) *honeycomb-web* (or *pyramid web*) in T of height n is the $\mathfrak{sl}_3$-web dual to the *n-triangulation* of T, oriented so that the outer-most edges are incoming to (resp. outgoing from) T. See the left picture in Figure 2 for an example. We will also use a short-hand presentation as shown in the right of Figure 2. The embedded image of a honeycomb web in Σ is simply called a *honeycomb*. The ends of a honeycomb can be connected with other oriented arcs or honeycombs on Σ.

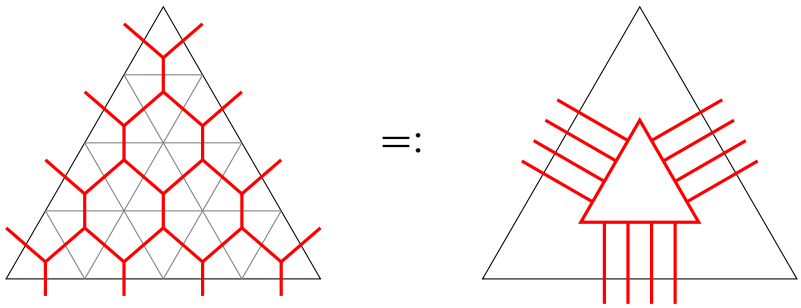

Figure 2: A honeycomb-web on a triangle T of height $n = 4$ (left) and its short-hand presentation (right).

A *signed web* is a web on Σ together with a sign ($+$ or $-$) assigned to each end incident to a puncture. The following patterns (and their orientation-reversals) of signed ends are called *bad ends*:

(2-3) 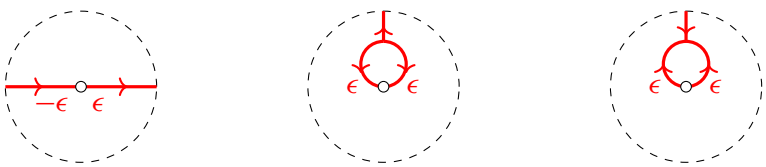

Here $\epsilon \in \{+, -\}$. A signed web is said to be *admissible* if it has no bad ends. In this paper, we always assume that the signed webs are admissible unless otherwise stated. A bounded web is naturally regarded as a signed web since we do not need to specify any signs.

Remark 2.3 The latter two types of bad ends will be excluded simply because they will not contribute to the shear coordinates. On the other hand, a pair of the first type will have nontrivial coordinates, while there is always another web that attains the same coordinates. So we only need admissible signed webs to realize the tropical space. It turns out that we need to include the bad ends of first type to define the Weyl group actions at punctures [28].

Elementary moves of signed webs We are going to introduce several elementary moves for signed webs. The first two are defined for a web without signs.

(E1) Loop parallel-move (aka *flip move* [19] or *global parallel move* [6]):

(2-4) 

(E2) Boundary H-move:

(2-5) 

Similarly for the opposite orientation. We call the face in the left-hand side a *boundary H-face*.

(E3) Puncture H-moves:

(2-6)

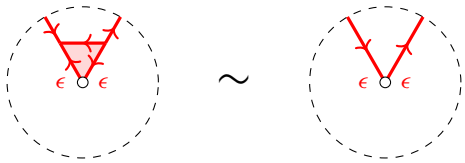

for $\epsilon \in \{+,-\}$, and

(2-7)

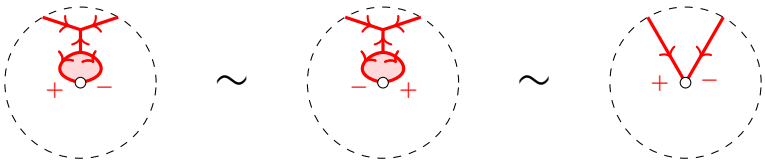

Similarly for the opposite orientation. We call the face in the left-hand side of (2-6) a *puncture H-face*.

The following lemma is verified by using (E2) and the first one in (E3):

Lemma 2.4 *From the boundary and puncture H-moves, we get the following "arc parallel-moves" swapping parallel arcs with opposite orientations*:

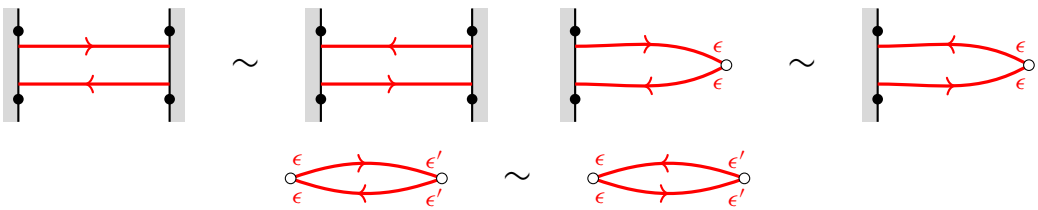

Here white (resp. black) circles stand for punctures (resp. special points), and $\epsilon, \epsilon' \in \{+,-\}$.

Also note that we can always transform any signed web to a signed web without boundary H-faces (resp. puncture H-faces) by applying (E2) and (E3), respectively. Slightly generalizing the terminology in [19], such a signed web is said to be *boundary-reduced* (resp. *puncture-reduced*). It is said to be *reduced* if it is both boundary- and puncture-reduced.

(E4) Peripheral move: removing or creating a peripheral component:

(2-8)

Moreover, we have the moves

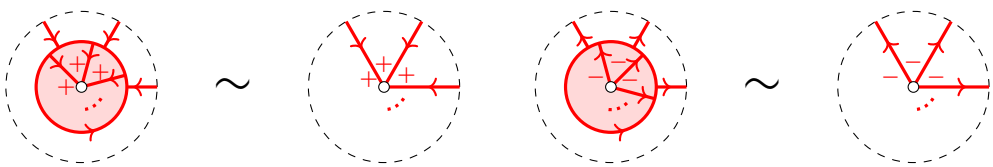

Similarly for the opposite orientation.

We will consider the equivalence relation on signed webs generated by isotopies of marked surfaces and the elementary moves (E1)–(E4). Observe that the moves (E1)–(E4) preserves the admissibility. On the other hand, a nonelliptic signed web may be equivalent to an elliptic web as the following example shows.

Example 2.5 We have

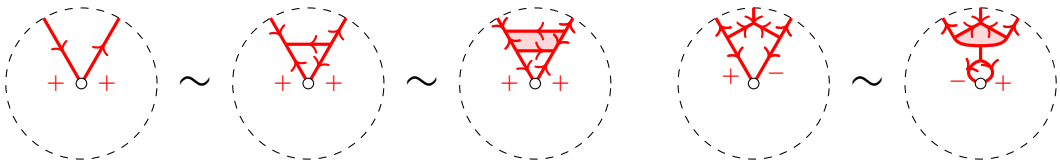

by the puncture H-moves (2-6) and (2-7), where the resulting signed webs are elliptic (having interior 4-gon faces).

Definition 2.6 (rational unbounded $\mathfrak{sl}_3$-laminations) A *rational unbounded* $\mathfrak{sl}_3$*-lamination* (or a rational $\mathfrak{sl}_3$-$\mathcal{X}$-lamination) on Σ is an admissible, nonelliptic signed $\mathfrak{sl}_3$-web W on Σ equipped with a positive rational number (called the *weight*) on each component, which is considered modulo the equivalence relation generated by isotopies and the following operations:

(1) Elementary moves (E1)–(E4) for the underlying signed webs. Here the corresponding components are assumed to have the same weights.

(2) Combine a pair of isotopic loops with the same orientation with weights u and v into a single loop with the weight $u+v$. Similarly combine a pair of isotopic oriented arcs with the same orientation (and with the same signs if some of their ends are incident to punctures) into a single one by adding their weights.

(3) For an integer $n \in \mathbb{Z}_{>0}$ and a rational number $u \in \mathbb{Q}_{>0}$, replace a component with weight nu with its *n-cabling* with weight u, which locally looks like

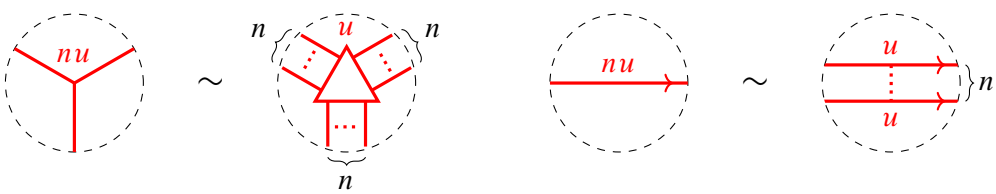

For a loop or arc component, it is just a successive applications of operation (2). One can also verify that the cabling operation is associative in the sense that the n-cabling followed by the m-cabling agrees with the nm-cabling, since nm-cabling is dual to the m^{th} subdivision of an n-triangulation (recall Figure 2).

See Figure 3 for a global example. Let $\mathcal{L}^{x}_{\mathfrak{sl}_3}(\Sigma,\mathbb{Q})$ denote the set of equivalence classes of the rational unbounded $\mathfrak{sl}_3$-laminations on Σ. We have a natural $\mathbb{Q}_{>0}$-action on $\mathcal{L}^{x}_{\mathfrak{sl}_3}(\Sigma,\mathbb{Q})$ that simultaneously rescales the weights. A rational unbounded $\mathfrak{sl}_3$-lamination is said to be *integral* if all the weights are integers. The subset of integral unbounded $\mathfrak{sl}_3$-laminations is denoted by $\mathcal{L}^{x}_{\mathfrak{sl}_3}(\Sigma,\mathbb{Z})$.

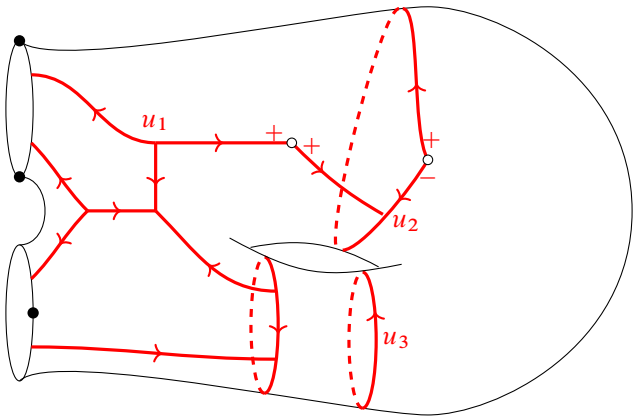

Figure 3: An example of a rational unbounded $\mathfrak{sl}_3$-lamination. Here u_1, u_2 and u_3 are arbitrary positive rational weights.

The sets $\mathcal{L}^x_{\mathfrak{sl}_3}(\Sigma,\mathbb{Q})$ and $\mathcal{L}^x_{\mathfrak{sl}_3}(\Sigma,\mathbb{Z})$ will be identified with the unfrozen part $\mathcal{X}^{\mathrm{uf}}_{\mathfrak{sl}_3,\Sigma}(\mathbb{Q}^T)$ and $\mathcal{X}^{\mathrm{uf}}_{\mathfrak{sl}_3,\Sigma}(\mathbb{Z}^T)$, respectively, of the tropical cluster $\mathcal{X}$-variety associated with the pair $(\mathfrak{sl}_3,\Sigma)$ (see Section A.3).

Notation 2.7 In view of the equivalence relation (4), we will occasionally use the following equivalent notations for honeycombs:

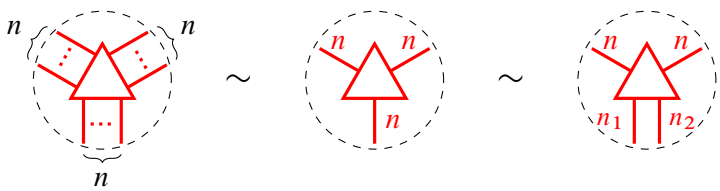

with $n_1+n_2=n$. We may also split an edge of weight n with k edges of weight $n_1,\dots,n_k$ with $n_1+\cdots+n_k=n$.

Definition 2.8 (Dynkin involution) The *Dynkin involution* is the involutive automorphism

$$*\colon \mathcal{L}^x_{\mathfrak{sl}_3}(\Sigma,\mathbb{Q})\to\mathcal{L}^x_{\mathfrak{sl}_3}(\Sigma,\mathbb{Q}),\quad \widehat{L}\mapsto\widehat{L}^*,$$

where $\widehat{L}^*$ is obtained from $\widehat{L}$ by reversing the orientation of every components of the underlying web, and keeping the signs at punctures intact. Since all the elementary moves (E1)–(E4) are equivariant under the orientation-reversion, this indeed defines an automorphism on $\mathcal{L}^x_{\mathfrak{sl}_3}(\Sigma,\mathbb{Q})$.

Bounded laminations and the ensemble map

Definition 2.9 (rational bounded $\mathfrak{sl}_3$-laminations) A *rational bounded $\mathfrak{sl}_3$-lamination* (or a *rational $\mathfrak{sl}_3$-$\mathcal{A}$-lamination*) on Σ is a bounded nonelliptic $\mathfrak{sl}_3$-web W on Σ equipped with a rational number (called the *weight*) on each component such that the weight on a nonperipheral component is positive. It is considered modulo the equivalence relation generated by isotopies and the operations (2)–(4) in Definition 2.6.

Let $\mathcal{L}^a_{\mathfrak{sl}_3}(\Sigma,\mathbb{Q})$ denote the space of rational bounded $\mathfrak{sl}_3$-laminations. We have a natural $\mathbb{Q}_{>0}$-action on $\mathcal{L}^a_{\mathfrak{sl}_3}(\Sigma,\mathbb{Q})$ that simultaneously rescales the weights. A rational bounded $\mathfrak{sl}_3$-lamination is said to be *integral* if all the weights are integers. The subset of integral bounded $\mathfrak{sl}_3$-laminations is denoted by $\mathcal{L}^a_{\mathfrak{sl}_3}(\Sigma,\mathbb{Z})$.

Remark 2.10 The space $\mathcal{L}^a_{\mathfrak{sl}_3}(\Sigma,\mathbb{Z})$ is the same one as the space $\mathcal{A}_L(\Sigma;\mathbb{Z})$ that appears in Kim's work [32, Definition 3.9].[3] The space $\mathcal{W}_\Sigma$ in Douglas and Sun's work [6, Definition 6] is the subset of $\mathcal{L}^a_{\mathfrak{sl}_3}(\Sigma,\mathbb{Z})$ consisting of elements with positive peripheral weights. It is straightforward to extend their coordinate systems by $\mathbb{Q}_{>0}$-equivariance to the rational case, and the space $\mathcal{L}^a_{\mathfrak{sl}_3}(\Sigma,\mathbb{Q})$ is identified with the tropical cluster $\mathcal{A}$-variety $\mathcal{A}_{\mathfrak{sl}_3,\Sigma}(\mathbb{Q}^T)$ [32, Theorem 3.39].[4]

By forgetting the peripheral components, we get the *geometric ensemble map*

$$p\colon \mathcal{L}^a_{\mathfrak{sl}_3}(\Sigma,\mathbb{Q}) \to \mathcal{L}^x_{\mathfrak{sl}_3}(\Sigma,\mathbb{Q}). \tag{2-9}$$

We will see in Section 4 that the geometric ensemble map coincides with the cluster ensemble map (A-2) via the Douglas–Sun coordinates and our shear coordinates.

3 Shear coordinates

3.1 Essential webs on polygons

Let $\mathbb{D}_k$ denote a disk with $k \geq 2$ special points. In what follows, we simply refer to $\mathbb{D}_k$ as a *k-gon*. We say that an $\mathfrak{sl}_3$-web W on $\mathbb{D}_k$ is *taut* if for any compact embedded arc α whose endpoints lie in a common boundary interval E, the number of intersection points of W with E does not exceed that of W with α. See Figure 4. Following [6], we call a nonelliptic, taut $\mathfrak{sl}_3$-web an *essential* web. These essential webs on polygons are basic building blocks for the bounded $\mathfrak{sl}_3$-laminations studied in [6]. We recall the concrete description of the essential webs for $k = 2, 3$ following [6, Sections 2.7 and 2.8] and [19, Sections 8 and 9], including additional infinite webs needed for our purpose.

The biangle (2-gon) case Let E_L and E_R denote the boundary intervals of a biangle $\mathbb{D}_2$. A (*finite*) *symmetric strand set* on $\mathbb{D}_2$ is a pair $S = (S_L, S_R)$ of finite collections of disjoint oriented strands (ie germs of oriented arcs), where the oriented strands in S_Z are located on E_Z for $Z \in \{L, R\}$ such that the number of incoming (resp. outgoing) strands on E_L is equal to the outgoing (resp. incoming) strands on E_R. See the left-most picture in Figure 5 for an example.

[3] Indeed, an element of our space $\mathcal{L}^a_{\mathfrak{sl}_3}(\Sigma,\mathbb{Z})$ can be represented by a reduced web [32, Definition 3.3] by applying the boundary H-moves, and we can rescale the weights on honeycombs to be 1 by the operation (4) in Definition 2.6.

[4] Here note that there is a subset of $\mathcal{L}^a_{\mathfrak{sl}_3}(\Sigma,\mathbb{Z})$ formed by *congruent* laminations [32, Definition 3.38] which is identified with the tropical cluster $\mathcal{A}$-variety $\mathcal{A}_{\mathfrak{sl}_3,\Sigma}(\mathbb{Z}^T)$.

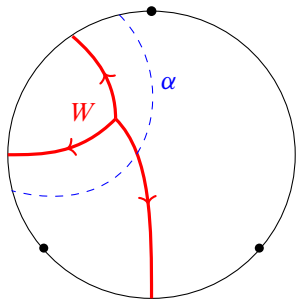

Figure 4: Example of a nontaut web in $\mathbb{D}_3$.

Given a symmetric strand set $S = (S_L, S_R)$, the associated *ladder-web* $W(S)$ on $\mathbb{D}_2$ is constructed as follows. First, let $W_{\mathrm{br}}(S)$ be the unique (up to ambient isotopy of $\mathbb{D}_2$) collection of oriented curves connecting strands in S_L with those in S_R in the order-preserving and minimally intersecting way. See the middle picture in Figure 5. It is characterized by the *pairing map* $f : S_L \to S_R$, which is an order-preserving bijection that maps each incoming (resp. outgoing) strand of S_L to an outgoing (resp. incoming) strand of S_R. The associated ladder-web $W(S)$ is obtained from $W_{\mathrm{br}}(S)$ by replacing each intersection with an H-web, as follows:

(3-1)

Conversely, the collection $W_{\mathrm{br}}(S)$ is called the *braid representation* of the ladder-web $W(S)$. It is known that all the essential webs on $\mathbb{D}_2$ arise in this way:

Proposition 3.1 [6, Proposition 19; 19, Section 8] *The ladder-web $W(S)$ is an essential web on $\mathbb{D}_2$ for any symmetric strand set S. Conversely, given an essential web W on $\mathbb{D}_2$, there exists a unique symmetric strand set S such that $W = W(S)$.*

For the study of unbounded $\mathfrak{sl}_3$-webs, we need the following infinite extension of the symmetric strand sets.

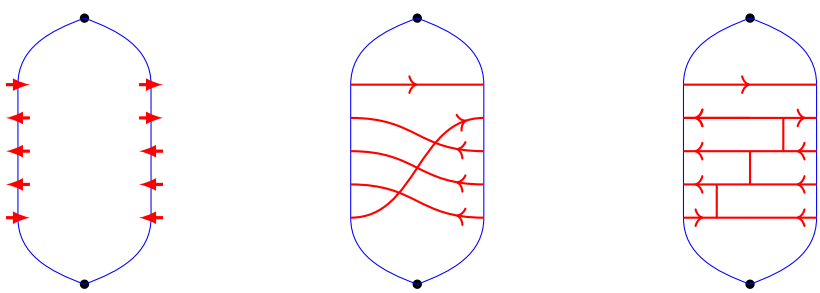

Figure 5: Construction of the ladder-webs. Left: a symmetric set S. Middle: the corresponding collection of oriented curves $W_{\mathrm{br}}(S)$. Right: the associated ladder-web $W(S)$.

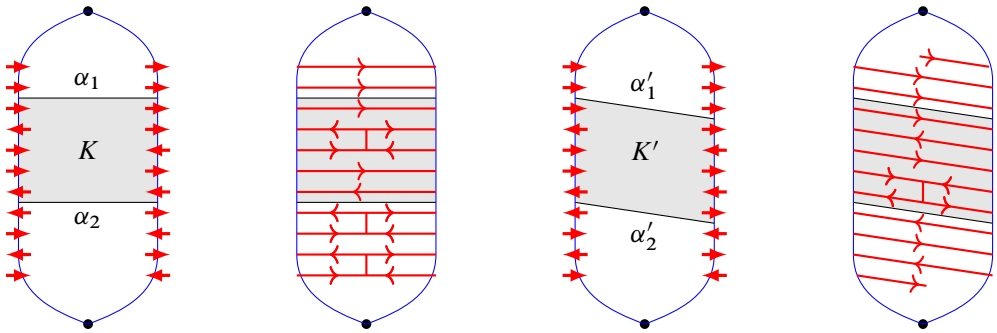

Figure 6: An asymptotically periodic symmetric strand set and the associated ladder webs corresponding to the two choices of compact strips K and K'.

Definition 3.2 (asymptotically periodic symmetric strand sets) An *asymptotically periodic symmetric strand set* $S = (S_L, S_R)$ on $\mathbb{D}_2$ consists of countable collections S_L and S_R of disjoint oriented strands, where the oriented strands in S_Z are located on E_Z without accumulation points for $Z \in \{L, R\}$. The oriented strands are required to be symmetric, and periodic away from a compact set (see Figure 6). Namely, we require that there exists a compact strip $K \subset \mathbb{D}_2 \setminus \mathbb{M}$ such that

- K is bounded by two parallel arcs, α_1 and α_2, transverse to the boundary intervals of $\mathbb{D}_2$, and $\alpha_1 \cup \alpha_2$ avoiding the strand sets S_L and S_R;
- the pair $(S_L \cap K, S_R \cap K)$ is a finite symmetric strand set;
- the orientation patterns of the strands in the sets S_L and S_R that belong to $\mathbb{D}_2 \setminus K$ are periodic, and the pairing map $f_K : S_L \cap K \to S_R \cap K$ of finite symmetric strand set can be extended to an order-preserving bijection $f : S_L \to S_R$ that maps each incoming (resp. outgoing) strand of S_L to an outgoing (resp. incoming) strand of S_R.

Unlike the finite case, the pairing map f may not be unique, as it depends on the choice of the compact strip K. Given such a pair (S, f), we get a collection $W_{\mathrm{br}}(S, f)$ of oriented curves mutually in a minimal position, and the associated ladder-web $W(S, f)$ just in the same manner as in the finite case. We call $W(S, f)$ the ladder-web associated with the pair (S, f). It is possibly an infinite web.

Definition 3.3 An *unbounded essential web* on $\mathbb{D}_2$ is the isotopy class of the ladder-web associated with a pair (S, f) as above.

Among the others, the following way of fixing a pairing map turns out to be useful in this paper.

Definition 3.4 A *pinning* of an asymptotically periodic symmetric strand set $S = (S_L, S_R)$ is a pair $\mathsf{p}_Z = (p_Z^+, p_Z^-)$ of points in E_Z away from the set S_Z for $Z \in \{L, R\}$. The resulting tuple $\widehat{S} := (S; \mathsf{p}_L, \mathsf{p}_R)$ is called a *pinned symmetric strand set*.

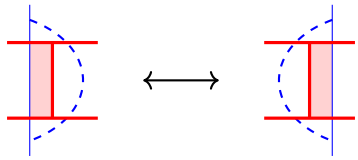

Figure 7: The H-move across an arc.

Then we define the pairing map as follows. For $Z \in \{L, R\}$, let us decompose $S_Z = S_Z^+ \sqcup S_Z^-$, where S_Z^+ (resp. S_Z^-) denotes the subset of incoming (resp. outgoing) strands. Then there exist orientation-reversing homeomorphisms $f_\pm \colon E_L \to E_R$ such that $f_\pm(S_L^\pm) = S_R^\mp$ and $f_\pm(p_L^\pm) = p_R^\mp$. Then we get the unique pairing map

$$f_{\widehat{S}} := f_+ \sqcup f_- \colon S_L^+ \sqcup S_L^- \to S_R^- \sqcup S_R^+,$$

which determines the collection $W_{\mathrm{br}}(\widehat{S}) := W_{\mathrm{br}}(S, f_{\widehat{S}})$ of oriented curves and the associated ladder-web $W(\widehat{S}) := W(S, f_{\widehat{S}})$.

The triangle (3-gon) case Let $\mathbb{D}_3$ be a triangle. Recall that we have honeycomb-webs on $\mathbb{D}_3$, which are dual to n-triangulations of $\mathbb{D}_3$.

Proposition 3.5 [6, Proposition 22; 19, Theorem 19] *A honeycomb-web is reduced (**rung-less** in terms of [6]) and essential. Conversely, any connected reduced essential web on $\mathbb{D}_3$ having at least one trivalent vertex is a honeycomb-web.*

Consequently, any reduced essential web on $\mathbb{D}_3$ consists of a unique (possibly empty) honeycomb component together with a collection of disjoint oriented arcs located on the corners of $\mathbb{D}_3$. These oriented arcs are called *corner arcs*. Similarly to the biangle case, we may allow the collection of corner arcs to be semi-infinite and asymptotically periodic.

Definition 3.6 An *unbounded reduced essential web* on $\mathbb{D}_3$ is the isotopy class of a disjoint union of a (possibly empty) reduced essential web on $\mathbb{D}_3$ and at most one semi-infinite periodic collection of corner arcs around each corner.

3.2 Good position of an unbounded $\mathfrak{sl}_3$-lamination

Let $\triangle$ be an ideal triangulation of Σ without self-folded triangles. Recall from [6, Section 3] that a bounded $\mathfrak{sl}_3$-web W on Σ is *generic* with respect to $\triangle$ if none of its trivalent vertices intersect with the edges of $\triangle$, and W intersects with $\triangle$ transversely. A *generic isotopy* is an isotopy of webs through generic webs. Recall the *parallel-equivalence* of bounded webs, which is the equivalence relation generated by isotopies of marked surface and the loop parallel-move (E1). A generic bounded web W is said to be in *minimal position* with respect to $\triangle$ if it minimizes the sum of the intersection numbers with the edges of $\triangle$ among those parallel-equivalent to W. Then we have:

Figure 8: The intersection reduction moves across an arc.

Proposition 3.7 [6, Proposition 27; 19, Section 6] *Any parallel-equivalence class of nonelliptic bounded webs on Σ has a representative in minimal position with respect to $\triangle$. Moreover, such a representative is unique up to a sequence of H-moves across edges of $\triangle$ (Figure 7), loop parallel-moves, and generic isotopies.*

Indeed, the minimal position is realized by appropriately applying the *intersection reduction moves* (aka *tightening moves*) across edges of $\triangle$ shown in Figure 8.

The *split ideal triangulation* $\widehat{\triangle}$ is obtained from $\triangle$ by replacing each edge E into a biangle B_E. We say that a bounded web W on Σ is in *good position* with respect to $\widehat{\triangle}$ if the restrictions $W \cap B_E$ for $E \in e(\triangle)$ (resp. $W \cap T$ for $T \in t(\triangle)$) are an essential (resp. reduced essential) webs. Then it is known that any parallel-equivalence class of nonelliptic bounded webs on Σ has a representative in good position with respect to $\widehat{\triangle}$; such a representative is unique up to a sequence of modified H-moves (Figure 9), loop parallel-moves, and generic isotopies for $\widehat{\triangle}$ [6, Proposition 30; 19, Corollary 18]. Using such a representative, the Douglas–Sun coordinates are defined [6, Section 4].

Now let us consider a signed web W on Σ. In this case, W is no more parallel-equivalent to a web in good position in the above sense. To resolve this, we introduce the following notion:

Definition 3.8 (spiraling diagram) Let W be a nonelliptic signed web on Σ. Then the associated *spiraling diagram* $\mathcal{W}$ is a (possibly infinite and noncompact) $\mathfrak{sl}_3$-web obtained by the following two steps.

(1) In a small disk neighborhood D_p of each puncture $p \in \mathbb{M}_\circ$, deform each end of W incident to p into an infinitely spiraling curve, according to their signs as shown in Figure 10. Let $\mathcal{W}'$ be the resulting diagram.

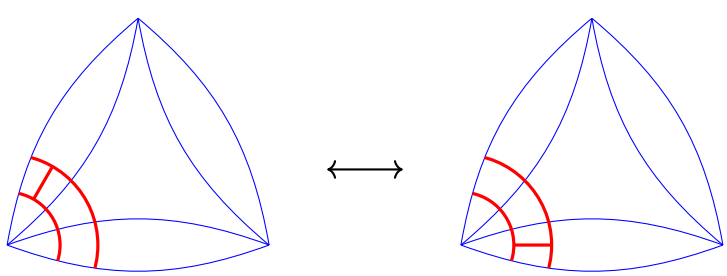

Figure 9: The modified H-move [6] (aka crossbar pass [19]) across a corner.

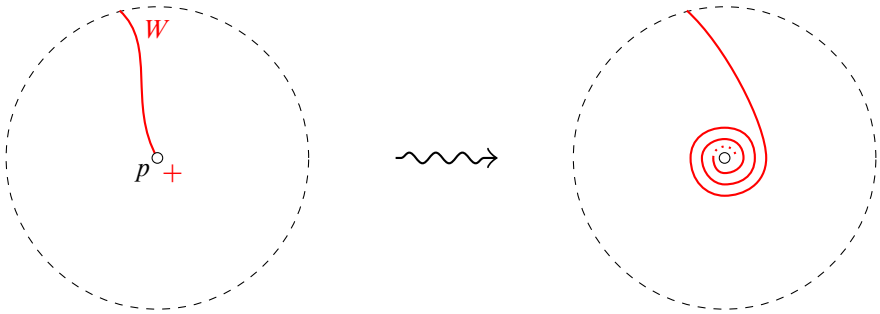

Figure 10: Construction of a spiraling diagram. The negative sign similarly produce an end spiraling counterclockwise.

(2) A pair of ends incident to a common puncture p with the opposite sign produce infinitely many intersections in $\mathcal{W}'$. We then modify these intersections into H-webs in a periodic manner, as follows. By applying an isotopy in D_p, we can make these intersections only occurring in a single half-biangle B_p in D_p with special point p, without producing additional intersections.[5] Then $\mathcal{W}' \cap B_p = W_{\mathrm{br}}(S_p)$ for an asymptotically periodic symmetric strand set S_p on B_p. By replacing the biangle part $W_{\mathrm{br}}(S_p)$ with the associated ladder-web $W(S_p)$, we get the spiraling diagram $\mathcal{W}$. Since $\mathcal{W} \cap (D_p \setminus B_p)$ consists of oriented corner arcs, the result does not depend on the choice of B_p.

See Figure 11 for a local example. A global example arising from Figure 3 is shown in Figure 12.

Definition 3.9 The spiraling diagram $\mathcal{W}$ is in a *good position* with respect to a split triangulation $\widehat{\triangle}$ if the intersection $\mathcal{W} \cap B_E$ (resp. $\mathcal{W} \cap T$) is an unbounded essential (resp. reduced essential) local web for each $E \in e(\triangle)$ and $T \in t(\triangle)$.

The loop parallel-move and the boundary H-move of a spiraling diagram are similarly defined as before, so that the construction of spiraling diagram from a signed web is equivariant under these moves. We define the *modified periodic H-move* of a spiraling diagram in a good position across a corner to be the periodic application of the modified H-move to be the periodic parts of the unbounded essential local webs on biangles. By a *strict isotopy* relative to a split triangulation $\widehat{\triangle}$, we mean an isotopy on a marked surface Σ which is the identity on each edge of $\widehat{\triangle}$ and a neighborhood of each puncture.

Theorem 3.10 (proof in Section 6.1) *Any spiraling diagram arising from a nonelliptic signed web on Σ can be isotoped into a good position with respect to $\widehat{\triangle}$ by a finite sequence of intersection reduction*

[5] Concretely, this can be done as follows. If we fix a polar coordinates (r, θ), $r < r_0$ for some $r_0 > 0$ on the punctured disk $D_p \setminus \{p\}$, each spiraling curve can be modeled by the logarithmic spiral $\ell_\pm(a)$: $\theta = \pm \log(ar)$ for some parameter $a > 0$. Then an elementary calculation shows that the intersection points of $\ell_+(a_1)$ and $\ell_-(a_2)$ lie on a single line, which is viewed as the union of two rays. Then we can collectively push these rays into a chosen half-biangle B_p only by smoothly varying the coordinate function θ. By the standard argument involving a smooth cut-off function, we can also modify this "angular" isotopy to be identity near ∂D_p.

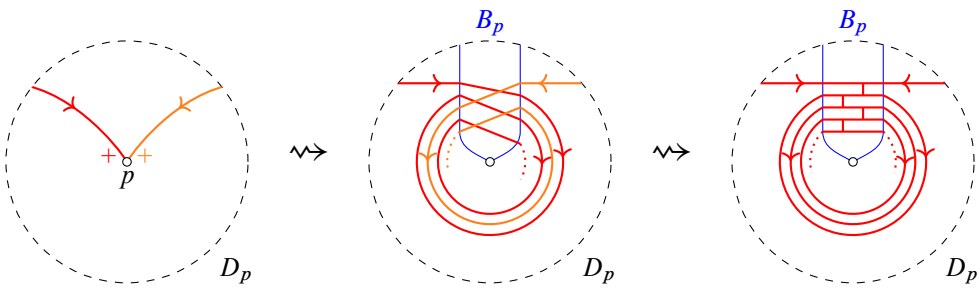

Figure 11: Construction of a spiraling diagram. Replace intersections with H-webs in a periodic manner.

moves, H-moves, and strict isotopies relative to $\widehat{\triangle}$*. Moreover, such a good position is unique up to a sequence of modified H-moves, modified periodic H-moves, loop parallel-moves, boundary H-moves, and strict isotopies relative to* $\widehat{\triangle}$*.*

Indeed, we can obtain a representative in a good position by successively applying the intersection reduction moves (Figure 8) and then pushing the H-faces into biangles by the H-move (Figure 7). An example of this procedure is illustrated in Figure 13. The main issue here is to ensure that this procedure always terminates in finite steps, which is discussed in Section 6.1 in detail.

While the spiraling diagram itself is suited to discuss its good position, the following *braid representation* will be useful to define the shear coordinates:

Definition 3.11 (braid representation of a spiraling diagram) Let $\mathcal{W}$ be a spiraling diagram in a good position with respect to $\widehat{\triangle}$. Then its *braid representation* $\mathcal{W}_{\mathrm{br}}^{\triangle}$ is obtained from $\mathcal{W}$ by replacing the unbounded essential web $\mathcal{W} \cap B_E$ on each biangle B_E with its braid representation.

The braid representation is closely related to (an unbounded version of) *global picture* [6, Definition 55]. See also Section 6.2.

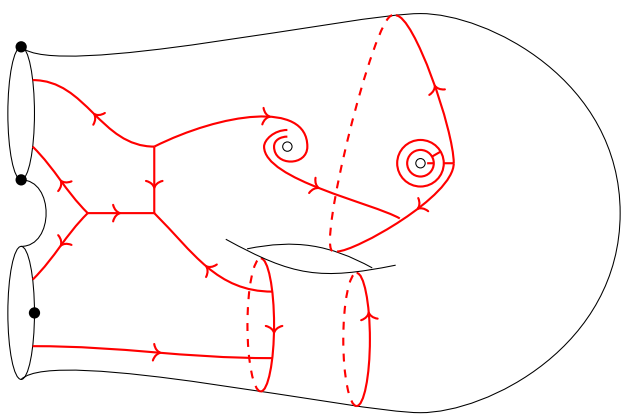

Figure 12: A global example of spiraling diagram arising from the underlying signed nonelliptic web in Figure 3.

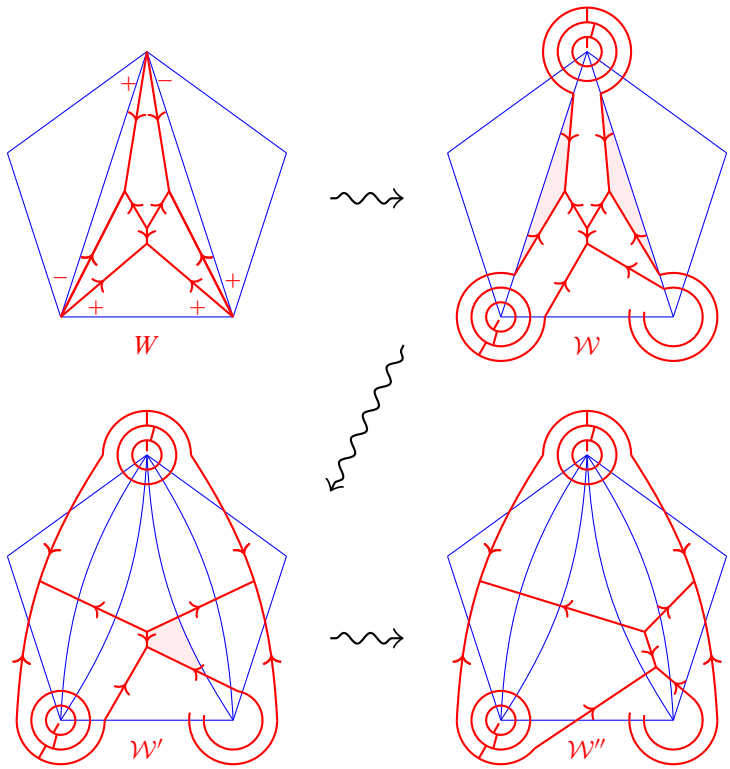

Figure 13: An example of the procedure to place a spiraling diagram in good position.

3.3 Definition of the shear coordinates

Now we define the shear coordinates associated with an ideal triangulation $\triangle$ of Σ without self-folded triangles. Let $\widehat{\triangle}$ be the associated split triangulation.

Given a rational $\mathfrak{sl}_3$-lamination $\widehat{L} \in \mathcal{L}^{x}_{\mathfrak{sl}_3}(\Sigma, \mathbb{Q})$, represent it by an $\mathfrak{sl}_3$-web W together with rational weights on its components and signs at the ends incident to punctures. Let $\mathcal{W}$ be the associated spiraling diagram together with rational weights on the components, placed in good position with respect to $\widehat{\triangle}$. Let $\mathcal{W}^{\triangle}_{\mathrm{br}}$ be its braid representation, together with well-assigned rational weights on its components. The shear coordinates of $\widehat{L}$ are going to be defined out of $\mathcal{W}^{\triangle}_{\mathrm{br}}$.

For each $E \in e_{\mathrm{int}}(\triangle)$, let Q_E be the unique quadrilateral containing E as its diagonal, regarded as the union of two triangles, T_L and T_R, and the biangle B_E. By Proposition 3.5, the restriction of $\mathcal{W}^{\triangle}_{\mathrm{br}}$ to each of T_L and T_R has at most one honeycomb web, which is represented by a triangular symbol as in Notation 2.7. We call any strand in the braid representative $\mathcal{W}^{\triangle}_{\mathrm{br}} \cap Q_E$ that is incident to the triangular symbol in T_L (if exists) a *T_L-strand*. Similarly, we define *T_R-strands*. It is possible that an arc is both T_L- and T_R-strand, in which case it connects the two honeycombs. By removing the T_L- and T_R-strands, remaining is a collection of (possibly intersecting) oriented curves, which we call the *curve components*. See Figure 17 below.

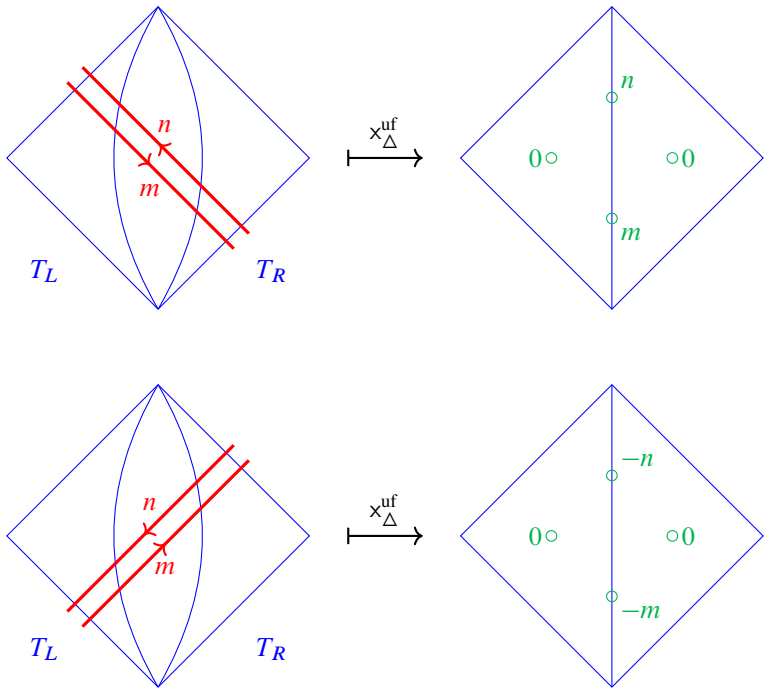

Figure 14: Contributions from curve components.

Definition 3.12 ($\mathfrak{sl}_3$-shear coordinates) The ($\mathfrak{sl}_3$-)*shear coordinate system*

$$x_\Delta^{\mathrm{uf}}(\widehat{L}) = (x_i^\Delta(\widehat{L}))_{i \in I_{\mathrm{uf}}(\Delta)} \in \mathbb{Q}^{I_{\mathrm{uf}}(\Delta)}$$

is defined as follows. First, for each $E \in e_{\mathrm{int}}(\Delta)$, the coordinates assigned to the four vertices in the interior of Q_E only depends on the restriction $\mathcal{W}_{\mathrm{br}}^\Delta \cap Q_E$.

(1) Each curve component contributes to the edge coordinates according to the rule shown in Figure 14.

(2) The honeycomb on the triangle T_L contributes to $x_\Delta^{\mathrm{uf}}(\widehat{L})$ as in Figure 15. Namely, the face coordinate counts the height of the honeycomb web, where a sink (resp. source) is counted positively (resp. negatively). The edge coordinates counts the contributions from T_L-strands, where we have n_1 left-turning ones, n_2 straight-going ones (which are also T_R-strands), and n_3 right-turning ones.

(3) The honeycomb on the triangle T_R and the T_R-strands contribute in the symmetric way with respect to the π rotation of the figure.

Then the shear coordinates are defined to be the weighted sums of these contributions.

Remark 3.13 (1) Notice that the rule shown in Figure 14 is an "oriented version" of the Thurston's shear coordinates (see Section 3.5). Indeed, the sign of contribution is determined by the crossing pattern as in the $\mathfrak{sl}_2$-case, and it contributes to the coordinates *on the right side* of the oriented curve.

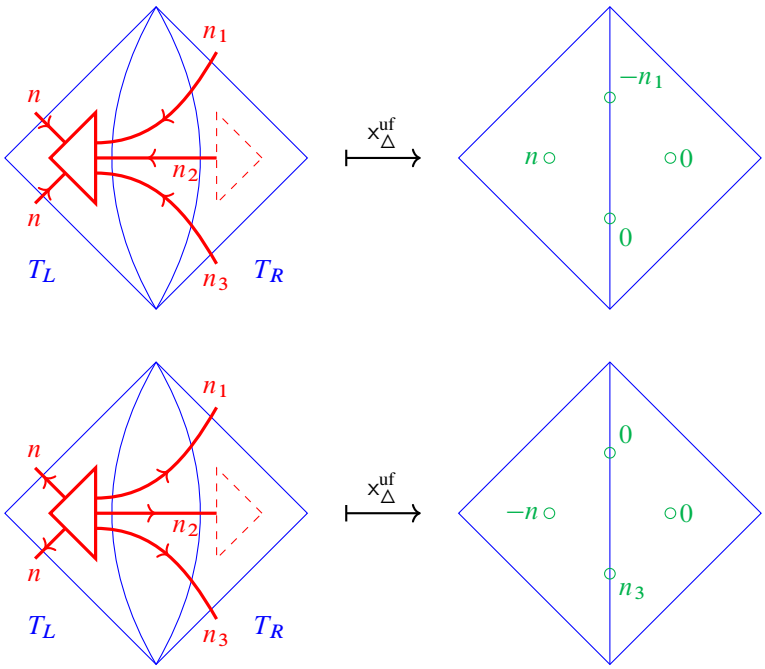

Figure 15: Contributions from the honeycomb of height $n = n_1 + n_2 + n_3$ on the triangle T_L. Observe that the n_2 straight-going T_L-strands do not contribute.

(2) The shear coordinates of the first honeycomb component shown in Figure 15 is the same as the sum of shear coordinates of the three honeycomb components shown in Figure 16.

Proposition 3.14 *The shear coordinate system $x^{\mathrm{uf}}_{\Delta}(\widehat{L}) \in \mathbb{Q}^{I_{\mathrm{uf}}(\Delta)}$ is well defined, and we get a map*

$$x^{\mathrm{uf}}_{\Delta} \colon \mathcal{L}^{x}_{\mathfrak{sl}_3}(\Sigma, \mathbb{Q}) \to \mathbb{Q}^{I_{\mathrm{uf}}(\Delta)}.$$

Proof It is not hard to see that the operations appearing in Theorem 3.10 that move a spiraling diagram in a good position to another good position do not change the shear coordinates. For example, the modified H-move always involves a pair of oriented curves in the opposite directions in the braid representation,

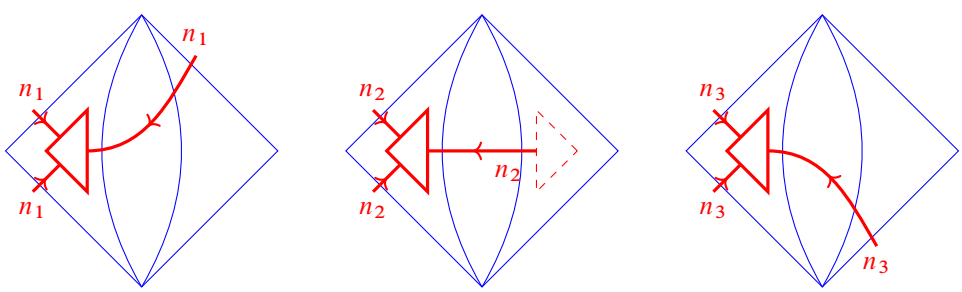

Figure 16: Basic honeycomb components.

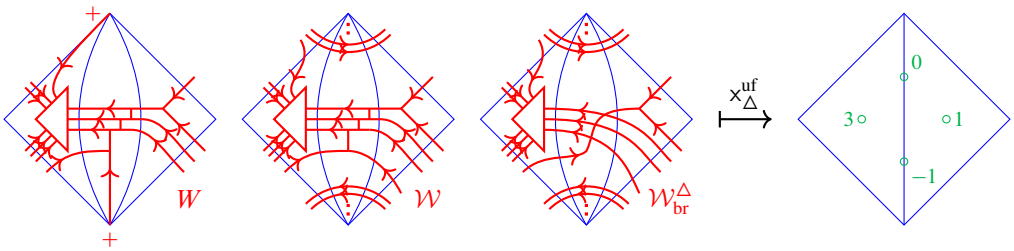

Figure 17: An example of a signed web W restricted to Q_E, the associated spiraling diagram $\mathcal{W}$, its braid representation $\mathcal{W}^{\triangle}_{\mathrm{br}}$, its shear coordinates are shown order. In $\mathcal{W}^{\triangle}_{\mathrm{br}}$, there are two honeycomb components and infinitely many curve components.

and hence preserves the contribution from the pair. It follows that the shear coordinates are well defined for a given spiraling diagram, not depending on the choice of a good position with respect to $\widehat{\triangle}$.

We need to check that the elementary moves (E1)–(E4) of signed webs do not change the shear coordinates. It is easy to see the invariance for the loop parallel-move (E1). The braid representatives of spiraling diagrams associated with the local signed webs in (2-5)–(2-7) are obtained as follows:

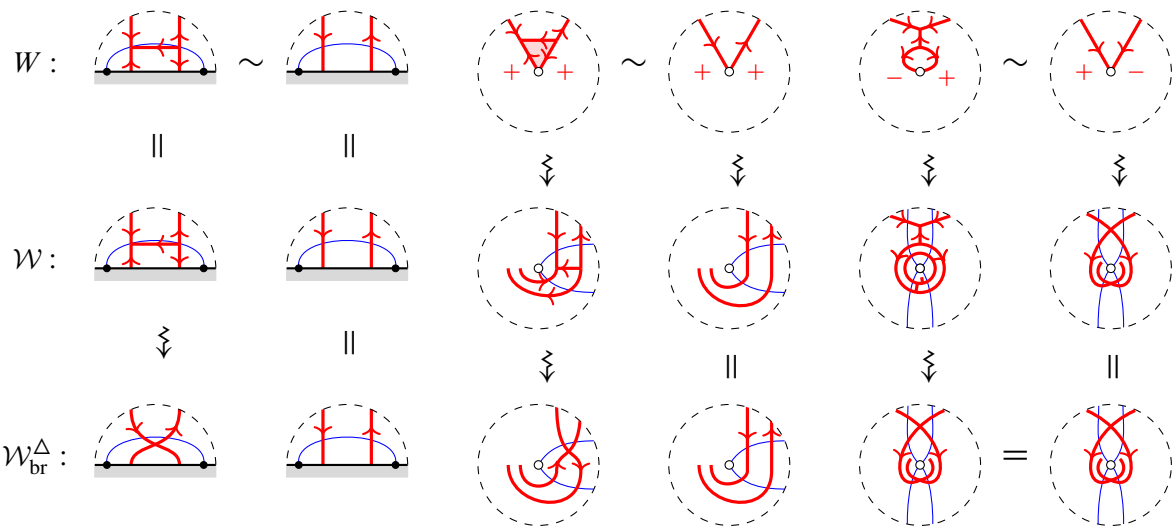

Here the braid representatives are not quite the same in the first two cases, but both have the same shear coordinates. Thus the shear coordinates are invariant under the moves (E2) and (E3). The invariance under the peripheral move (E4) is similarly verified, where the signed web in the left-hand side produces a peripheral component in its spiraling diagram.

The shear coordinates are clearly invariant under operations (2) and (3) in Definition 2.6, and hence do not depend on the choice of a signed $\mathbb{Q}_{>0}$-weighted web representing an unbounded $\mathfrak{sl}_3$-lamination. □

Notation 3.15 We will write $x^{\triangle}_T := x^{\triangle}_{i(T)}$ for a triangle T of $\triangle$, and $x^{\triangle}_{E,s} := x^{\triangle}_{i^s(E)}$ for an oriented edge E of $\triangle$ and $s = 1, 2$. Here recall the notations in Section 2.1.

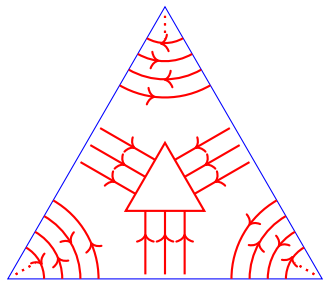

Figure 18: The building block for reconstruction from the shear coordinates when $x_T = +3$.

3.4 Reconstruction

We are going to give an inverse map $\xi_\triangle : \mathbb{Q}^{I_{\mathrm{uf}}(\triangle)} \to \mathcal{L}^x_{\mathfrak{sl}_3}(\Sigma, \mathbb{Q})$ of the shear coordinate system associated with an ideal triangulation $\triangle$.

Given $(\tilde{x}_i)_i \in \mathbb{Q}^{I_{\mathrm{uf}}(\triangle)}$, choose a positive integer $u \in \mathbb{Z}_{>0}$ such that $x_i := u\tilde{x}_i$ are integral for all $i \in I_{\mathrm{uf}}(\triangle)$. We will use a notation similar to Notation 3.15 for these tuples. On each triangle $T \in t(\triangle)$, first draw a honeycomb web of height $|x_T|$ of sink type (resp. source type) if $x_T \geq 0$ (resp. $x_T < 0$). Moreover, on each corner of T, draw an semi-infinite collection of disjoint corner arcs with alternating orientations such that

- they are disjoint from the honeycomb web (placed on the center of T),
- they accumulate only at the marked points of the triangle, and
- the farthest one from the marked point is oriented clockwise.

See Figure 18. Then we get an unbounded reduced essential web W_T on each triangle T. We are going to glue these local blocks together to form an integral unbounded $\mathfrak{sl}_3$-lamination $\xi_\triangle((x_i)_i) \in \mathcal{L}^x_{\mathfrak{sl}_3}(\Sigma, \mathbb{Z})$.

Now let us concentrate on a quadrilateral Q_E in the ideal triangulation $\triangle$ which contains two triangles T_L and T_R that share an interior edge E. We fix an orientation of E such that T_L lies on the left; hence we have two edge coordinates $x_{E,1}$ and $x_{E,2}$ as well as two face coordinates x_{T_L} and x_{T_R}:

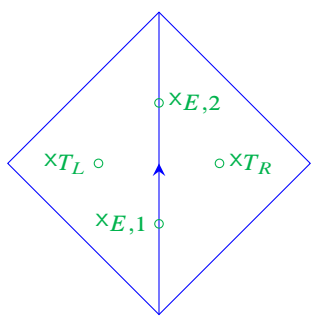

Consider a biangle B_E in the split ideal triangulation $\widehat{\triangle}$ obtained by fattening E, which is bounded by boundary intervals E_L and E_R of T_L and T_R, respectively. For $Z \in \{L, R\}$, let $S_Z = S_Z^+ \sqcup S_Z^-$

denote the set of ends of the web W_{T_Z} on E_Z, where S_Z^+ (resp. S_Z^-) consists of the ends incoming to (resp. outgoing from) the biangle B_E. Then $S = (S_L, S_R)$ defines an asymptotically periodic symmetric strand set (Definition 3.2). Let us define its pinning by the following rule:

- For $Z \in \{L, R\}$, choose orientation-preserving parametrizations
$$\phi_Z^{\pm}\colon \mathbb{R} \to E_Z$$
so that $\phi_Z^{\pm}\left(\frac{1}{2}+\mathbb{Z}\right) = S_Z^{\pm}$, and $\phi_Z^{\pm}(\mathbb{R}_{<0}) \cap S_Z^{\pm}$ consists of all the strands coming from the corner arcs around the initial marked point of E_Z.
- Let $p_Z^{\pm} := \phi_Z^{\pm}(n_Z^{\pm}) \in E_Z$ for $Z \in \{L, R\}$, where $n_Z^{\pm} \in \mathbb{Z}$ are given by

(3-2)
$$n_L^+ := \mathsf{x}_{E,1}, \quad n_L^- := [\mathsf{x}_{T_L}]_+, \quad n_R^+ := \mathsf{x}_{E,2}, \quad n_R^- := [\mathsf{x}_{T_R}]_+,$$

where we use the notation $[x]_+ := \max\{0, x\}$.

Then we get a pinned symmetric strand set $\widehat{S}_E := (S; \mathsf{p}_L, \mathsf{p}_R)$ with the pinnings $\mathsf{p}_Z := (p_Z^+, p_Z^-)$ for $Z \in \{L, R\}$. Let $W_{\mathrm{br}}(\widehat{S}_E)$ denote the associated collection of oriented curves in B_E.

Remark 3.16 The resulting collection $W_{\mathrm{br}}(\widehat{S}_E)$ is invariant under the transformation
$$n_L^+ \mapsto n_L^+ - k, \quad n_L^- \mapsto n_L^- - l, \quad n_R^+ \mapsto n_R^+ + l, \quad n_R^- \mapsto n_R^- + k,$$
for $k, l \in \mathbb{Z}$.

Gluing together the local webs W_T for $T \in t(\triangle)$ and the curves in $W_{\mathrm{br}}(\widehat{S}_E)$ for $E \in e(\triangle)$, we get a (possibly infinite) collection $\mathcal{W}_{\mathrm{br}}^{\triangle}((\mathsf{x}_i)_i)$ of webs on Σ. The following lemma shows that it has correct shear coordinates.

Lemma 3.17 *We have* $\mathsf{x}_k^{\triangle}(\mathcal{W}_{\mathrm{br}}^{\triangle}((\mathsf{x}_i)_i)) = \mathsf{x}_k$ *for all* $k \in I_{\mathrm{uf}}(\triangle)$.

Proof Let us concentrate on a quadrilateral $Q = T_L \cup B_E \cup T_R$. It is easy to see $\mathsf{x}_{T_Z}^{\triangle}(\widehat{L}) = \mathsf{x}_{T_Z}$ for $Z \in \{L, R\}$. The equalities $\mathsf{x}_{E,1}^{\triangle}(\widehat{L}) = \mathsf{x}_{E,1}$ and $\mathsf{x}_{E,2}^{\triangle}(\widehat{L}) = \mathsf{x}_{E,2}$ can be also verified case-by-case, divided according to the signs of x_{T_L} and x_{T_R}. See Figures 19–21. Here we draw the pictures by separating the gluing procedures $S_L^- \to S_R^+$ and $S_L^+ \to S_R^-$ into two sheets; the result is obtained by overlaying the two diagrams drawn on the right.

For example, let us consider the example shown in Figure 19. In the case $\mathsf{x}_{E,2} \geq 0$ (as in this example), there are $\mathsf{x}_{E,2}$ many lines from south-east to north-west that contribute positively. One can imagine the other cases by varying this example: if we decrease $\mathsf{x}_{E,2}$, then the point p_R^+ moves upward and the gluing pattern is shifted. When $-\mathsf{x}_{T_L} \leq \mathsf{x}_{E,2} < 0$, negative contributions come from the honeycomb in T_L. When $\mathsf{x}_{E,2} < -\mathsf{x}_{T_L}$, there are also lines from south-west to north-east that contribute negatively. Thus we get $\mathsf{x}_{E,2}^{\triangle}(\widehat{L}) = \mathsf{x}_{E,2}$. The check for $\mathsf{x}_{E,1}$ is similar. One can check the other cases from Figures 20 and 21 in a similar manner. □

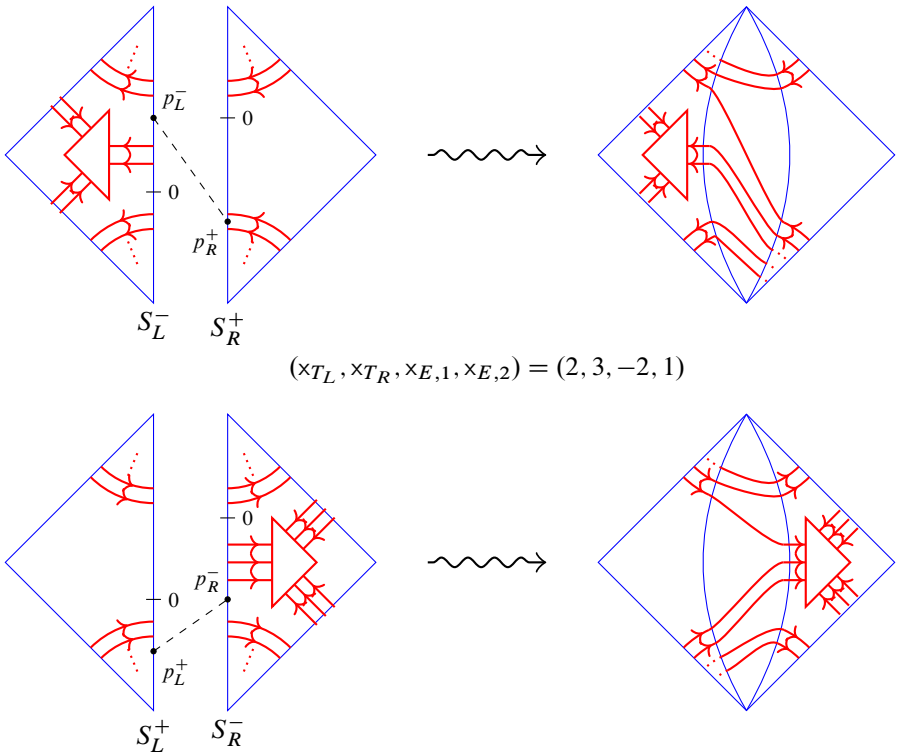

Figure 19: An example for the case $x_{T_L} \geq 0$ and $x_{T_R} \geq 0$.

The collection $\mathcal{W}_{\mathrm{br}}^{\triangle}((x_i)_i)$ is the braid representative of the spiraling diagram associated to an unbounded integral $\mathfrak{sl}_3$-lamination $\xi_{\triangle}((x_i)_i)$, which is obtained as follows:

Step 1 First remove the peripheral components around the marked points (both special points and punctures) from $\mathcal{W}_{\mathrm{br}}^{\triangle}((x_i)_i)$. Then, remaining are finitely many components.

Step 2 Replace each spiraling end around a puncture p with an end incident to p, while encoding the spiraling directions in signs by reversing the rule in Figure 10. Then we get a collection $W_{\mathrm{br}}^{\triangle}((x_i)_i)$ of signed webs, which we call a *braid representative* of a signed web. It contains at most finitely many intersections of curves only in biangles. Here we can rearrange $W_{\mathrm{br}}^{\triangle}((x_i)_i)$ so that no pair of curves form a bigon by applying a Reidemeister II-type isotopy if necessary (cf *square removing algorithm* in [6]). See Figure 22. Observe that this operation does not affect the shear coordinates.

Step 3 Replace each intersection of curves in a biangle with an H-web by the rule (3-1). Then we get a signed $\mathfrak{sl}_3$-web W on Σ, which has no elliptic faces. Indeed, we have no 0-gon or 2-gon faces by construction, and possible emergence of 4-gon faces has been eliminated in Step 2.

Then $\xi_{\triangle}((x_i)_i) \in \mathcal{L}^x_{\mathfrak{sl}_3}(\Sigma, \mathbb{Z})$ is defined to be the unbounded integral $\mathfrak{sl}_3$-lamination represented by the nonelliptic signed web W (with weight 1 on each component). Set

$$\xi_{\triangle}((\tilde{x}_i)_i) := u^{-1} \cdot \xi_{\triangle}((x_i)_i) \in \mathcal{L}^x_{\mathfrak{sl}_3}(\Sigma, \mathbb{Q}).$$

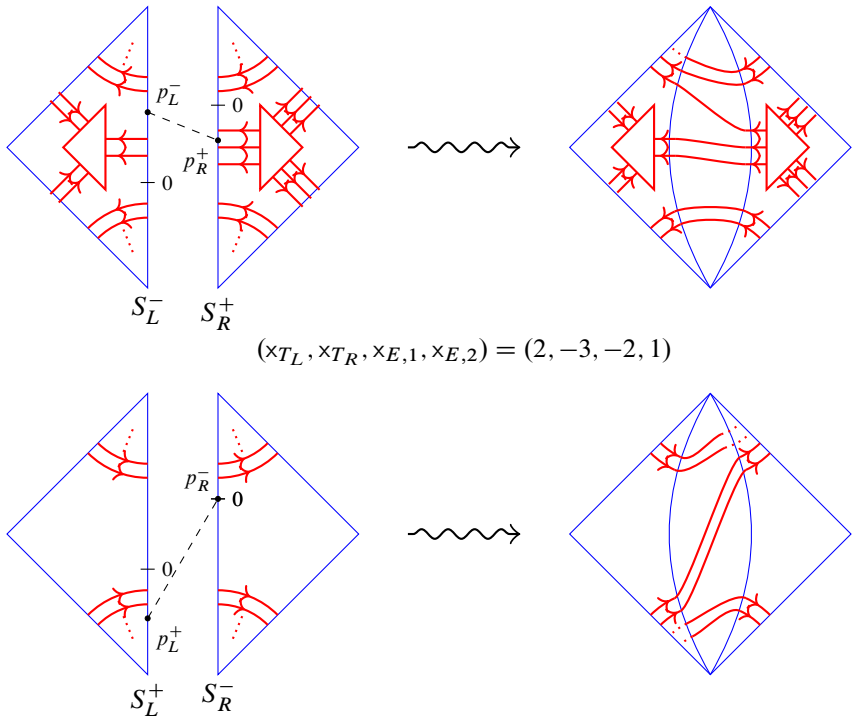

Figure 20: An example for the case $\mathsf{x}_{T_L} \geq 0$ and $\mathsf{x}_{T_R} \leq 0$. The case $\mathsf{x}_{T_L} \leq 0$ and $\mathsf{x}_{T_R} \geq 0$ follows by symmetry (Remark 3.16).

Thus we get the map $\xi_\triangle \colon \mathbb{Q}^{I_{\mathrm{uf}}(\triangle)} \to \mathcal{L}^{\mathcal{X}}_{\mathfrak{sl}_3}(\Sigma, \mathbb{Q})$, which is clearly $\mathbb{Q}_{>0}$-equivariant. We are going to show that this map indeed gives the inverse map of $\mathsf{x}^{\mathrm{uf}}_\triangle$. The following direction is easier:

Proposition 3.18 *We have* $\mathsf{x}^{\mathrm{uf}}_\triangle \circ \xi_\triangle = \mathrm{id}_{\mathbb{Q}^{I_{\mathrm{uf}}(\triangle)}}$.

Proof By $\mathbb{Q}_{>0}$-equivariance, it suffices to consider an integral tuple $(\mathsf{x}_i)_i \in \mathbb{Z}^{I_{\mathrm{uf}}(\triangle)}$. Notice that by construction, the collection $\mathcal{W}^\triangle_{\mathrm{br}}((\mathsf{x}_i)_i)$ arising from the gluing construction above is exactly the braid representative of the spiraling diagram associated with the underlying signed web of the $\mathfrak{sl}_3$-lamination $\widehat{L} := \xi_\triangle((\mathsf{x}_i)_i) \in \mathcal{L}^{\mathcal{X}}_{\mathfrak{sl}_3}(\Sigma, \mathbb{Z})$. Therefore the shear coordinates $(\mathsf{x}^\triangle_i(\widehat{L}))$ can be directly read off from the collection $\mathcal{W}^\triangle_{\mathrm{br}}((\mathsf{x}_i)_i)$. Hence the assertion follows from Lemma 3.17. □

Theorem 3.19 (proof in Section 6.2) *We have* $\xi_\triangle \circ \mathsf{x}^{\mathrm{uf}}_\triangle = \mathrm{id}_{\mathcal{L}^{\mathcal{X}}_{\mathfrak{sl}_3}(\Sigma,\mathbb{Q})}$. *In particular, the shear coordinates gives a bijection* $\xi_\triangle \colon \mathbb{Q}^{I_{\mathrm{uf}}(\triangle)} \xrightarrow{\sim} \mathcal{L}^{\mathcal{X}}_{\mathfrak{sl}_3}(\Sigma, \mathbb{Q})$.

See Section 6.2 for a proof. The main ingredient of the proof is an unbounded version of the fellow-traveler lemma [6, Lemma 57] with respect to the shear coordinates.

Recall from Section A.3 that the ideal triangulations $\triangle$ correspond to certain seeds in the mutation class $\mathsf{s}(\Sigma, \mathfrak{sl}_3)$. The following theorem states that the associated shear coordinate systems $\mathsf{x}^{\mathrm{uf}}_\triangle$ are related by tropical cluster Poisson transformations:

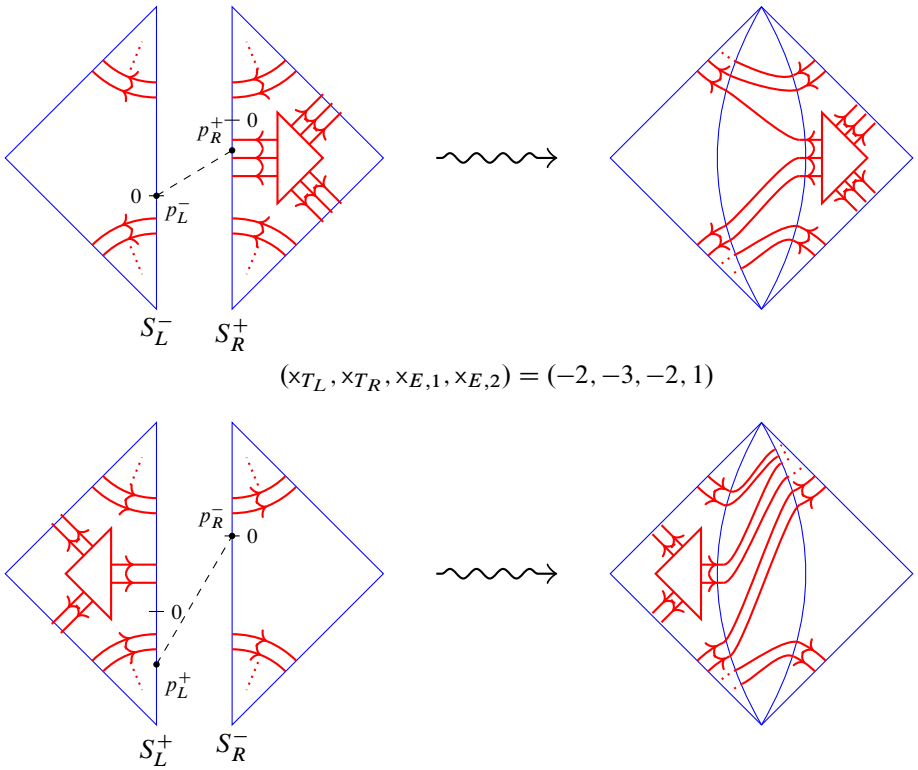

Figure 21: An example for the case $x_{T_L} \le 0$ and $x_{T_R} \le 0$.

Theorem 3.20 *For any two ideal triangulations $\triangle$ and $\triangle'$ of Σ, the coordinate transformation*

$$x^{\mathrm{uf}}_{\triangle'} \circ (x^{\mathrm{uf}}_{\triangle})^{-1} : \mathbb{Q}^{I_{\mathrm{uf}}(\triangle)} \to \mathbb{Q}^{I_{\mathrm{uf}}(\triangle)}$$

is a composite of tropical cluster Poisson transformations. In particular, we get an $\mathrm{MC}(\Sigma)$-equivariant identification $x^{\mathrm{uf}}_{\bullet} : \mathcal{L}^{x}_{\mathfrak{sl}_3}(\Sigma, \mathbb{Q}) \xrightarrow{\sim} \mathcal{X}^{\mathrm{uf}}_{\mathfrak{sl}_3,\Sigma}(\mathbb{Q}^T)$.

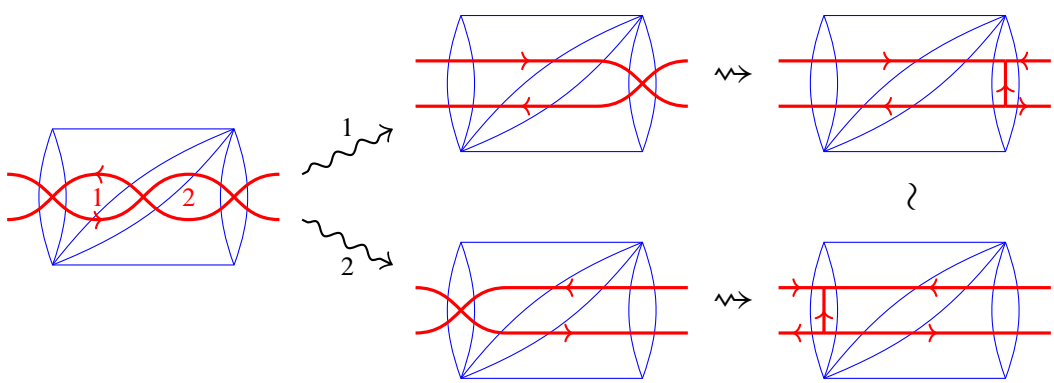

Figure 22: Reidemeister II-type isotopy. We have two ways of applications of this isotopy, which produce equivalent webs.

Since it is classically known that any two ideal triangulations of the same marked surface can be connected by a finite sequence of flips, it suffices to show that a flip corresponds to a composite of tropical cluster Poisson transformations. Although it can be directly checked in a similar way to [7, Section 4], we are going to reduce it to Douglas and Sun's result via the ensemble map and the gluing technique developed in Section 4.

3.5 Relation to the rational unbounded $\mathfrak{sl}_2$-laminations

Recall the space $\mathcal{L}^{x}_{\mathfrak{sl}_2}(\Sigma, \mathbb{Q})$ of rational unbounded ($\mathfrak{sl}_2$-)laminations from [11]. It consists of the following data:

- A collection of immersed unoriented loops and arcs such that each endpoint lies in $\mathbb{M}_\circ \cup \partial^* \Sigma$, and the other part is embedded in $\operatorname{int} \Sigma$. It is required to have no elliptic faces (the first one in (2-1) or the first and last ones in (2-2)).
- A positive rational weight on each component.
- A sign $\sigma_p \in \{+, 0, -\}$ for each puncture $p \in \mathbb{M}_\circ$ such that $\sigma_p = 0$ if and only if there are no components incident to p.

They are considered modulo removal/creation of peripheral components as in (2-8), and the weighted isotopy as in Definition 2.6(2). Given an ideal triangulation $\triangle$ of Σ, the ($\mathfrak{sl}_2$-)shear coordinate

$$x_\triangle = (x_E^\triangle)_{E \in e(\triangle)} \colon \mathcal{L}^{x}_{\mathfrak{sl}_2}(\Sigma, \mathbb{Q}) \xrightarrow{\sim} \mathbb{Q}^{e(\triangle)}$$

(see [11]) is defined by first constructing a spiraling diagram according to the sign σ_p, and counting contributions with weights from the curves in that diagram, as in Figure 23.

An embedding $\iota_{\mathrm{prin}} \colon \mathcal{L}^{x}_{\mathfrak{sl}_2}(\Sigma, \mathbb{Q}) \to \mathcal{L}^{x}_{\mathfrak{sl}_3}(\Sigma, \mathbb{Q})$ is defined so that

- each curve γ with weight $u \in \mathbb{Q}_{>0}$ is sent to its parallel copies, γ_1 and γ_2, with the same weight u with the opposite orientations;
- if an arc γ is incident to a puncture p, then the corresponding ends of the oriented curves γ_1 and γ_2 are assigned the sign $\sigma_p \in \{+, -\}$.

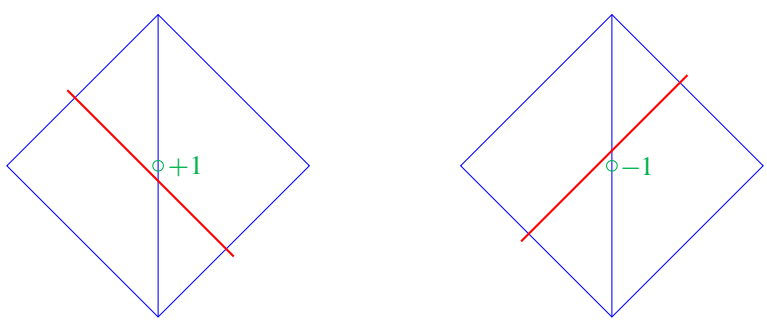

Figure 23: Contributions to the $\mathfrak{sl}_2$-shear coordinates.

One can easily verify that it is indeed well defined. We call ι_{prin} the *principal embedding*, as it is a tropical analogue of the morphism $\mathcal{X}_{\mathrm{SL}_2,\Sigma} \to \mathcal{X}_{\mathrm{SL}_3,\Sigma}$ induced by the principal embedding $\mathfrak{sl}_2 \to \mathfrak{sl}_3$. The following is a tropical analogue of the statement given in [12, Section 2.5.3]:

Proposition 3.21 *The image $\iota_{\mathrm{prin}}(\mathcal{L}^x_{\mathfrak{sl}_2}(\Sigma,\mathbb{Q}))$ coincides with the fixed point locus of the Dynkin involution $*$ (Definition 2.8). In the shear coordinate system $\mathrm{x}_\triangle$ associated with any ideal triangulation $\triangle$, it is characterized by the equations*

$$\mathrm{x}^{\triangle}_{E,1} = \mathrm{x}^{\triangle}_{E,2} \quad \text{for each } E \in e(\triangle),$$
$$\mathrm{x}^{\triangle}_{T} = 0 \quad \text{for each } T \in t(\triangle).$$

Proof The first assertion follows from the second one, by Proposition 4.13 below. The second assertion is easily verified by comparing the definitions of $\mathfrak{sl}_2$- and $\mathfrak{sl}_3$-shear coordinates. Indeed, we have $\mathrm{x}^{\triangle}_E(\widehat{L}) = \mathrm{x}^{\triangle}_{E,1}(\iota_{\mathrm{prin}}(\widehat{L})) = \mathrm{x}^{\triangle}_{E,2}(\iota_{\mathrm{prin}}(\widehat{L}))$ and $\mathrm{x}^{\triangle}_T(\iota_{\mathrm{prin}}(\widehat{L})) = 0$, where $(\mathrm{x}^{\triangle}_E)_{E\in e(\triangle)}$ denotes the $\mathfrak{sl}_2$-shear coordinate system. □

4 Rational $\mathcal{P}$-laminations, their gluing and the mutation equivariance

In this section, we introduce the space of *rational $\mathcal{P}$-laminations* by considering some additional data on boundary intervals and define a coordinate system $\mathrm{x}_\triangle$ extending $\mathrm{x}^{\mathrm{uf}}_\triangle$. These additional data allow us to introduce the *gluing map* between these spaces. Under this extended situation, we discuss the relation to Douglas and Sun's tropical $\mathcal{A}$-coordinates [6], and prove that the coordinates $\mathrm{x}_\triangle$ transform correctly under flips.

4.1 Rational unbounded $\mathfrak{sl}_3$-laminations with pinnings

It has been stated that the space $\mathcal{L}^x_{\mathfrak{sl}_3}(\Sigma,\mathbb{Q})$ of rational unbounded $\mathfrak{sl}_3$-laminations is identified with the unfrozen part $\mathcal{X}^{\mathrm{uf}}_{\mathfrak{sl}_3,\Sigma}(\mathbb{Q}^T)$ of the tropical cluster $\mathcal{X}$-variety. In order to obtain the entire tropical cluster $\mathcal{X}$-variety, we further equip the rational laminations with additional data on boundary intervals. Let $\mathsf{P}^\vee = \mathbb{Z}\varpi_1^\vee \oplus \mathbb{Z}\varpi_2^\vee$ be the coweight lattice of $\mathfrak{sl}_3$, and $\mathsf{P}^\vee_{\mathbb{Q}} := \mathsf{P}^\vee \otimes \mathbb{Q}$. Let us consider the direct sum

$$H_\partial(\mathbb{Q}^T) := \bigoplus_{E\in\mathbb{B}} \mathsf{P}^\vee_{\mathbb{Q}}$$

of the coweight lattices over $\mathbb{Q}$, one for each boundary interval.

Definition 4.1 (rational unbounded $\mathfrak{sl}_3$-laminations with pinnings) We introduce the space

$$\mathcal{L}^p_{\mathfrak{sl}_3}(\Sigma,\mathbb{Q}) := \mathcal{L}^x_{\mathfrak{sl}_3}(\Sigma,\mathbb{Q}) \times H_\partial(\mathbb{Q}^T),$$

and call its elements *rational unbounded $\mathfrak{sl}_3$-laminations with pinnings* (or *rational ($\mathfrak{sl}_3$-)$\mathcal{P}$-laminations*). The datum in the second factor is written as $\nu = (\nu_E)_{E\in\mathbb{B}}$ with $\nu_E = \nu_E^+\varpi_1^\vee + \nu_E^-\varpi_2^\vee$, $\nu_E^\pm \in \mathbb{Q}$.

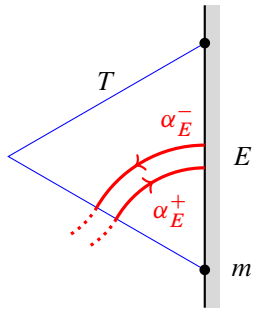

Figure 24: The corner arcs relevant to the boundary shear coordinate.

The data $\nu = (\nu_E)_E$ will be related to the pinning in the sense of Definition 3.4 when we consider their gluings, thus the terminology. We have a natural $\mathbb{Q}_{>0}$-action on $\mathcal{L}^p_{\mathfrak{sl}_3}(\Sigma, \mathbb{Q})$ given by

$$u.(\widehat{L}, \nu) := (u.\widehat{L}, (u\nu_E)_E)$$

for $u \in \mathbb{Q}_{>0}$ and $(\widehat{L}, \nu = (\nu_E)_E) \in \mathcal{L}^p_{\mathfrak{sl}_3}(\Sigma, \mathbb{Q})$. The Dynkin involution (Definition 2.8) is extended as

$$*\colon \mathcal{L}^p_{\mathfrak{sl}_3}(\Sigma, \mathbb{Q}) \to \mathcal{L}^p_{\mathfrak{sl}_3}(\Sigma, \mathbb{Q}), \quad (\widehat{L}, (\nu_E)_{E\in\mathbb{B}}) \mapsto (\widehat{L}^*, (\nu_E^*)_{E\in\mathbb{B}}), \tag{4-1}$$

where $\nu^* = (\nu_E^*)_{E\in\mathbb{B}}$ is obtained from ν by the Dynkin involution on the coweight lattice: $\varpi_s^* := \varpi_{3-s}$ for $s = 1, 2$. There is a projection

$$\pi_{\mathrm{uf}}\colon \mathcal{L}^p_{\mathfrak{sl}_3}(\Sigma, \mathbb{Q}) \to \mathcal{L}^x_{\mathfrak{sl}_3}(\Sigma, \mathbb{Q})$$

forgetting the second factor, which is equivariant under these structures. A rational $\mathcal{P}$-lamination $(\widehat{L}, \nu)$ is said to be *integral* if $\widehat{L} \in \mathcal{L}^x_{\mathfrak{sl}_3}(\Sigma, \mathbb{Z})$ and $p_E \in \mathsf{P}^\vee$ for all $E \in \mathbb{B}$.

Remark 4.2 The space $\mathcal{L}^p_{\mathfrak{sl}_3}(\Sigma, \mathbb{Q})$ is introduced as a tropical analogue of the moduli space $\mathcal{P}_{\mathrm{PGL}_3,\Sigma}$ of framed PGL_3-local systems with pinnings on Σ [21]. We have a dominant morphism $\mathcal{P}_{\mathrm{PGL}_3,\Sigma} \to \mathcal{X}_{\mathrm{PGL}_3,\Sigma}$, which is a principal $H_\partial := H^{\mathbb{B}}$-bundle over its image. Here $H \subset \mathrm{PGL}_3$ denote the Cartan subgroup. As a tropical analogue, we may naturally consider the bundle

$$0 \to H_\partial(\mathbb{Q}^T) \to \mathcal{P}_{\mathrm{PGL}_3,\Sigma}(\mathbb{Q}^T) \to \mathcal{X}_{\mathrm{PGL}_3,\Sigma}(\mathbb{Q}^T) \to 0. \tag{4-2}$$

The space $\mathcal{L}^p_{\mathfrak{sl}_3}(\Sigma, \mathbb{Q})$ is regarded as the total space $\mathcal{P}_{\mathrm{PGL}_3,\Sigma}(\mathbb{Q}^T)$ with a fixed trivialization. See also Remark 4.8 below.

Shear coordinates on $\mathcal{L}^p_{\mathfrak{sl}_3}(\Sigma, \mathbb{Q})$ Given an ideal triangulation $\triangle$ of Σ, we are going to define a shear coordinate system

$$\mathsf{x}_\triangle = (\mathsf{x}_i^\triangle)_{i\in I(\triangle)}\colon \mathcal{L}^p_{\mathfrak{sl}_3}(\Sigma, \mathbb{Q}) \to \mathbb{Q}^{I(\triangle)}$$

which extends $\mathsf{x}^{\mathrm{uf}}_\triangle$ on $\mathcal{L}^x_{\mathfrak{sl}_3}(\Sigma, \mathbb{Q})$. For $(\widehat{L}, \nu) \in \mathcal{L}^p_{\mathfrak{sl}_3}(\Sigma, \mathbb{Q})$ and an unfrozen index $i \in I_{\mathrm{uf}}(\triangle)$, let $\mathsf{x}_i^\triangle(\widehat{L}, \nu) := \mathsf{x}_i^\triangle(\widehat{L})$ be the shear coordinate of the underlying rational unbounded lamination.

We define the frozen coordinate $\mathsf{x}^\triangle_{E,s}(\widehat{L}, \nu)$ for $s = 1, 2$ associated to a boundary interval $E \in \mathbb{B}$, as follows. Let W be a nonelliptic signed $\mathbb{Q}_{>0}$-weighted web without peripheral components representing $\widehat{L}$,

and $\mathcal{W}$ its spiraling diagram in a good position with respect to the split triangulation $\widehat{\triangle}$. By convention, E is endowed with the orientation induced from $\partial\Sigma$. Then $\mathrm{x}^{\triangle}_{E,1}$ (resp. $\mathrm{x}^{\triangle}_{E,2}$) is assigned to the vertex of the $\mathfrak{sl}_3$-triangulation on E closer to the initial (resp. terminal) endpoint. Let $m \in \mathbb{M}_\partial$ be the initial endpoint of E, and $T \in t(\triangle)$ the unique triangle having E as an edge. Let $\alpha^+_E(\widehat{L})$ (resp. $\alpha^-_E(\widehat{L})$) be the total weight of the oriented corner arcs in $\mathcal{W} \cap T$ bounding the special point m in the clockwise (resp. counterclockwise) direction, hence incoming to (resp. outgoing from) the external biangle B_E if we consider the split triangulation $\widehat{\triangle}$. See Figure 24. Then we define

$$\begin{aligned} \mathrm{x}^{\triangle}_{E,1}(\widehat{L}, \nu) &:= \nu^+_E - \alpha^+_E(\widehat{L}), \\ \mathrm{x}^{\triangle}_{E,2}(\widehat{L}, \nu) &:= \nu^-_E - \alpha^-_E(\widehat{L}) - [\mathrm{x}_T(\widehat{L})]_+. \end{aligned} \tag{4-3}$$

Proposition 4.3 *The shear coordinate system gives a bijection $\mathrm{x}_{\triangle}\colon \mathcal{L}^p_{\mathfrak{sl}_3}(\Sigma, \mathbb{Q}) \xrightarrow{\sim} \mathbb{Q}^{I(\triangle)}$.*

Proof Given $(\mathrm{x}_i)_{i \in I(\triangle)} \in \mathbb{Q}^{I(\triangle)}$, we can reconstruct the underlying rational unbounded lamination $\widehat{L}$ from the unfrozen part $(\mathrm{x}_i)_{i \in I(\triangle)_{\mathrm{uf}}}$ as in Section 3.4. Then the datum ν is uniquely determined by the relation (4-3). □

The following is immediate from the definition:

Lemma 4.4 *The map $\pi_{\mathrm{uf}}\colon \mathcal{L}^p_{\mathfrak{sl}_3}(\Sigma, \mathbb{Q}) \to \mathcal{L}^x_{\mathfrak{sl}_3}(\Sigma, \mathbb{Q})$ is a **cluster projection**. Namely, we have a commutative diagram*

$$\begin{array}{ccc} \mathcal{L}^p_{\mathfrak{sl}_3}(\Sigma, \mathbb{Q}) & \xrightarrow{\mathrm{x}_{\triangle}} & \mathbb{Q}^{I(\triangle)} \\ \downarrow{\scriptstyle \pi_{\mathrm{uf}}} & & \downarrow \\ \mathcal{L}^x_{\mathfrak{sl}_3}(\Sigma, \mathbb{Q}) & \xrightarrow[\mathrm{x}^{\mathrm{uf}}_{\triangle}]{} & \mathbb{Q}^{I_{\mathrm{uf}}(\triangle)} \end{array}$$

for any ideal triangulation $\triangle$ of Σ, where the right vertical map is the projection forgetting the frozen coordinates.

4.2 Gluing of laminations

Let Σ be a (possibly disconnected) marked surface, and $E_L, E_R \in B(\Sigma)$ distinct boundary intervals. Then we can form a new marked surface Σ' from Σ by gluing E_L with E_R. As a tropical analogue of the gluing morphism $\mathcal{P}_{\mathrm{PGL}_3,\Sigma} \to \mathcal{P}_{\mathrm{PGL}_3,\Sigma'}$ [21, Lemma 2.14], we are going to introduce a map

$$q_{E_L,E_R}\colon \mathcal{L}^p_{\mathfrak{sl}_3}(\Sigma, \mathbb{Q}) \to \mathcal{L}^p_{\mathfrak{sl}_3}(\Sigma', \mathbb{Q})$$

between the corresponding spaces of rational $\mathcal{P}$-laminations. The map q_{E_L,E_R} will be defined to be equivariant with respect to the $\mathbb{Q}_{>0}$-action, and invariant under the action $\alpha_{E_L,E_R}\colon \mathsf{P}^\vee_{\mathbb{Q}} \curvearrowright \mathcal{L}^p_{\mathfrak{sl}_3}(\Sigma, \mathbb{Q})$ given by the shift

$$\mu.(\nu_{E_L}, \nu_{E_R}) := (\nu_{E_L} + \mu, \nu_{E_R} - \mu^*) \tag{4-4}$$

for $\mu = a\varpi_1^\vee + b\varpi_2^\vee \in \mathsf{P}^\vee_{\mathbb{Q}}$, where $\mu^* := b\varpi_1^\vee + a\varpi_2^\vee$, and keeping other ν_E, $E \neq E_L, E_R$ intact.

Let $(\widehat{L}, \nu) \in \mathcal{L}^p_{\mathfrak{sl}_3}(\Sigma, \mathbb{Z})$ be an integral $\mathcal{P}$-lamination. Represent the integral unbounded $\mathfrak{sl}_3$-lamination $\widehat{L}$ by a nonelliptic signed web W with weight 1 on every component. Around each special point of E_L and E_R, draw a semi-infinite collection of disjoint corner arcs with alternating orientations that accumulates only at the special point so that they are disjoint from W. Here we choose the orientation of the farthest corner arc from the special point to be clockwise, as in Section 3.4. Insert a biangle B between E_L and E_R, and identify $\Sigma' = \Sigma \cup B$. Notice that the ends of W on E_L and E_R, together with those of the additional corner arcs, defines an asymptotically periodic symmetric strand set $S = (S_L, S_R)$ on B. We equip S with a pinning $\mathsf{p}^{\pm}_Z$ for $Z \in \{L, R\}$ by the following rule:

- Choose continuous parametrizations $\psi^{\pm}_Z : \mathbb{R} \to E_Z$ so that $\psi^{\pm}_Z\left(\frac{1}{2} + \mathbb{Z}\right) = S^{\pm}_Z$, and $\psi^{\pm}_Z(\mathbb{R}_{<0}) \cap S^{\pm}_Z$ consists of all the strands coming from the additional corner arcs around the initial marked point of E_Z.
- Then set $p^{\pm}_Z := \psi^{\pm}_Z(\nu^{\pm}_{E_Z}) \in E_Z$.

Then we get a pinned symmetric strand set $\widehat{S} := (S; \mathsf{p}_L, \mathsf{p}_R)$ on the biangle B. Let $W_{\mathrm{br}}(\widehat{S})$ be the associated collection of oriented curves in B. Gluing the web W with the collection $W_{\mathrm{br}}(\widehat{S})$, we get an infinite collection $\mathcal{W}'_{\mathrm{br}}$ of webs on $\Sigma' = \Sigma \cup B$. The initial (resp. terminal) marked point of E_L is identified with the terminal (resp. initial) marked point of E_R, and regarded as new marked points in Σ'. For each of these new marked points, do the following:

- If it is a special point, then remove the peripheral components around this point from $\mathcal{W}'_{\mathrm{br}}$.
- If it is a puncture, then remove the peripheral components and replace each spiraling end around this point with a signed end, while encoding the spiraling directions in signs by reversing the rule in Figure 10. Then there remain at most finitely many intersections in B.
- Finally, replace each intersection of curves in B with an H-web by the rule (3-1).

Thus we get a nonelliptic signed web W' on Σ', which represents an integral $\mathcal{P}$-lamination

$$\widehat{L}' = q_{E_L, E_R}(\widehat{L}) \in \mathcal{L}^p_{\mathfrak{sl}_3}(\Sigma, \mathbb{Z}).$$

The construction is clearly invariant for the action of $H_\partial(\mathbb{Q}^T)$ by Remark 3.16, and $\mathbb{Z}_{>0}$-equivariant. Thus it can be extended $\mathbb{Q}_{>0}$-equivariantly.

Definition 4.5 The thus obtained map $q_{E_L, E_R} : \mathcal{L}^p_{\mathfrak{sl}_3}(\Sigma, \mathbb{Q}) \to \mathcal{L}^p_{\mathfrak{sl}_3}(\Sigma', \mathbb{Q})$ is called the *gluing map* along E_L and E_R.

In view of Remark 3.16, we immediately have:

Lemma 4.6 *The gluing map q_{E_L, E_R} is invariant under the shift action (4-4) of $\mathsf{P}^\vee_{\mathbb{Q}}$.*

Any ideal triangulation $\triangle$ of Σ naturally induces a triangulation $\triangle'$ of Σ', where the edges E_L and E_R are identified and give an interior edge E of $\triangle$. The points in $I(\triangle)$ on these edges are identified as $i^s(E_L) = i^{s^*}(E_R)$ for $s = 1, 2$ with $s^* := 3 - s$. The points of $I(\triangle)$ away from the edges E_L and E_R are naturally identified with the corresponding points of $I(\triangle')$.

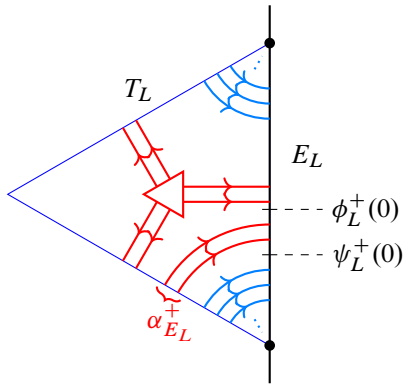

Figure 25: Comparison of two edge parametrizations. A part of the web representing $\widehat{L}$ which will be incoming to the bigon B_E is shown in red, and the additional corner arcs are shown in blue.

Theorem 4.7 *The gluing map q_{E_L,E_R} is the **tropicalized amalgamation**. Namely, for any ideal triangulation $\triangle$ of Σ and the induced triangulation $\triangle'$ of Σ', it satisfies*

$$q_{E_L,E_R}^* \mathrm{x}_{E,s}^{\triangle'} = \mathrm{x}_{E_L,s}^{\triangle} + \mathrm{x}_{E_R,s^*}^{\triangle}$$

for $s = 1, 2$. Here E inherits an orientation from E_L (so that from the bottom to the top, when we draw E_L on the left). The other coordinates are kept intact: $q_{E_L,E_R}^* \mathrm{x}_i^{\triangle'} = \mathrm{x}_i^{\triangle}$ for $i \in I(\triangle') \setminus \{i^s(E)\}_{s=1,2}$.

Proof The last statement is clear from the definition. To see the relation between the coordinates on the edges E_L, E_R and E, it suffices to consider an integral lamination $\widehat{L} \in \mathcal{L}^p_{\mathfrak{sl}_3}(\Sigma, \mathbb{Z})$ by $\mathbb{Q}_{>0}$-equivariance. Write $L' := q_{E_L,E_R}(\widehat{L})$ and $\mathrm{x}_i := \mathrm{x}_i^{\triangle}(\widehat{L})$ for $i \in I(\triangle)$. Recall the reconstruction procedure of the integral lamination $\widehat{L}'$ from its shear coordinates, and compare the gluing parameters

$$\begin{aligned} \nu^+_{E_L} &= \mathrm{x}_{E_L,1} + \alpha^+_{E_L}, & \nu^-_{E_R} &= \mathrm{x}_{E_R,2} + [\mathrm{x}_{T_R}]_+ + \alpha^-_{E_R}, \\ \nu^-_{E_L} &= \mathrm{x}_{E_L,2} + [\mathrm{x}_{T_L}]_+ + \alpha^-_{E_L}, & \nu^+_{E_R} &= \mathrm{x}_{E_R,1} + \alpha^+_{E_R}, \end{aligned} \tag{4-5}$$

with the integers appearing in (3-2). By Lemma 4.6, the result of gluing is unchanged under the modification

$$\begin{aligned} \tilde{\nu}^+_{E_L} &:= (\mathrm{x}_{E_L,1} + \mathrm{x}_{E_R,2}) + \alpha^+_{E_L}, & \tilde{\nu}^-_{E_R} &:= [\mathrm{x}_{T_R}]_+ + \alpha^-_{E_R}, \\ \tilde{\nu}^-_{E_L} &:= [\mathrm{x}_{T_L}]_+ + \alpha^-_{E_L}, & \tilde{\nu}^+_{E_R} &:= (\mathrm{x}_{E_L,2} + \mathrm{x}_{E_R,1}) + \alpha^+_{E_R} \end{aligned} \tag{4-6}$$

by the shift action (4-4). On the other hand, since there are "original" corner arcs of $\widehat{L}$ in T_L and T_R before adding infinite collections of corner arcs in the gluing procedure, the parametrizations of edges are related by

$$\phi^{\pm}_Z(n) = \psi^{\pm}_Z(n + \alpha^{\pm}_{E_Z})$$

for $n \in \mathbb{Z}$ and $Z \in \{L, R\}$. See Figure 25. These comparisons on the two gluing constructions show that $\widehat{L}' = q_{E_L,E_R}(\widehat{L})$ if and only if $\mathrm{x}_{E,s}(\widehat{L}') = \mathrm{x}_{E_L,s}(\widehat{L}) + \mathrm{x}_{E_R,s^*}(\widehat{L})$ for $s = 1, 2$. □

Remark 4.8 In view of the gluing construction presented above, the definition of the integral unbounded $\mathfrak{sl}_3$-laminations with pinnings can be modified slightly more geometrically as integral unbounded $\mathfrak{sl}_3$-laminations equipped with infinitely many corner arcs around special points and choices of points $p_E^{\pm} \in E$ for each $E \in \mathbb{B}$, in place of the datum $\nu_E \in \mathsf{P}^\vee$. It gives a right description of the tropical analogue of $\mathcal{P}_{\mathrm{PGL}_3,\Sigma}(\mathbb{Z}^T)$ without fixing a trivialization of the bundle (4-2). We do not pursue an extension of this description to the rational case.

4.3 Extended ensemble map

Recall the geometric ensemble map (2-9). We extend it by

$$\tilde{p}\colon \mathcal{L}^a_{\mathfrak{sl}_3}(\Sigma,\mathbb{Q}) \to \mathcal{L}^p_{\mathfrak{sl}_3}(\Sigma,\mathbb{Q}), \quad L \mapsto (p(L),(\nu_E)_E),$$

where ν_E^+ (resp. ν_E^-) is minus the total weight of the peripheral components with the clockwise (resp. counterclockwise) orientation around the initial marked point of E. We have a commutative diagram

$$\begin{array}{ccc} \mathcal{L}^a_{\mathfrak{sl}_3}(\Sigma,\mathbb{Q}) & \xrightarrow{\tilde{p}} & \mathcal{L}^p_{\mathfrak{sl}_3}(\Sigma,\mathbb{Q}) \\ & \searrow^{p} & \downarrow{\scriptstyle \pi_{\mathrm{uf}}} \\ & & \mathcal{L}^x_{\mathfrak{sl}_3}(\Sigma,\mathbb{Q}) \end{array}$$

Lemma 4.9 *If Σ has no punctures, then $\tilde{p}\colon \mathcal{L}^a_{\mathfrak{sl}_3}(\Sigma,\mathbb{Q}) \to \mathcal{L}^p_{\mathfrak{sl}_3}(\Sigma,\mathbb{Q})$ gives a bijection.*

Proof In this case, the only datum that the map p loses is the weights of peripheral components around special points. This can be uniquely recovered from the tuple $(\nu_E)_E$. □

On the integral points, we have $\tilde{p}(\mathcal{L}^a_{\mathfrak{sl}_3}(\Sigma,\mathbb{Z})) \subset \mathcal{L}^p_{\mathfrak{sl}_3}(\Sigma,\mathbb{Z})$.

Proposition 4.10 *The extended geometric ensemble map $\tilde{p}\colon \mathcal{L}^a_{\mathfrak{sl}_3}(\Sigma,\mathbb{Q}) \to \mathcal{L}^p_{\mathfrak{sl}_3}(\Sigma,\mathbb{Q})$ coincides with the Goncharov–Shen extension of the ensemble map (A-6). Namely, it satisfies*

$$\tilde{p}^* \mathsf{x}_i^{\triangle} = \sum_{j \in I(\triangle)} (\varepsilon_{ij}^{\triangle} + m_{ij}) \mathsf{a}_j^{\triangle} \tag{4-7}$$

for any ideal triangulation $\triangle$ of Σ and $i \in I(\triangle)$, where

- *$(\mathsf{a}_j^{\triangle})_{j\in I(\triangle)}$ denotes the tropical $\mathcal{A}$-coordinates on $\mathcal{L}^a_{\mathfrak{sl}_3}(\Sigma,\mathbb{Q})$ associated with $\triangle$, which is one-third of the Douglas–Sun coordinates;*
- *$\varepsilon^{\triangle} = (\varepsilon_{ij}^{\triangle})_{i,j\in I(\triangle)}$ denotes the exchange matrix defined in Section A.3;*
- *$M = (m_{ij})_{i,j\in I_{\mathrm{f}}(\triangle)}$ is the half-integral symmetric matrix given in (A-5).*

In particular, by forgetting the pinnings and frozen coordinates, we see that the geometric ensemble map $p\colon \mathcal{L}^a_{\mathfrak{sl}_3}(\Sigma,\mathbb{Q}) \to \mathcal{L}^x_{\mathfrak{sl}_3}(\Sigma,\mathbb{Q})$ coincides with the ensemble map (A-2).

Proof In view of the local nature of the definitions of coordinate systems and the exchange matrix, it suffices to consider the case where Σ is a triangle or a quadrilateral. Indeed, for $i = i(T) \in I^{\mathrm{tri}}(\triangle)$, it suffices to focus on the triangle T containing it; for $i = i^s(E) \in I^{\mathrm{edge}}(\triangle) \cap I_{\mathrm{uf}}(\triangle)$ consider the quadrilateral containing the interior edge E as a diagonal; for $i = i^s(E) \in I^{\mathrm{edge}}(\triangle) \cap I_{\mathrm{f}}(\triangle)$ consider the triangle T having the boundary interval E as one of its sides.

Triangle case For the $\mathfrak{sl}_3$-quiver associated with the unique ideal triangulation of a triangle T, label its vertices as:

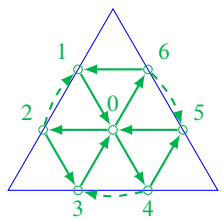

Then the expected relation (4-7) reads as

$$\begin{aligned}
\tilde{p}^* x_0 &= a_2 + a_4 + a_6 - (a_1 + a_3 + a_5),\\
\tilde{p}^* x_1 &= a_0 - a_1 - a_6,\\
\tilde{p}^* x_2 &= a_1 + a_3 - a_2 - a_0,\\
\tilde{p}^* x_3 &= a_0 - a_3 - a_2,\\
\tilde{p}^* x_4 &= a_3 + a_5 - a_4 - a_0,\\
\tilde{p}^* x_5 &= a_0 - a_5 - a_4,\\
\tilde{p}^* x_6 &= a_5 + a_1 - a_6 - a_0.
\end{aligned}$$

The tropical $\mathcal{A}$-coordinates of essential webs on T are defined as the weighted sum of the coordinates of its components. See [6, Section 4.3]. Therefore it suffices to check the relations for the corner arcs and the sink-/source-honeycombs of height 1, whose coordinates are shown in Figure 26. Then the relations between the two coordinates can be easily verified.

Quadrilateral case For the $\mathfrak{sl}_3$-quiver associated with an ideal triangulation $\triangle$ of a quadrilateral Q, label its vertices as:

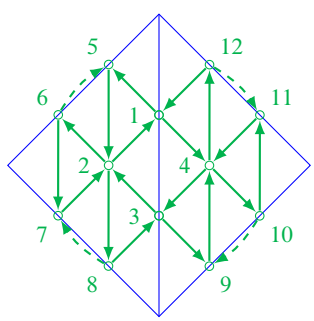

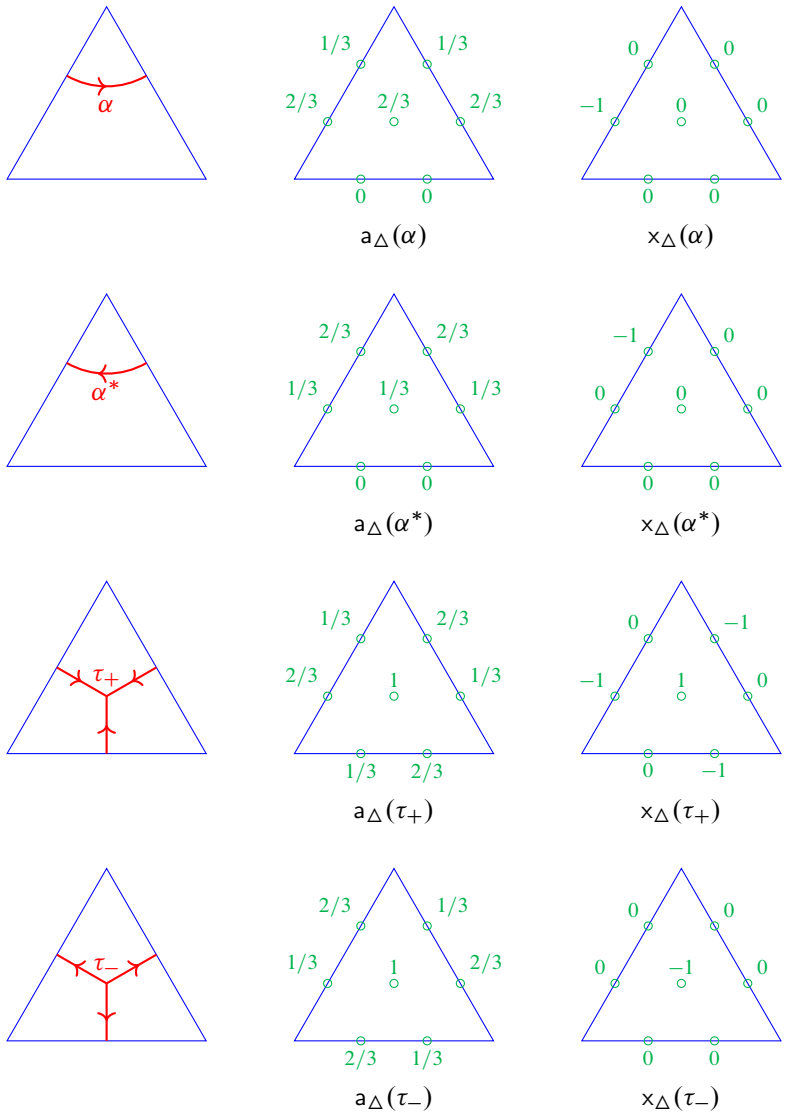

Figure 26: Two types of coordinates of component webs on a triangle T. All the webs shown here have weight 1.

The remaining relations to be checked are

$$\begin{aligned}\tilde{p}^*\mathsf{x}_1 &= \mathsf{a}_5 + \mathsf{a}_4 - \mathsf{a}_2 - \mathsf{a}_{12},\\ \tilde{p}^*\mathsf{x}_3 &= \mathsf{a}_2 + \mathsf{a}_9 - \mathsf{a}_4 - \mathsf{a}_8.\end{aligned} \tag{4-8}$$

The tropical $\mathcal{A}$-coordinate assigned to a vertex $i \in I(\triangle)$ only depends on the restriction of a given web to the triangle which contains i. In particular, we can choose the braid representative with respect to $\widehat{\triangle}$ for the computation, since the biangle part does not matter. Then both $\mathcal{A}$- and $\mathcal{X}$-coordinates are weighted sums of contributions from the components of the braid representative. It is easy to verify that the both sides of the

equations in (4-8) vanish for the corner arcs around the marked points Q. For the curve and honeycomb components that contribute to the shear coordinates, the expected relations are easily verified from Figures 27 and 28. Here notice that, for instance, the coordinates of the honeycomb component H_{n_1,n_2,n_3} shown in the top of Figure 15 can be computed as $\mathtt{z}_\triangle(H_{n_1,n_2,n_3}) = n_1\mathtt{z}_\triangle(\tau_+^L) + n_2\mathtt{z}_\triangle(h) + n_3\mathtt{z}_\triangle(\tau_+^R)$ for $\mathtt{z} \in \{\mathtt{a}, \mathtt{x}\}$. Together with this observation, the eight patterns shown in Figures 27 and 28 exhausts all the patterns up to symmetry. □

The following states an extension of Theorem 3.20 with pinnings/frozen variables, as promised before.

Theorem 4.11 *For any two ideal triangulations $\triangle$ and $\triangle'$ of Σ, the coordinate transformation*

$$\mathtt{x}_{\triangle,\triangle'} := \mathtt{x}_{\triangle'} \circ \mathtt{x}_\triangle^{-1} : \mathbb{Q}^{I(\triangle)} \to \mathbb{Q}^{I(\triangle)}$$

is a composite of tropical cluster Poisson transformations. In particular, we get an $\mathrm{MC}(\Sigma)$-equivariant identification $\mathtt{x}_\bullet : \mathcal{L}^p_{\mathfrak{sl}_3}(\Sigma,\mathbb{Q}) \xrightarrow{\sim} \mathcal{X}_{\mathfrak{sl}_3,\Sigma}(\mathbb{Q}^T)$.

As a corollary, combining with Lemma 4.4, we get a proof of Theorem 3.20.

Proof From Lemma 4.9 and Proposition 4.10, the statement is true when Σ has no puncture (in particular, a quadrilateral). Indeed, the corresponding transformation $\mathtt{a}_{\triangle,\triangle'} := \mathtt{a}_{\triangle'} \circ \mathtt{a}_\triangle^{-1} : \mathbb{Q}^{I(\triangle)} \to \mathbb{Q}^{I(\triangle)}$ is shown to be a composite of tropical cluster $\mathcal{A}$-transformations [7, Proposition 4.2]. Then $\mathtt{x}_{\triangle,\triangle'} = (\tilde{p}^{-1})^* \circ \mathtt{a}_{\triangle,\triangle'} \circ \tilde{p}^*$ is the corresponding composite of tropical cluster $\mathcal{X}$-transformations, since the extended ensemble map commutes with the tropical cluster transformations and is a bijection in this case.

For the general case, it suffices to consider two triangulations, $\triangle$ and $\triangle'$, related by a single flip along an edge $E \in e_{\mathrm{int}}(\triangle)$. Let Q be the unique quadrilateral in $\triangle$ containing E as a diagonal, and $\Sigma' := \Sigma \setminus \operatorname{int} Q$ the complement marked surface. It is obvious that the shear coordinates assigned to the vertices outside Q are unchanged. On the other hand, the coordinates assigned to the vertices on Q transform correctly from the argument above under the corresponding coordinate transformation on $\mathcal{L}^p_{\mathfrak{sl}_3}(Q,\mathbb{Q})$. Since Σ is obtained by gluing Q with Σ' and the shear coordinates are obtained by amalgamating those on $\mathcal{L}^p_{\mathfrak{sl}_3}(Q,\mathbb{Q})$ and $\mathcal{L}^p_{\mathfrak{sl}_3}(\Sigma',\mathbb{Q})$ by Theorem 4.7; the statement follows from the fact that the amalgamations commute with cluster $\mathcal{X}$-transformations [9, Lemma 2.2]. □

Remark 4.12 For an unpunctured surface Σ, the fastest way to introduce the coordinate system $\mathtt{x}_\triangle$ on $\mathcal{L}^p_{\mathfrak{sl}_3}(\Sigma,\mathbb{Q})$ which transforms correctly under the flips would be to define it via the relation (4-7) in view of Lemma 4.9. Then, however, it becomes rather difficult to obtain the amalgamation formula in Theorem 4.7, since the (tropical) $\mathcal{A}$-coordinates do not behave so simply as the (tropical) $\mathcal{X}$-coordinates under the gluing. Indeed, the following naive diagram does not commute:

$$\begin{array}{ccc} \mathcal{A}_{\mathfrak{sl}_3,\Sigma}(\mathbb{Q}^T) & \longrightarrow & \mathcal{A}_{\mathfrak{sl}_3,\Sigma'}(\mathbb{Q}^T) \\ \downarrow{\scriptstyle \tilde{p}_\Sigma} & & \downarrow{\scriptstyle \tilde{p}_{\Sigma'}} \\ \mathcal{X}_{\mathfrak{sl}_3,\Sigma}(\mathbb{Q}^T) & \xrightarrow[q_{E_L,E_R}]{} & \mathcal{X}_{\mathfrak{sl}_3,\Sigma'}(\mathbb{Q}^T). \end{array}$$

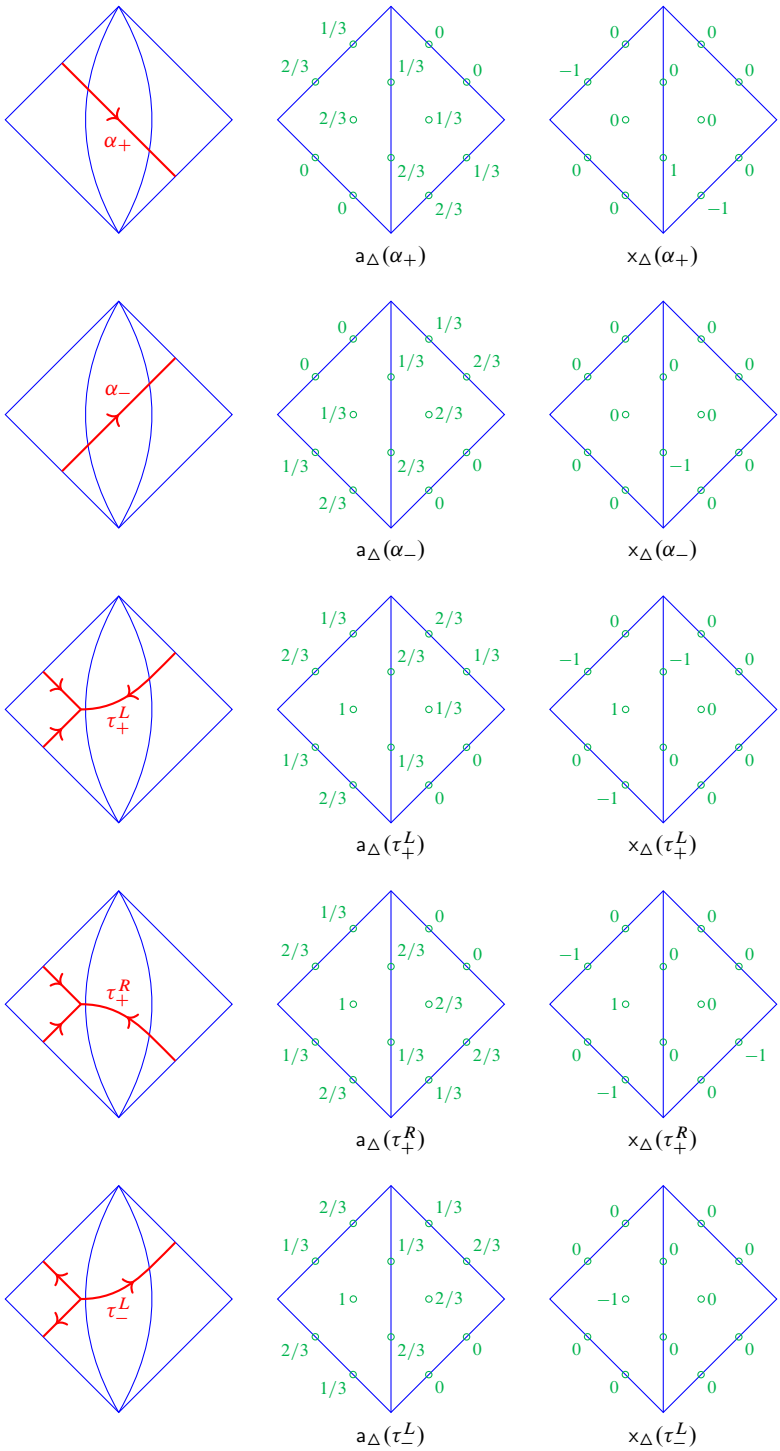

Figure 27: Two types of coordinates of component webs on a quadrilateral Q. All the webs shown here have weight 1. (Continued in Figure 28.)

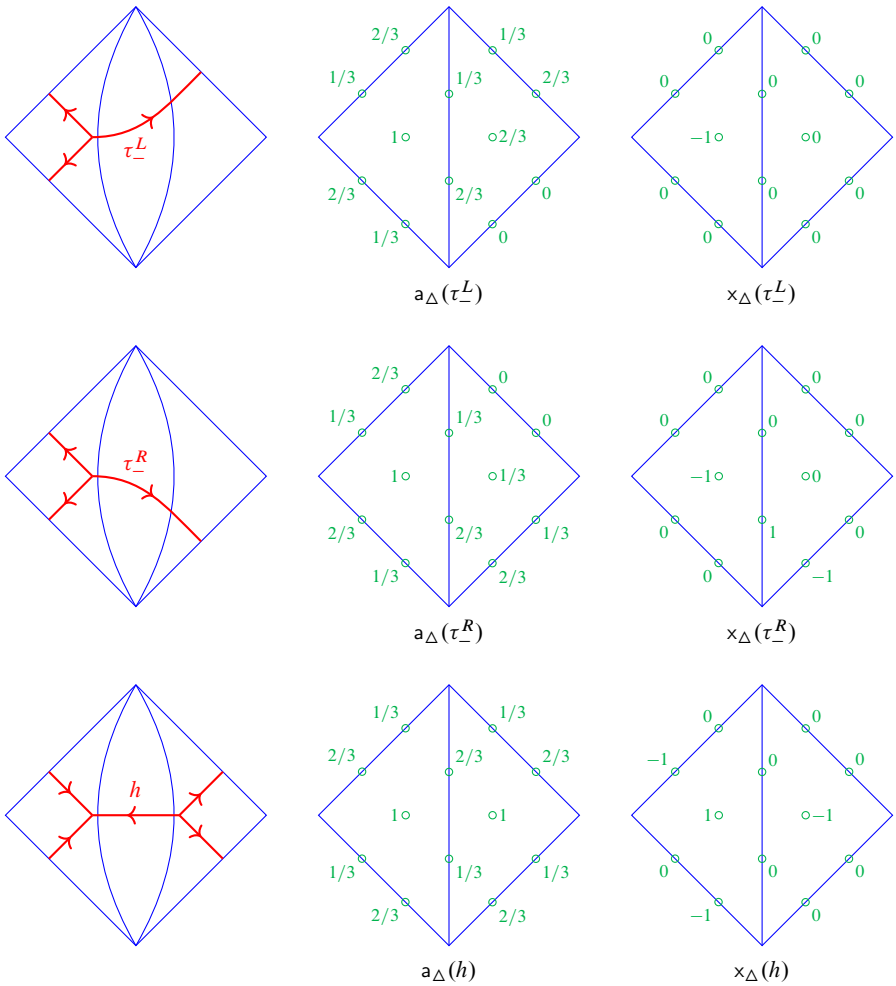

Figure 28: Two types of coordinates of component webs on a quadrilateral Q. All the webs shown here have weight 1. (Continued from Figure 27.)

Here the top right arrow denotes the quotient map given by the equation $\mathsf{a}_i = \mathsf{a}_j$ for any pair $\{i, j\}$ of quiver vertices that are identified under the gluing. Actually, we need to "rescale" some of the $\mathcal{A}$-coordinates for a correct gluing; see [29, Section 6.1] for a more detail. In particular, the sum $\tilde{p}^*_\Sigma \mathsf{x}_i^\triangle + \tilde{p}^*_\Sigma \mathsf{x}_j^\triangle$ does not compute $\tilde{p}^*_{\Sigma'} \mathsf{x}_{\bar{i}}^{\triangle'}$, where the pair $\{i, j\}$ is amalgamated into $\bar{i}$.

4.4 Dynkin involution

Let us discuss the equivariance of the shear coordinates under the Dynkin involution (4-1). The *cluster action* $*_\triangle$ (see the last paragraph of the appendix) of the Dynkin involution in the cluster chart associated to $\triangle$ is given by the mutation sequence

$$\mu_\gamma = \sigma_{e(\triangle)} \circ \mu_{t(\triangle)},$$

where $\sigma_{e(\triangle)}$ denotes the composite of the transpositions of the labels of the two vertices on each edge of $\triangle$, and $\mu_{t(\triangle)}$ is the composite of mutations at the vertex on each triangle of $\triangle$. It induces the tropical cluster $\mathcal{X}$-transformation

$$\begin{aligned} *^{x}_{\triangle} : x_T &\mapsto -x_T && \text{for } T \in t(\triangle), \\ x_{E,1} &\mapsto x_{E,2} + [x_{T_L}]_+ - [-x_{T_R}]_+, \\ x_{E,2} &\mapsto x_{E,1} + [x_{T_R}]_+ - [-x_{T_L}]_+ && \text{for } E \in e(\triangle), \end{aligned}$$

where we use the local labeling as in Section 3.4 for each edge E.

Proposition 4.13 *We have the commutative diagram*

$$\begin{array}{ccc} \mathcal{L}^{p}_{\mathfrak{sl}_3}(\Sigma,\mathbb{Q}) & \xrightarrow{x_\triangle} & \mathbb{Q}^{I(\Delta)} \\ \downarrow{\scriptstyle *} & & \downarrow{\scriptstyle *_\triangle} \\ \mathcal{L}^{p}_{\mathfrak{sl}_3}(\Sigma,\mathbb{Q}) & \xrightarrow[x_\triangle]{} & \mathbb{Q}^{I(\Delta)}. \end{array}$$

In particular, the orientation-reversing action of the Dynkin involution coincides with the cluster action.

Proof Mutations commute with amalgamations [9, Lemma 2.2]. Moreover, the permutation term $\sigma_{e(\triangle)}$ also commutes with the amalgamation of edge vertices corresponding to the gluing. Hence $*_\triangle$ commutes with the gluing map. It is also clear from the definitions that the Dynkin involution (4-1) commutes with gluing maps. Therefore it suffices to prove the statement for triangles.

It is easy to verify the equation

$$*_\triangle \circ x_\triangle(W) = x_\triangle(W^*) \tag{4-9}$$

for each component web W shown in Figure 26 by inspection. Consider a disjoint union $W = W_1 \sqcup W_2$ of webs on a triangle T, and suppose that the (4-9) is true for $W = W_1, W_2$. Since sink/source honeycombs cannot coexist, we have $\{\operatorname{sgn} x_T(W_1), \operatorname{sgn} x_T(W_2)\} \neq \{+,-\}$. Therefore the coordinate vectors $x_\triangle(W_1)$ and $x_\triangle(W_2)$ belong to the same cone on which the tropical cluster transformation $*_\triangle$ is linear. Hence,

$$\begin{aligned} *_\triangle \circ x_\triangle(W) &= *_\triangle(x_\triangle(W_1) + x_\triangle(W_1)) \\ &= *_\triangle \circ x_\triangle(W_1) + *_\triangle \circ x_\triangle(W_2) = x_\triangle(W_1^*) + x_\triangle(W_2^*) = x_\triangle(W^*). \end{aligned}$$

□

5 A relation to the graphical basis and quantum duality map

Let Σ be a marked surface without punctures. Recall from [30] the skein algebra $\mathcal{S}^{q}_{\mathfrak{sl}_3,\Sigma}$, which is a noncommutative algebra over $\mathbb{Z}_q := \mathbb{Z}[q^{\pm 1/2}]$ consisting of tangled trivalent graphs in Σ with endpoints in $\mathbb{M}$, subject to the $\mathfrak{sl}_3$-skein relations

(5-1)

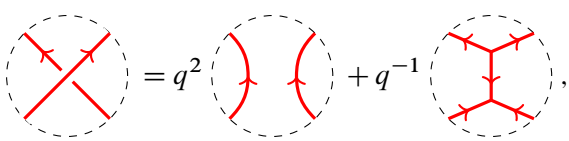

(5-2)

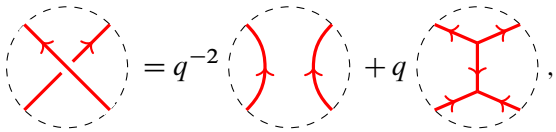

(5-3)

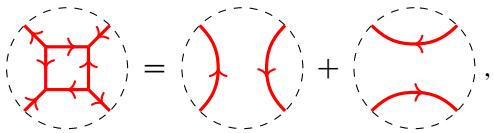

(5-4)

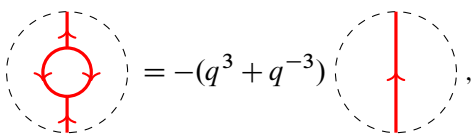

(5-5)

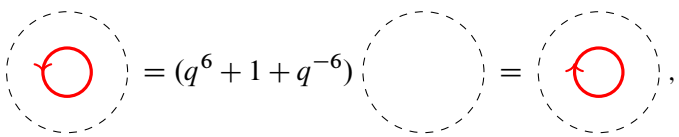

and the boundary skein relations

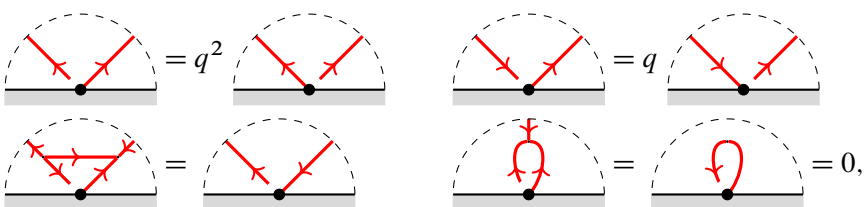

together with their Dynkin involutions. We included the square-root parameter $q^{1/2}$ so that we can consider the *simultaneous crossing* (or the *Weyl normalization*) as

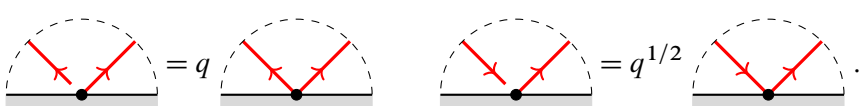

It is proved in [30] that the localized skein algebra $\mathcal{S}^q_{\mathfrak{sl}_3,\Sigma}[\partial^{-1}]$ along the oriented arcs parallel to boundary intervals is contained in the quantum cluster algebra [3] $\mathcal{A}^q_{\mathfrak{sl}_3,\Sigma}$ associated with a certain choice of compatibility pairs over the mutation class $\mathfrak{s}(\mathfrak{sl}_3,\Sigma)$ At least in the classical limit $q=1$, we have the equalities [29]

$$\mathcal{S}^1_{\mathfrak{sl}_3,\Sigma}[\partial^{-1}] = \mathcal{A}_{\mathfrak{sl}_3,\Sigma} = \mathcal{O}(\mathcal{A}_{\mathfrak{sl}_3,\Sigma}). \tag{5-6}$$

The skein algebra $\mathcal{S}^q_{\mathfrak{sl}_3,\Sigma}$ has a natural $\mathbb{Z}_q$-basis $\mathsf{BWeb}_{\mathfrak{sl}_3,\Sigma}$ consisting of *nonelliptic flat trivalent graphs*. Here a flat trivalent graph is an immersed oriented uni-trivalent graph on Σ such that each univalent vertex lies in $\mathbb{M}$, and the other part is embedded into $\operatorname{int}\Sigma$. In particular, it is required to have simultaneous crossings at each special point. It is said to be nonelliptic if it has none of the following *elliptic faces*:

(5-7)

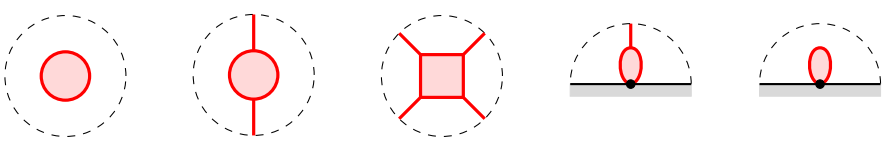

Elements of $\mathsf{BWeb}_{\mathfrak{sl}_3,\Sigma}$ are also called the *basis webs*. We are going to relate the integral $\mathfrak{sl}_3$-laminations with pinnings to the basis webs.

Definition 5.1 (negative $\mathbb{M}$-shifting of webs (cf "moving left" in [36, Figure 2])) Given a web W on Σ in the sense of Section 2.2, let $W^{\mathbb{M}} \in \mathcal{S}^q_{\mathfrak{sl}_3,\Sigma}$ be the flat trivalent graph obtained by shifting the endpoints of W to the nearest special point in the negative direction along the boundary (with respect to the orientation induced from Σ), and taking the simultaneous crossing. See Figure 30.

For an integral $\mathfrak{sl}_3$-lamination with pinnings $(\widehat{L}, \nu) \in \mathcal{L}^p_{\mathfrak{sl}_3}(\Sigma, \mathbb{Z})$, represent $\widehat{L}$ by a nonelliptic $\mathfrak{sl}_3$-web W only with components with weight one, and define

$$\mathbb{I}^q_{\mathcal{X}}(\widehat{L}) := \left[W^{\mathbb{M}} \cdot \prod_{E \in \mathbb{B}} (e^+_E)^{\nu^+_E} (e^-_E)^{\nu^-_E} \right] \in \mathcal{S}^q_{\mathfrak{sl}_3,\Sigma}[\partial^{-1}].$$

Here $\nu_E = \nu^+_E \varpi_1^\vee + \nu^-_E \varpi_2^\vee \in \mathsf{P}^\vee$ for each $E \in \mathbb{B}$, and the symbol $[-]$ stands for the Weyl normalization. Then $\mathbb{I}^q_{\mathcal{X}}(\widehat{L})$ does not depend on the choice of the representative W, since the loop parallel-move is also realized in the skein algebra (by using the Reidemeister II move twice), and the boundary H-move exactly corresponds to the third boundary skein relation. Moreover, it is a basis web since the two notions of elliptic faces correspond to each other via the shift of endpoints.

Note that $\mathbb{I}^q_{\mathcal{X}}(\widehat{L}) \in \mathcal{S}^q_{\mathfrak{sl}_3,\Sigma}$ if and only if $\nu_E \in \mathsf{P}^\vee_+ := \mathbb{Z}_+ \varpi_1^\vee + \mathbb{Z}_+ \varpi_2^\vee$ for all $E \in \mathbb{B}$. In this case, we say that $(\widehat{L}, (\nu_E)) \in \mathcal{L}^p_{\mathfrak{sl}_3}(\Sigma, \mathbb{Z})$ is *dominant*. Let $\mathcal{L}^p_{\mathfrak{sl}_3}(\Sigma, \mathbb{Z})_+ \subset \mathcal{L}^p_{\mathfrak{sl}_3}(\Sigma, \mathbb{Z})$ denote the subspace of dominant integral $\mathfrak{sl}_3$-laminations. From the above discussion, we get:

Theorem 5.2 *Assume that Σ has no punctures. Then we have an $\mathrm{MC}(\Sigma)\times\mathrm{Out}(\mathrm{SL}_3)$-equivariant bijection*

$$\mathbb{I}^q_{\mathcal{X}} \colon \mathcal{L}^p_{\mathfrak{sl}_3}(\Sigma, \mathbb{Z})_+ \xrightarrow{\sim} \mathsf{BWeb}_{\mathfrak{sl}_3,\Sigma} \subset \mathcal{S}^q_{\mathfrak{sl}_3,\Sigma}.$$

Moreover, it is extended to a map $\mathbb{I}^q_{\mathcal{X}} \colon \mathcal{L}^p_{\mathfrak{sl}_3}(\Sigma, \mathbb{Z}) \hookrightarrow \mathcal{S}^q_{\mathfrak{sl}_3,\Sigma}[\partial^{-1}]$, whose image again gives a $\mathbb{Z}_q$-basis.

The latter correspondence should be a basic ingredient for a construction of Fock and Goncharov's *quantum duality map* [13] (see [41, Conjecture 4.14] for a finer formulation as well as [5]), which requires a basis of the quantum upper cluster algebra parametrized by the tropical set $\mathcal{X}_{\mathfrak{sl}_3,\Sigma}(\mathbb{Z}^T) = \mathcal{L}^p_{\mathfrak{sl}_3}(\Sigma, \mathbb{Z})$ with certain positivity properties. Let us interpret Theorem 5.2 in this context.

Langlands dual coordinates It turns out that it is more convenient to use a slight modification[6] of frozen shear coordinates to make the correspondence suited to the Fock–Goncharov conjecture. For an ideal triangulation $\triangle$ of Σ, we define the *Langlands dual coordinates*

$$\check{\mathrm{x}}_\triangle = (\check{\mathrm{x}}^\triangle_i)_{i \in I(\triangle)} \colon \mathcal{L}^p_{\mathfrak{sl}_3}(\Sigma, \mathbb{Q}) \xrightarrow{\sim} \mathbb{Q}^{I(\triangle)}$$

[6] In the language of Goncharov and Shen [21], it amounts to take the decoration at the *terminal* endpoint of a boundary interval rather than its *initial* endpoint along the boundary orientation to make a pinning.

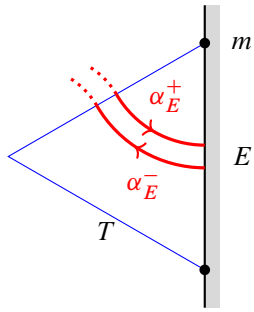

Figure 29: The corner arcs relevant to the Langlands dual coordinate.

as follows. For $i \in I_{\mathrm{uf}}(\triangle)$, let $\check{\mathrm{x}}_i^{\triangle} := \mathrm{x}_i^{\triangle}$. For $E \in \mathbb{B}$, we define the frozen coordinates on E by

$$\check{\mathrm{x}}_{E,1}^{\triangle}(\widehat{L}, \nu) := \nu_E^+ + \check{\alpha}_E^+(\widehat{L}) + [\mathrm{x}_T(\widehat{L})]_+,$$
$$\check{\mathrm{x}}_{E,2}^{\triangle}(\widehat{L}, \nu) := \nu_E^- + \check{\alpha}_E^-(\widehat{L}).$$

Here T is the unique triangle having E as an edge; $\check{\alpha}_E^+(\widehat{L})$ (resp. $\check{\alpha}_E^-(\widehat{L})$) is the total weight of the oriented corner arcs in $\mathcal{W} \cap T$ bounding the *terminal* endpoint of E in the counterclockwise (resp. clockwise) direction. Compare with (4-3). The map $\check{\mathrm{x}}_{\triangle}$ gives a bijection, which can be verified similarly to the proof of Proposition 4.3.

We define the *Langlands dual ensemble map*

$$\check{p}\colon \mathcal{L}^a_{\mathfrak{sl}_3}(\Sigma, \mathbb{Q}) \to \mathcal{L}^p_{\mathfrak{sl}_3}(\Sigma, \mathbb{Q}) \tag{5-8}$$

by forgetting the peripheral components, and defining the pinning $\nu_E^+ \in \mathbb{Q}$ (resp. $\nu_E^- \in \mathbb{Q}$) to be the weight of the peripheral component around the *terminal* endpoint of E in the counterclockwise (resp. clockwise) direction. The name "Langlands dual" is inspired by the following property:

Proposition 5.3 *The Langlands dual ensemble map (5-8) satisfies*

$$\check{p}^* \mathrm{x}_i^{\triangle} = \sum_{j \in I(\triangle)} (\varepsilon_{ij}^{\triangle} - m_{ij}) \mathrm{a}_j^{\triangle}$$

for any ideal triangulation.

Compare with (A-2), and observe that the presentation matrix is changed to the Langlands dual

$$-(\varepsilon^{\triangle} + M)^{\top} = \varepsilon^{\triangle} - M.$$

The verification of Proposition 5.3 is similar to Proposition 4.10, which is left to the reader.

For each $v \in \mathbb{E}\mathrm{xch}_{\mathfrak{sl}_3,\Sigma}$ and $k \in I$, the *elementary lamination* is the tropical point $\ell_k^{(v)} \in \mathcal{X}_{\mathfrak{sl}_3,\Sigma}(\mathbb{Z}^T)$ characterized by $\check{\mathrm{x}}_i^{(v)}(\ell_k^{(v)}) = \delta_{i,k}$. We have the cone

$$\mathcal{C}_{(v)}^+ := \mathrm{span}_{\mathbb{R}_+}\{\ell_k^{(v)} \mid k \in I\} = \{\ell \in \mathcal{X}_{\mathfrak{sl}_3,\Sigma}(\mathbb{R}^T) \mid \check{\mathrm{x}}_k^{(v)}(\ell) \geq 0 \text{ for all } k \in I\}$$

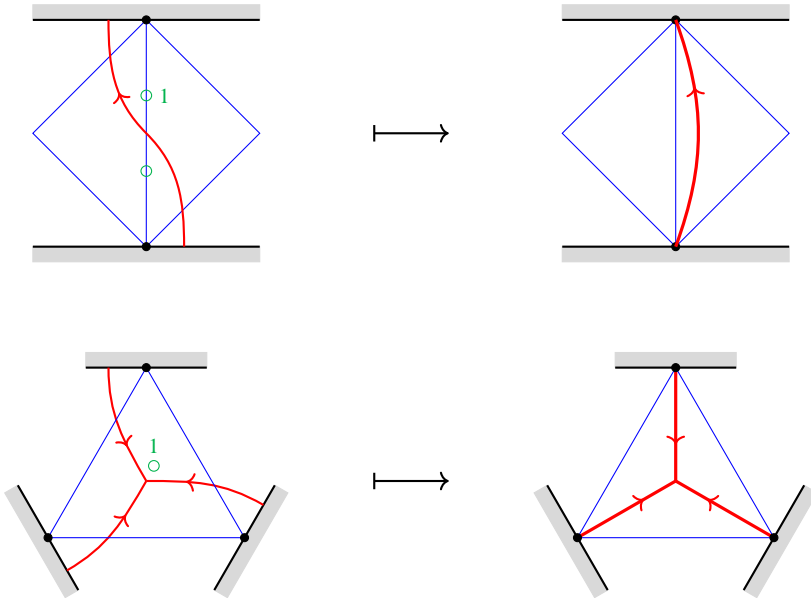

Figure 30: Negative $\mathbb{M}$-shifting of elementary laminations associated with a triangulation. Here exactly one of the Langlands dual coordinates $\check{x}_i^{\triangle}$ is $+1$, while the others are zero (including the frozen ones).

and its integral points $\mathcal{C}^+_{(v)}(\mathbb{Z}) := \mathcal{C}^+_{(v)} \cap \mathcal{X}_{\mathfrak{sl}_3,\Sigma}(\mathbb{Z}^T)$. The following gives a partial verification of a condition for the quantum duality map:

Lemma 5.4 *For any elementary lamination $\ell_k^{(v)}$ associated with a labeled $\mathfrak{sl}_3$-triangulation $v = (\triangle, \ell)$ in $\mathbb{E}\mathrm{xch}_{\mathfrak{sl}_3,\Sigma}$, the element $\mathbb{I}^q_{\mathcal{X}}(\ell_k^{(v)})$ coincides with the quantum cluster variable $A_k^{(v)} \in \mathscr{A}^q_{\mathfrak{sl}_3,\Sigma}$. In particular, any point $\ell = \sum_k x_k \ell_k^{(v)} \in \mathcal{C}^+_{(v)}(\mathbb{Z})$ gives a quantum cluster monomial $\big[\prod_k (A_k^{(v)})^{x_k}\big]$.*

Proof Via the isomorphism

$$\check{x}_{\triangle}^{-1} \colon \mathcal{X}_{\mathfrak{sl}_3,\Sigma}(\mathbb{Z}^T) \cong \mathcal{L}^p_{\mathfrak{sl}_3}(\Sigma, \mathbb{Z}),$$

the elementary laminations $\ell_k^{(v)}$ for unfrozen $k \in I(\triangle)_{\mathrm{uf}}$ correspond to the integral $\mathfrak{sl}_3$-laminations as shown in the left of Figure 30. The elementary laminations $\ell_k^{(v)}$ for frozen $k = i^s(E) \in I(\triangle)_{\mathrm{f}}$ with $E \in \mathbb{B}$ and $s \in \{1, 2\}$ correspond to the pinning data $v_E = \varpi_s^\vee$. Then via the quantum duality map

$$\mathbb{I}^q_{\mathcal{X}} \colon \mathcal{L}^p_{\mathfrak{sl}_3}(\Sigma, \mathbb{Z})_+ \xrightarrow{\sim} \mathsf{BWeb}_{\mathfrak{sl}_3,\Sigma} \subset \mathcal{S}^q_{\mathfrak{sl}_3,\Sigma}$$

these laminations are sent to the *elementary webs* associated with $\triangle$ in the sense of [30]. They correspond to the quantum cluster variables [30, Section 5]. □

Remark 5.5 By the equivariance of the map $\mathbb{I}^q_{\mathcal{X}}$ under the Dynkin involution, the above lemma can be immediately generalized for *decorated triangulations* (see [30, Section 1]).

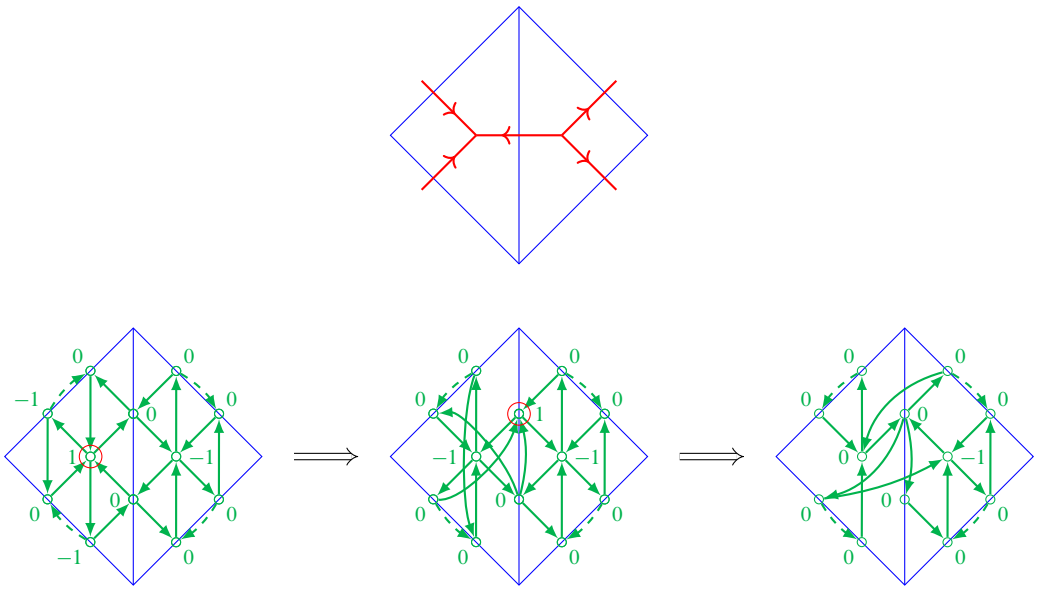

Figure 31: An elementary lamination of H-shape. Its shear coordinates associated with a triangulation is shown in the bottom left, and their transformations under the mutation sequence shown in red circles continue to the right.

Remark 5.6 When Σ is not a k-gon with $k = 3, 4, 5$, the mutation class $\mathfrak{s}(\mathfrak{sl}_3, \Sigma)$ is of infinite-mutation type. In this case, the union $\bigcup_{v \in \mathbb{E}\mathrm{xch}_{\mathfrak{sl}_3,\Sigma}} \mathcal{C}^+_{(v)}$ is not dense in $\mathcal{X}_{\mathfrak{sl}_3,\Sigma}(\mathbb{R}^{\mathrm{trop}})$ [44, Theorem 2.27]. Therefore Lemma 5.4 is far from characterizing the map $\mathbb{I}^q_{\mathcal{X}}$.

For the simplest cases that Σ is a triangle or a quadrilateral (where the mutation class $\mathfrak{s}(\mathfrak{sl}_3, \Sigma)$ is finite types A_1 and D_4, respectively), we actually get a quantum duality map:

Proposition 5.7 *When Σ is a triangle or a quadrilateral, the image $\mathbb{I}^q_{\mathcal{X}}(\mathcal{L}^p_{\mathfrak{sl}_3}(\Sigma, \mathbb{Z})) \subset \mathcal{O}_q(\mathcal{A}_{\mathfrak{sl}_3,\Sigma})$ gives a $\mathbb{Z}_q$-basis consisting of quantum cluster monomials. In particular, it has positive structure constants.*

Proof For these cases, it is easy to see that $\mathcal{S}^q_{\mathfrak{sl}_3,\Sigma}[\partial^{-1}] = \mathcal{A}^q_{\mathfrak{sl}_3,\Sigma} = \mathcal{O}_q(\mathcal{A}_{\mathfrak{sl}_3,\Sigma})$ [30, Corollary 6.1]. Moreover, the tropical set $\mathcal{X}_{\mathfrak{sl}_3,\Sigma}(\mathbb{Z}^T)$ is covered by finitely many cones $\mathcal{C}^+_{(v)}(\mathbb{Z}^T)$ for $v \in \mathbb{E}\mathrm{xch}_{\mathfrak{sl}_3,\Sigma}$.

For the triangle case, we have only two clusters (up to permutations), and hence Lemma 5.4 with Remark 5.5 already gives the desired statement. For the quadrilateral case (type D_4), we have 16 unfrozen variables and 8 frozen variables. For instance, see [30, Appendix A and Corollary 6.1]. Up to symmetry, we have already seen in the proof of Lemma 5.4 (see Figure 30) that all of them are the images of some elementary laminations under the map $\mathbb{I}^q_{\mathcal{X}}$, except for the one represented by the elementary web

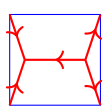

This one also comes from an elementary lamination, as seen from Figure 31. □

Conjecture 5.8 The basis $\mathbb{I}^q_{\mathcal{X}}(\mathcal{L}^p_{\mathfrak{sl}_3}(\Sigma,\mathbb{Z}))$ is *parametrized by tropical points* in the sense of [41, Definition 4.13]. Namely, for any integral $\mathfrak{sl}_3$-lamination $\widehat{L} \in \mathcal{L}^p_{\mathfrak{sl}_3}(\Sigma,\mathbb{Z})$, the quantum Laurent expression of $\mathbb{I}^q_{\mathcal{X}}(\widehat{L}) \in \mathcal{A}^q_{\mathfrak{sl}_3,\Sigma}$ in the quantum cluster $\{A_i\}_{i\in I}$ associated with a vertex $\omega \in \mathbb{E}\mathrm{xch}_{\mathfrak{sl}_3,\Sigma}$ has the leading term $\left[\prod_{i\in I} A_i^{\check{\mathrm{x}}_i}(\widehat{L})\right]$ with respect to the dominance order [41, Definition 4.6], where $\check{\mathrm{x}}^{(\omega)} = (\check{\mathrm{x}}_i)_{i\in I}$ is the Langlands dual shear coordinate system associated with ω.

Classical limit Recall that the set $\mathsf{BWeb}_{\mathfrak{sl}_3,\Sigma}$ also gives a $\mathbb{Z}$-basis of the classical (commutative) skein algebra $\mathcal{S}^1_{\mathfrak{sl}_3,\Sigma}$. Then Theorem 5.2 tells us that the map $\mathbb{I}^q_{\mathcal{X}}$ induces a bijection

$$\mathbb{I}_{\mathcal{X}} \colon \mathcal{L}^p_{\mathfrak{sl}_3}(\Sigma,\mathbb{Z})_+ \xrightarrow{\sim} \mathsf{BWeb}_{\mathfrak{sl}_3,\Sigma} \subset \mathcal{S}^1_{\mathfrak{sl}_3,\Sigma},$$

which is also extended to a map $\mathbb{I}_{\mathcal{X}} \colon \mathcal{L}^p_{\mathfrak{sl}_3}(\Sigma,\mathbb{Z}) \hookrightarrow \mathcal{S}^1_{\mathfrak{sl}_3,\Sigma}[\partial^{-1}]$. Then by (5-6), we get the following:

Corollary 5.9 *The image $\mathbb{I}_{\mathcal{X}}(\mathcal{L}^p_{\mathfrak{sl}_3}(\Sigma,\mathbb{Z}))$ gives a $\mathbb{Z}$-basis of the cluster algebra $\mathcal{A}_{\mathfrak{sl}_3,\Sigma}$.*

6 Proofs of Theorems 3.10 and 3.19

6.1 Proof of Theorem 3.10

General position Recall that an *ideal arc* in $(\Sigma,\mathbb{M})$ is an immersed arc γ in Σ with endpoints in $\mathbb{M}$ which has no self-intersection except possibly at its endpoints, and not isotopic to one point. In particular γ is one-sided differentiable at each endpoint p, hence there exists a small coordinate neighborhood D_p of p such that $D_p \cap \gamma$ consists of (at most two) rays incident to p.

We say that two immersed arcs or webs in Σ are in *general position* with each other if their intersections are finite, transverse and avoiding the trivalent vertices. Moreover, we say that the spiraling diagram $\mathcal{W}$ (Definition 3.8) associated with a nonelliptic signed web is in *general position* with an ideal arc if their intersection points do not accumulate in $\operatorname{int}\Sigma$, transverse and avoiding the trivalent vertices. We may always assume the general position by the concrete construction of a spiraling diagram as logarithmic spirals near punctures.

Relative intersection number Let γ and γ' be two ideal arcs isotopic to each other with common endpoints $p_1, p_2 \in \mathbb{M}$, and $\mathcal{W}$ a spiraling diagram. Assume that these three are in a general position with each other. Then the ideal arcs γ and γ' bounds a region $B(\gamma,\gamma')$, which is a union of finitely many biangles (or such a region minus small biangles; see γ and γ'_2 in Figure 35).

By the construction of the spiraling diagram, there exists a small disk neighborhood $p_i \in D_i$ for $i = 1,2$ such that $\rho_i := \gamma \cap D_i$ and $\rho'_i := \gamma' \cap D_i$ are rays incident to p_i, and $\mathcal{W} \cap D_i$ is a logarithmic spiral. The rays ρ_i and ρ'_i separate D_i into two sectors, and exactly one of them corresponds to the region bounded by γ and γ'. Then we can find a circular segment in this sector which does not intersect with $\mathcal{W}$, and the restriction of $\mathcal{W}$ to the circular sector separated by this segment is a periodic ladder-web. We call this circular sector $S(p_i)$ a *cut-off sector* at p_i. See Figure 32. Then $\mathcal{W}_{\mathrm{reg}} := \mathcal{W} \cap (B \setminus S(p_1) \cup S(p_2))$ is a finite web.

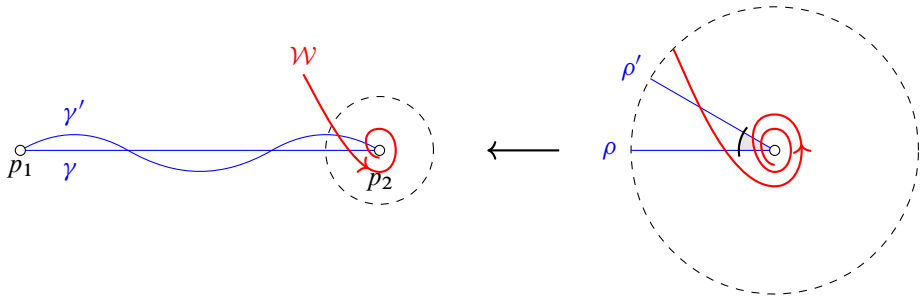

Figure 32: Two isotopic ideal arcs and a spiraling diagram. A cut-off sector is shown in gray in the right.

Definition 6.1 (relative intersection number) Let γ, γ' and $\mathcal{W}$ be as above, and choose cut-off sectors $S(p_1)$ and $S(p_2)$ at the common endpoints $p_1, p_2 \in \mathbb{M}$. Then we define the *relative intersection number* of $\mathcal{W}$ with (γ, γ') to be

$$i(\mathcal{W}; \gamma, \gamma') := i(\mathcal{W}_{\mathrm{reg}}, \gamma) - i(\mathcal{W}_{\mathrm{reg}}, \gamma').$$

Here $i(-,-)$ denotes the usual geometric intersection number of two webs.

Notice that it is independent of the choice of the cut-off sectors since a periodic ladder-web has an equal number of intersections with γ and γ' in each of its period. Clearly, we have $i(\mathcal{W}; \gamma', \gamma) = -i(\mathcal{W}; \gamma, \gamma')$.

Lemma 6.2 *Let γ_1, γ_2 and γ_3 be three ideal arcs isotopic to each other with common endpoints, and $\mathcal{W}$ a spiraling diagram. Assume that they are in general position with each other. Then we have*

$$i(\mathcal{W}; \gamma_1, \gamma_3) = i(\mathcal{W}; \gamma_1, \gamma_2) + i(\mathcal{W}; \gamma_2, \gamma_3).$$

Proof Immediately verified by choosing a common cut-off sector. □

Definition 6.3 We say that an ideal arc γ is in *minimal position* with a spiraling diagram $\mathcal{W}$ if it satisfies $i(\mathcal{W}; \gamma', \gamma) \geq 0$ for any ideal arc γ' isotopic to γ with common endpoints, and in general position with $\mathcal{W}$.

See Figure 33 for an example of an ideal arc not in a minimal position.

Realization of a minimal position We are going to prove:

Proposition 6.4 (unbounded version of [19, Corollary 12]) *Let $\mathcal{W}$ be the spiraling diagram associated with a nonelliptic signed web, and γ an ideal arc in a general position with $\mathcal{W}$. Then we can isotope $\mathcal{W}$*

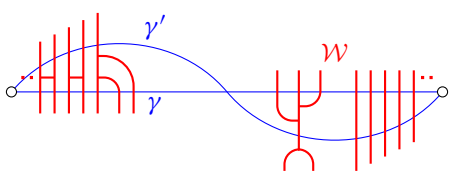

Figure 33: A spiraling diagram $\mathcal{W}$ that is not in minimal position with an ideal arc γ. Indeed, $i(\mathcal{W}; \gamma', \gamma) = -4$.

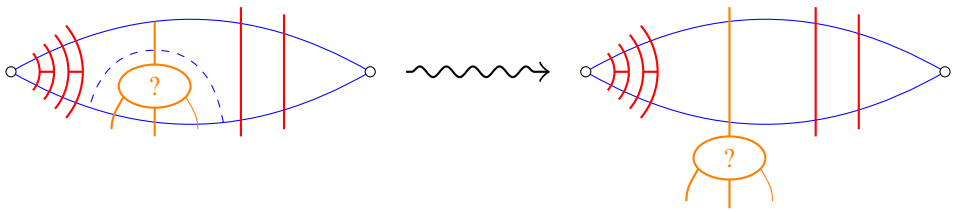

Figure 34: The restriction of a spiraling diagram $\mathcal{W}$ to a biangle bounded by two ideal arcs. Its loose part is shown in orange, which can be pushed out through a sequence of intersection reduction moves and H-moves.

into a spiraling diagram $\mathcal{W}'$ in minimal position with γ via a finite sequence of intersection reduction moves, H-moves, and an isotopy relative to γ.

To prove this, the following lemma is useful:

Lemma 6.5 (unbounded version of [19, Lemma 15]) *Let B be a biangle in Σ bounded by two immersed arcs α and α', and $\mathcal{W}$ a spiraling diagram in a general position. If some of the endpoints of α and α' are punctures, then choose any cut-off sectors and consider $\mathcal{W}_{\mathrm{reg}}$ as above. Otherwise, set $\mathcal{W}_{\mathrm{reg}} := \mathcal{W}$. Then $\mathcal{W}_{\mathrm{reg}}$ can be isotoped through a finite number of intersection reduction moves and H-moves so that $\mathcal{W}_{\mathrm{reg}} \cap B$ consists of disjoint parallel arcs connecting α and α'. This can be done by preserving the cut-off sectors, and the resulting web does not depend on the choice of cut-offs.*

Proof Since $\mathcal{W}_{\mathrm{reg}}$ is finite, the statement follows from [19, Lemma 15]. □

Notice that each of the H-moves and the intersection reduction moves are accompanied with a small biangle (shown by dashed lines in Figures 7 and 8) that cuts out a part of the web which we push out. Therefore the finite sequence of these moves in Lemma 6.5 is accompanied with a finite collection $\{B^{(j)}\}_{j\in J}$ of biangles that is partially ordered for the inclusion according to the order of moves, which we call the *tightening biangles*. Let us denote by $W^{(j)}$ the part of $\mathcal{W}$ cut out by the tightening biangle $B^{(j)}$, which we call the *loose part* of $\mathcal{W}$. See Figure 34.

The following lemma ensures that the intersection reduction procedures of a spiraling diagram associated with a nonelliptic signed web always terminate in finite steps.

Lemma 6.6 *For any spiraling diagram $\mathcal{W}$ associated with a nonelliptic signed web W and an ideal arc γ in general position, the relative intersection number $i(\mathcal{W};\gamma,\gamma')$ is bounded from above when γ' runs over the ideal arcs homotopic to γ and in general position with γ and $\mathcal{W}$.*

Proof If W has punctured H-faces, then applying appropriate puncture H-moves, we obtain another signed web W' which is puncture-reduced. The corresponding spiraling diagrams $\mathcal{W}$ and $\mathcal{W}'$ differ only by some finitely many H-shaped parts in the spiraling part, and hence $i(\mathcal{W};\gamma,\gamma') = i(\mathcal{W}';\gamma,\gamma')$. Therefore it suffices to consider the case where the signed web W giving rise to $\mathcal{W}$ is puncture-reduced.

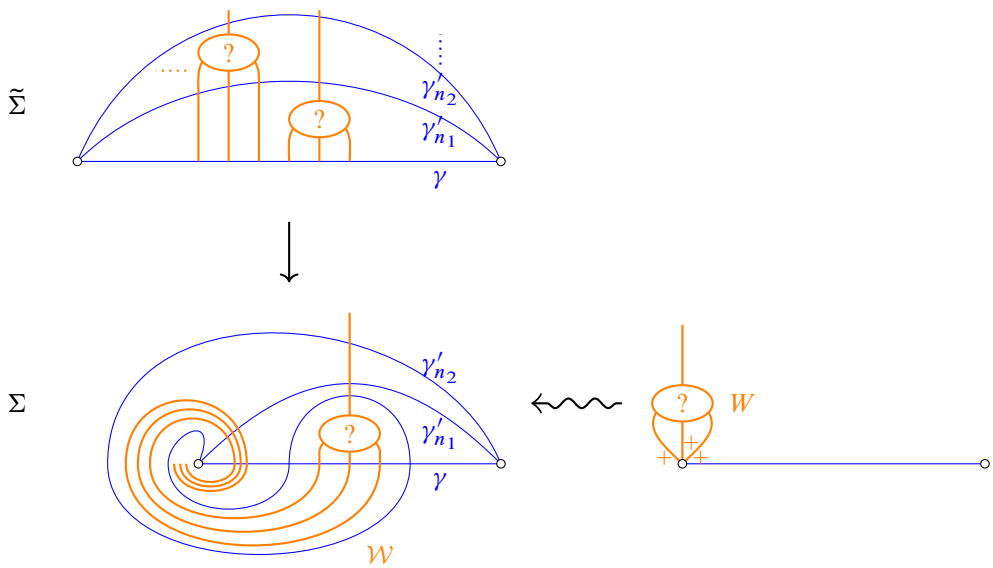

Figure 35: The situation that the relative intersection numbers $i(\mathcal{W};\gamma,\gamma'_n)$ diverge. The top left shows a covering of Σ around the puncture. The infinite sequence of portions are projected to the same portion of $\mathcal{W}$.

We prove the assertion by contradiction: suppose that there exists a sequence $\gamma'_n \simeq \gamma$ of ideal arcs satisfying the condition and $i(\mathcal{W};\gamma,\gamma'_n) \geq n$ for all $n \in \mathbb{Z}_{\geq 0}$. Let $\{B_n^{(j)}\}_{j\in J_n}$ be the collection of tightening biangles for the pair (γ,γ'_n), and $W_n^{(j)} \subset \mathcal{W}$ the corresponding loose part.

(a) Since we are interested in a sequence γ'_n such that $i(\mathcal{W};\gamma,\gamma'_n)$ diverges, we may assume that all of the tightening biangles $B_n^{(j)}$ are stuck to γ rather than γ'_n. Otherwise, a biangle stuck to γ'_n contributes negatively to $i(\mathcal{W};\gamma,\gamma'_n)$. Then we may isotope γ'_n to avoid this biangle without decreasing $i(\mathcal{W};\gamma,\gamma'_n)$.

(b) Shrinking each tightening biangle (without changing the intersection number of its boundary with $\mathcal{W}$) if necessary, we may assume that either $B_n^{(j)} \cap B_m^{(\ell)} = \varnothing$, $B_n^{(j)} \subset B_m^{(\ell)}$ or $B_m^{(\ell)} \subset B_n^{(j)}$ holds for any pair in this collection. Also we can ensure that each tightening biangle does not intersect with the cut-off sectors at punctures.

Let us consider the compact interval $K = \gamma \setminus (\text{cut-off sectors})$. From the assumption of general position, the intersection of $\mathcal{W}$ with K is finite. The intersections $I_n^{(j)} := \gamma \cap \operatorname{int} B_n^{(j)}$ give open intervals in K. Observe that the union $\bigcup_{n\geq 0,\ j\in J_n} I_n^{(j)}$ has finitely many path-connected components, since each such component contains a distinct point in $\mathcal{W}\cap K$, which is finite. Therefore we see that there exist subsequences n_k and $j_k \in J_{n_k}$ such that $B_{n_k}^{(j_k)} \subset B_{n_{k+1}}^{(j_{k+1})}$.

Such a nested situation is illustrated in Figure 35. Indeed, the situation says that distinct reduction moves are applied infinitely many times, while the original signed web W is finite. It means that there is a portion P of the signed web that is referred infinitely many times. Therefore the nested biangles $B_{n_k}^{(j_k)}$ (or the

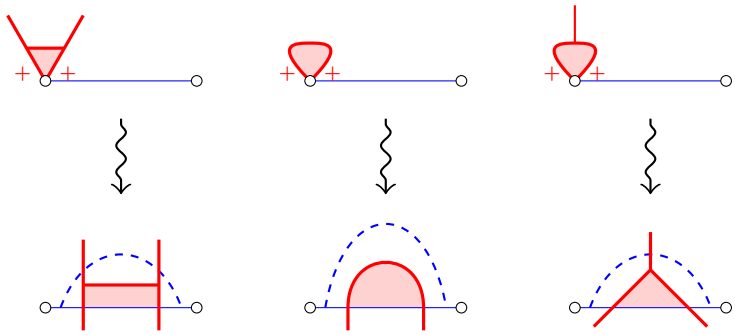

Figure 36: The correspondence between the puncture-faces (top) and the faces stuck to γ (bottom).

arcs γ'_{n_k}) must be winding around one of the punctures p_1 or p_2, while the portion $\mathcal{P}$ in $\mathcal{W}$ corresponding to P is spiraling around the same puncture as in the bottom left of the figure. Notice that such a spiraling diagram $\mathcal{W}$ arises from the signed web W shown in the bottom right.

Moreover, observe the correspondence shown in Figure 36 between the faces stuck to γ and the puncture-faces. Therefore, the sequence of loose parts $W_{n_k}^{(j_k)}$ must come from these puncture-faces in the signed web W, which contradicts to either the puncture-reduced assumption, nonelliptic condition, or the no bad ends condition. Thus the assertion is proved. □

Proof of Proposition 6.4 Suppose that $\mathcal{W}$ is not in minimal position with γ. Then there exists an ideal arc $\gamma_0 \simeq \gamma$ such that $i(\mathcal{W};\gamma,\gamma_0) > 0$ and in general position with γ and $\mathcal{W}$. Choose γ_0 so that $i(\mathcal{W};\gamma,\gamma_0)$ is maximal, whose existence is ensured by Lemma 6.6. Then for any other ideal arc γ' isotopic to γ, we have

$$i(\mathcal{W};\gamma',\gamma_0) = i(\mathcal{W};\gamma',\gamma) + i(\mathcal{W};\gamma,\gamma_0) = -i(\mathcal{W};\gamma,\gamma') + i(\mathcal{W};\gamma,\gamma_0) \geq 0$$

by Lemma 6.2 and the maximality of γ_0. It implies that γ_0 is in minimal position with $\mathcal{W}$, as desired. □

Corollary 6.7 (cf [19, Corollary 12 and Proposition 13]) *Any spiraling diagram $\mathcal{W}$ associated with a signed web on Σ can be isotoped through a finite number of intersection reduction moves and H-moves so that it is in minimal position simultaneously with any disjoint finite collection $\{\gamma_i\}_{i=1}^N$ of ideal arcs. Such a minimal position with $\{\gamma_i\}_{i=1}^N$ is unique up to isotopy relative to these arcs, H-moves, periodic H-moves and parallel moves.*

Proof As in the discussion above, we isotope the arcs instead of the spiraling diagram. Let $\{\gamma_i\}_i$ be the original collection of ideal arcs, and $\{\gamma'_i\}_i$ the collection of modified arcs such that $i(\mathcal{W};\gamma_i,\gamma'_i)$ is maximal. Let B_i be the biangle bounded by γ_i and γ'_i. We claim that we can slightly modify B_i as in (b) above so that it does not cross γ'_j for any $i \neq j$. Indeed, suppose B_i crosses γ'_j. If we can shrink B_i without changing the intersection with $\mathcal{W}$, do so. Otherwise, it implies that γ_i and γ'_j bound together at least one biangle $B' \subset B_j$, for which we can apply a reduction move (see Figure 37). It contradicts to the maximality of $i(\mathcal{W};\gamma_j,\gamma'_j)$.

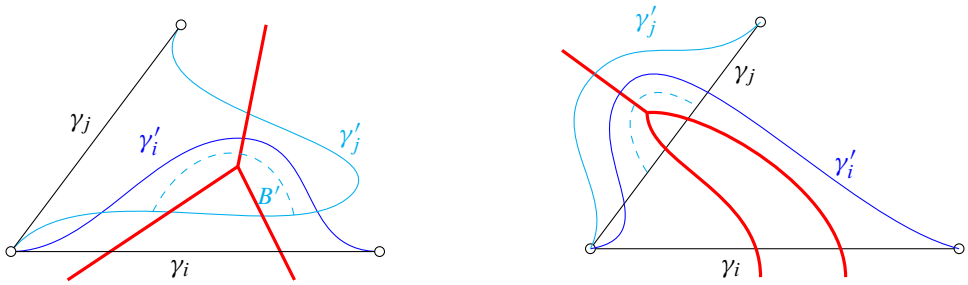

Figure 37: Situations where B_i essentially crosses γ_j' (left) and B_i crosses γ_j essentially (right). Both pictures show the case where B_i intersects B_j only once.

Hence, the biangle B_i is either disjoint from B_j or intersect with B_j only through γ_j. In the former case, the reduction moves are independently applied. In the latter case, some of the reduction moves are common for γ_i and γ_j but still the minimal positions can be simultaneously realized. Thus we get the first statement.

The second one is proved by induction on the number N of arcs, just in the same way as the proof of [19, Proposition 13]. □

Proof of Theorem 3.10: realization of a good position By Corollary 6.7, we can place any spiraling diagram $\mathcal{W}$ in a minimal position with the ideal arcs in the split triangulation $\widehat{\triangle}$. Then by applying a finite number of H-moves and periodic H-moves, we can push all the *ladders* as in Figure 38 into biangles (the "tidying up" operation in [19]). Assume that these moves can be no longer applied to $\mathcal{W}$. We are going to prove that this position (the "joy-sparking" position in [19]) is a good position with respect to $\widehat{\triangle}$.

For each $E \in e(\triangle)$, the intersection $\mathcal{W} \cap B_E$ is an unbounded essential web by Lemma 6.5, since it is in minimal position with the ideal arcs bounding B_E. For each $T \in t(\triangle)$, we see that the only components of $\mathcal{W} \cap T$ which do not touch all sides of T are corner arcs by Lemma 6.5. Indeed, such a component can be viewed as a web in a biangle obtained from T by collapsing one edge that is not touched, and the ladders in the periodic part have been pushed into the biangles neighboring to T. Let W' be the web

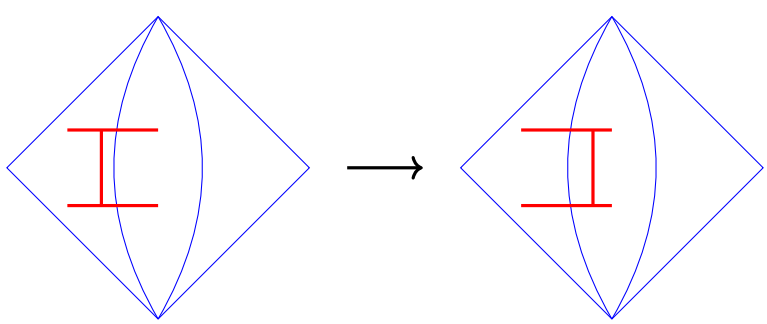

Figure 38: Pushing a ladder into a biangle.

obtained from $\mathcal{W} \cap T$ by removing these corner arcs, which must be finite. Then we see that W' must be a honeycomb in the same as in the last part in the proof of [19, Theorem 19]. Hence $\mathcal{W} \cap T$ is an unbounded rung-less essential web. The uniqueness statement follows from that of Corollary 6.7. Thus Theorem 3.10 is proved.

6.2 Proof of Theorem 3.19

We are going to prove Theorem 3.19 by following the strategy for the proof of [6, Theorem 47]. We remark here that another proof of the latter statement is given in [19, Section 14] based on the graded skein algebras.

The main issue here is that we have fixed the periodic pattern of corner arcs in the reconstruction procedure. Hence the resulting spiraling diagram may differ from the original one by a periodic permutation of corner arcs ("periodic local parallel-moves") on each triangle. Our claim is that these local adjustments glue together to give a global parallel-move, thus we get equivalent $\mathfrak{sl}_3$-laminations. See Figure 40 for a typical example.

By the $\mathbb{Q}_{>0}$-equivariance, it suffices to consider integral unbounded $\mathfrak{sl}_3$-laminations, which are represented by signed nonelliptic webs. Therefore it suffices to prove the following statement:

Proposition 6.8 *If two signed nonelliptic webs W_1 and W_2 have the same shear coordinates $(x_i)_{i \in I_{\mathrm{uf}}(\triangle)}$ with respect to an ideal triangulation $\triangle$, then W_1 and W_2 are equivalent as unbounded $\mathfrak{sl}_3$-laminations.*

In what follows, the index $\nu \in \{1, 2\}$ will always given to the objects associated to the web W_ν. For a discrete subset $A \subset \mathbb{R}$ (eg $A = \mathbb{Z}$), we call a subset $I \subset A$ of the form $I = [a, b] \cap A$ for a (possibly unbounded) interval $[a, b] \subset \mathbb{R}$ an *interval* in A.

Global pictures Let W_1 and W_2 be as in Proposition 6.8. For $\nu = 1, 2$, we may assume that the associated spiraling diagram $\mathcal{W}_\nu$ is placed in a good position with respect to the split triangulation $\widehat{\triangle}$ by Theorem 3.10. Then its braid representative $\mathcal{W}_{\nu,\mathrm{br}}^{\triangle}$ has at most one honeycomb component on each triangle. Let Σ° be the holed surface, which is a compact surface obtained by removing a small open disk D_T in each $T \in t(\triangle)$ from Σ. We may isotope the unique honeycomb component of $\mathcal{W}_{\nu,\mathrm{br}}^{\triangle}$ into the disk D_T, so that $\langle \mathcal{W}_\nu \rangle := \mathcal{W}_{\nu,\mathrm{br}}^{\triangle} \cap \Sigma^\circ$ is a collection of oriented curves, whose ends either lie on $\partial\Sigma^\circ$ or spiral around punctures. Following [6], we call $\langle \mathcal{W}_\nu \rangle$ the *global picture* associated with $\mathcal{W}_{\nu,\mathrm{br}}^{\triangle}$. It is obvious to reconstruct the braid representative from its global picture. We call each oriented curve in $\langle \mathcal{W}_\nu \rangle$ a *traveler*.

Recall from Steps 1 and 2 in the reconstruction procedure (Section 3.4) that we can construct a braid representative $W_{\nu,\mathrm{br}}^{\triangle}$ of signed web by replacing the spiraling ends with signed ends. We similarly define its global picture by $\langle W_\nu \rangle := W_{\nu,\mathrm{br}}^{\triangle} \cap \Sigma^\circ$. For the scheme of our proof, see Figure 39. Our strategy is as follows:

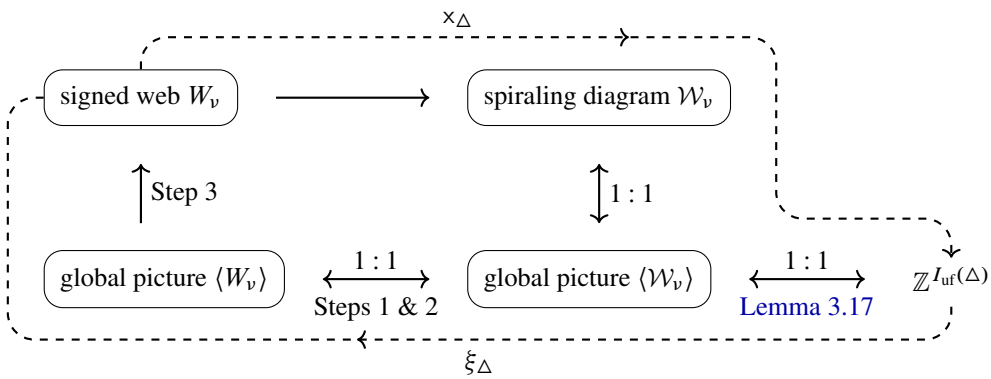

Figure 39: The scheme for a proof of Proposition 6.8. It is obvious that the three objects $\mathcal{W}_v$, $\langle \mathcal{W}_v \rangle$ and $\langle W_v \rangle$ are in one-to-one correspondences (up to strict isotopies), when one fixes a triangulation $\triangle$. It will be proved that we get the identity (up to equivalence of signed webs) after going through the square.

(1) Starting from the assumption in Proposition 6.8, we are going to make a correspondence between the topological data of global pictures $\langle W_1 \rangle$ and $\langle W_2 \rangle$ (namely, their travelers and intersection points among them) by an unbounded version of the "fellow-traveler lemma" [6, Lemma 57].

(2) From such a correspondence, we can describe a sequence of elementary moves relation W_1 and W_2 by just following the argument of Douglas and Sun [6, Section 7.4] for the bounded case.

Unbounded fellow-traveler lemma For each traveler γ in $\langle \mathcal{W}_v \rangle$, fix a basepoint $x_0 \in \gamma$ so that it does not lie on any edge of $\triangle$. Associated to such a based traveler (γ, x_0) is the *route* $(E_i)_{i \in I}$, where $I \subset \mathbb{Z}$ is an interval and E_i is the i^{th} edge of $\triangle$ crossed by γ listed in order according to the orientation of γ: the 0^{th} edge is the first one encountered by γ after passing x_0. We also define the *turning pattern* $(\tau_i)_{i \in I} \subset \{L, S, R\}^I$ of the based traveler (γ, x_0) as follows:

$$\tau_i := \begin{cases} L & \text{if } E_{i+1} \text{ follows } E_i \text{ in the counterclockwise direction at their common endpoints,} \\ S & \text{if } \gamma \text{ ends at the boundary of } D_T \text{ right after passing } E_i, \\ R & \text{if } E_{i+1} \text{ follows } E_i \text{ in the clockwise direction at their common endpoints.} \end{cases}$$

The following is immediately verified:

Lemma 6.9 *The topological types of the travelers γ are distinguished by the periodicity of the data $(E_i, \tau_i)_{i \in I}$, as follows*:

- *γ is a bounded arc both of whose ends lie on $\partial\Sigma^\circ$ if $I \subset \mathbb{Z}$ is bounded*;
- *γ is a loop if $I = \mathbb{Z}$ and the route is totally periodic (namely, $E_{i+k} = E_i$ for some $k \in \mathbb{Z}$). Moreover, it is peripheral if the turning pattern $(\tau_i)_{i \in I}$ is constant*;
- *γ has an end spiraling to a puncture p, say in the forward direction, if $I \subset \mathbb{Z}$ is unbounded from above, the route $(E_i)_i$ is not totally periodic but eventually periodic, and the turning pattern $(\tau_i)_i$ is eventually constant in the forward direction.*

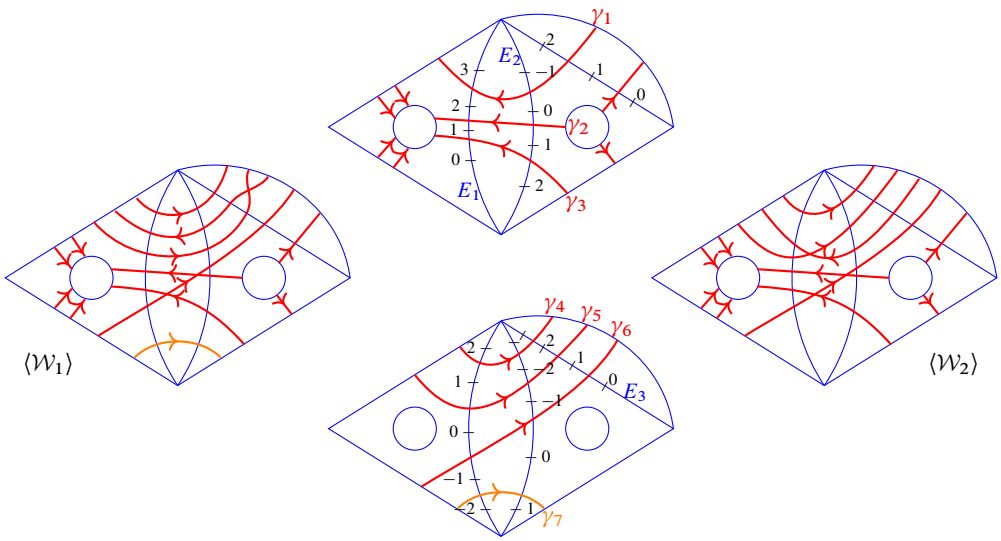

Figure 40: Example of local picture of a pair $(\langle\mathcal{W}_1\rangle, \langle\mathcal{W}_2\rangle)$ having the same shear coordinates. Here the top (resp. bottom) picture shows the collection of oriented curves going through the central biangle from the right to the left (resp. from the left to the right), which is common for $\langle\mathcal{W}_1\rangle$ and $\langle\mathcal{W}_2\rangle$ except for γ_7.

We say that two travelers $\gamma^{(1)}$ in $\langle\mathcal{W}_1\rangle$ and $\gamma^{(2)}$ in $\langle\mathcal{W}_2\rangle$ are *fellow-travelers* if their data $(E_i^{(1)}, \tau_i^{(1)})_{i\in I_1}$ and $(E_i^{(2)}, \tau_i^{(2)})_{i\in I_2}$ are the same, in the sense that there exists an order-preserving bijection $f: I_1 \to I_2$ such that $E_{f(i)}^{(2)} = E_i^{(1)}$ and $\tau_{f(i)}^{(2)} = \tau_i^{(1)}$ for all $i \in I_1$. Notice that the notion of fellow-traveler does not depend on the choice of basepoints, and that two fellow-travelers have the same topological type by Lemma 6.9.

Lemma 6.10 (unbounded fellow-traveler lemma, cf [6, Lemma 57]) *Under the assumption of Proposition 6.8, there exists a bijection*

$$\varphi: \{\text{nonperipheral travelers in } \langle\mathcal{W}_1\rangle\} \xrightarrow{\sim} \{\text{nonperipheral travelers in } \langle\mathcal{W}_2\rangle\}$$

such that γ and $\varphi(\gamma)$ are fellow-travelers.

Traveler identifier In order to prove Lemma 6.10, let us introduce another data that identifies the traveler and can be characterized by the shear coordinates. Let us consider two triangles $T_L, T_R \in t(\triangle)$ that shares a biangle B_E. For $Z \in \{L, R\}$, let E_Z denote the edge of $\widehat{\triangle}$ shared by T_Z and B_E. Let $S_{E_Z}^{+,(\nu)}$ (resp. $S_{E_Z}^{-,(\nu)}$) denote the set of strands on E_Z incoming to (resp. outgoing from) the biangle B_E, which are given by the intersections of travelers in $\langle\mathcal{W}_\nu\rangle$ and E_Z for $\nu = 1, 2$. We endow E_Z with the orientation induced from the triangle T_Z.

Choose two orientation-preserving parametrizations of E_Z in the same way as in Section 3.4. Namely, choose $\phi_{E_Z}^{\pm,(\nu)}: \mathbb{R} \to E_Z$ so that the inverse image of $S_{E_Z}^{\pm,(\nu)}$ is an interval $I_{E_Z}^{\pm,(\nu)} \subset \frac{1}{2} + \mathbb{Z}$, and $\phi_{E_Z}^{\pm,(\nu)}(\mathbb{R}_{<0}) \cap S_{E_Z}^{\pm,(\nu)}$ consists of all the strands coming from the corner arcs around the initial marked

point of E_Z. Let $f_{E_Z}^{\pm,(\nu)}\colon E_Z \to \mathbb{R}$ be the inverse map of $\phi_{E_Z}^{\pm,(\nu)}$. For a traveler $\gamma^{(\nu)}$ in $\langle \mathcal{W}_\nu \rangle$ that intersects with the edge E_Z at a point x, its *traveler identifier* at E_Z is the pair $(k,\epsilon) \in \left(\frac{1}{2}+\mathbb{Z}\right)\times\{\pm 1\}$ given by

$$(k,\epsilon) := \begin{cases} (f_{E_Z}^{+,(\nu)}(x),+) & \text{if } \gamma \text{ enters } B_E \text{ from } E_Z, \\ (f_{E_Z}^{-,(\nu)}(x),-) & \text{if } \gamma \text{ exits } B_E \text{ from } E_Z. \end{cases}$$

Then we write $\gamma^{(\nu)} = \gamma_{E_Z}^{(\nu)}(k,\epsilon)$.

Example 6.11 In the example shown in Figure 40, we have

$$\begin{aligned}
\gamma_1 &= \gamma_{E_1}^{(\nu)}(5/2,-) = \gamma_{E_2}^{(\nu)}(-1/2,+) = \gamma_{E_3}^{(\nu)}(3/2,-),\\
\gamma_2 &= \gamma_{E_1}^{(\nu)}(3/2,-) = \gamma_{E_2}^{(\nu)}(1/2,+),\\
\gamma_3 &= \gamma_{E_1}^{(\nu)}(1/2,-) = \gamma_{E_2}^{(\nu)}(3/2,+),\\
\gamma_4 &= \gamma_{E_1}^{(\nu)}(3/2,+) = \gamma_{E_2}^{(\nu)}(-5/2,-) = \gamma_{E_3}^{(\nu)}(5/2,+),\\
\gamma_5 &= \gamma_{E_1}^{(\nu)}(1/2,+) = \gamma_{E_2}^{(\nu)}(-3/2,-) = \gamma_{E_3}^{(\nu)}(3/2,+),\\
\gamma_6 &= \gamma_{E_1}^{(\nu)}(-1/2,+) = \gamma_{E_2}^{(\nu)}(-1/2,-) = \gamma_{E_3}^{(\nu)}(1/2,+),\\
\gamma_7 &= \gamma_{E_1}^{(\nu)}(-3/2,+) = \gamma_{E_2}^{(\nu)}(1/2,+).
\end{aligned}$$

Lemma 6.12 *Let $\gamma^{(\nu)}$ be a traveler in $\langle \mathcal{W}_\nu \rangle$ that passes through B_E from E_L to E_R. Let $(k_L,+)$ and $(k_R,-)$ be its traveler identifier at E_L and E_R, respectively. Then we have*

$$k_L + k_R = \times_{E,1}(W_\nu) + [\times_{T_R}(W_\nu)]_+.$$

If $\gamma^{(\nu)}$ passes through B_E from E_R to E_L, then its traveler identifiers $(k_R,+)$ and $(k_L,+)$ satisfy $k_L + k_R = \times_{E,2}(W_\nu) + [\times_{T_L}(W_\nu)]_+$.

Proof Just observe that our choice of parametrizations $\phi_{E_Z}^{\pm,(\nu)}$ is the same as in the reconstruction procedure (Section 3.4), except for the difference that we do not necessarily have an infinite number of corner arcs here. Then the assertion is obtained from the gluing rule (3-2). □

Lemma 6.13 *The traveler identifiers characterizes the traveler and its topological type. Namely,*

(1) *the traveler identifier determines the data $(E_i,\tau_i)_{i\in I}$ for each traveler;*

(2) *if $\gamma_E^{(1)}(k,\epsilon) = \gamma_{E'}^{(1)}(k',\epsilon')$ for two edges E and E' of the split triangulation $\widehat{\triangle}$, then*

$$\gamma_E^{(2)}(k,\epsilon) = \gamma_{E'}^{(2)}(k',\epsilon').$$

Proof (1) The initial edge E_0 is determined from the basepoint x_0. Assume that we have determined the data E_i for $0 \le i \le k$ and τ_j for $0 \le j \le k-1$. Let $E := E_k$. Then E_{k-1} and τ_{k-1} tell us from which direction our traveler passes through the biangle B_E. Assume it is from T_L to T_R, without loss of

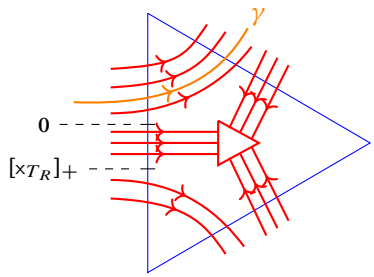

Figure 41: The turning pattern determined by the value of k_R.

generality. Then by Lemma 6.12, we have $k_R = \times_{E,1}(W_v) + [\times_{T_R}(W_v)]_+ - k_L$. Then by the choice of the parametrization $\phi_{E_R}^{-,(v)}$, we see that

$$\tau_k = \begin{cases} L & \text{if } k_R < 0, \\ S & \text{if } 0 < k_R < [\times_{T_R}(W_v)]_+, \\ R & \text{if } k_R > [\times_{T_R}(W_v)]_+. \end{cases}$$

See Figure 41. Moreover, the pattern τ_k tells us the next edge E_{k+1} or its absence.

(2) Recall that the shear coordinates of W_1 and W_2 are the same. Since the reconstruction given in (1) is characterized by the shear coordinates, the assertion follows. □

Proof of Lemma 6.10 Define the bijection φ by

$$\varphi\colon \gamma_E^{(1)}(k,\epsilon) \mapsto \gamma_E^{(2)}(k,\epsilon). \tag{6-1}$$

It is well defined by Lemma 6.13(2), and preserves the topological types of travelers by Lemma 6.13(1). □

Remark 6.14 From the proof of Lemma 6.12, a traveler $\gamma = \gamma_E^{(1)}(k,\epsilon)$ with $k \in I_E^{\epsilon,(1)} \setminus I_E^{\epsilon,(2)}$ must be peripheral. For example, if $\gamma = \gamma_{E_L}^{(1)}(k_L,+)$ and $k_L < \min I_{E_L}^{\epsilon,(2)}$ is a lower excess, then it must have $\tau_k = R$, since otherwise it has a nontrivial contribution to the edge coordinates. It follows that such a traveler also has an identifier of lower excess in the next biangle, concluding $\tau_k = R$ for all $k \in \mathbb{Z}$ inductively for both directions. See γ_7 in Figure 40 for an example.

Correspondence between the global pictures $\langle W_1 \rangle$ and $\langle W_2 \rangle$ Let W_1 and W_2 be as in Proposition 6.8. Then by the unbounded fellow-traveler Lemma, we have a bijective correspondence φ between the travelers in $\langle \mathcal{W}_1 \rangle$ and $\langle \mathcal{W}_2 \rangle$. Let us consider the global pictures $\langle W_1 \rangle$ and $\langle W_2 \rangle$, and call each oriented curve in $\langle W_v \rangle$ a traveler again. Since the bijection φ preserves the spiraling types of travelers in $\langle \mathcal{W}_v \rangle$, it induces a bijection

$$\varphi\colon \{\text{travelers in } \langle W_1 \rangle\} \xrightarrow{\sim} \{\text{travelers in } \langle W_2 \rangle\}. \tag{6-2}$$

Here we make the intersection of each traveler in $\langle W_v \rangle$ with each edge of $\widehat{\triangle}$ minimal, by applying the same isotopy for each pair $(\gamma, \varphi(\gamma))$ of travelers. Notice that each traveler in $\langle W_v \rangle$ is either a closed loop or a compact arc, and their intersections are finite. Therefore we can proceed by applying Douglas and Sun's argument [6, Section 7.4] for the rest of discussion.

Recall the notion of a *shared route* of two ordered travelers (γ, γ') from [6, Definition 59]. Roughly speaking, it is a maximal interval shared by the routes of two travelers with opposite orientations. The definition is extended for the travelers in $\langle W_\nu \rangle$ in a straightforward way. A shared route is either *crossing* or *noncrossing*. A noncrossing shared route is said to be *left-oriented* if one traveler is always seen on the left from the other traveler. A crossing shared route is said to be *left-oriented* if the same situation occurs near its source-end [6, Definition 61].

By applying the boundary and puncture H-moves if necessary, we may assume that these webs are reduced. Then we see that each shared route has at most one intersection point (see [6, Lemma 60]). Indeed, two intersecting travelers cannot have a common endpoint at a puncture, since such a situation would come from a puncture H-face. Hence the situation regarding the crossing shared routes is exactly the same as in the bounded case. From these observations, together with the bijection (6-2), we get:

Lemma 6.15 (cf [6, Corollary 64]) *For $\nu = 1, 2$, let $P_{\langle W_\nu \rangle}$ denote the set of intersections of travelers in $\langle W_\nu \rangle$. Then we have a bijection*

$$\varphi_{\mathrm{int}} \colon P_{\langle W_1 \rangle} \xrightarrow{\sim} P_{\langle W_2 \rangle}$$

such that the unique intersection point p of a left-oriented shared route of two travelers (γ, γ') in $\langle W_1 \rangle$ is sent to the unique intersection point $\varphi_{\mathrm{int}}(p)$ of the corresponding shared route of $(\varphi(\gamma), \varphi(\gamma'))$ in $\langle W_2 \rangle$.

Proof of Proposition 6.8: a sequence of elementary moves relating W_1 and W_2 As in the previous paragraph, we may assume that W_1 and W_2 are reduced by applying the boundary/puncture H-moves. Moreover by applying the loop parallel-moves and the arc parallel-moves (Lemma 2.4), we may assume that both W_1 and W_2 are *left-oriented* in the sense that for each pair of parallel loop or arc components with opposite orientations, one is always seen on the left from the other. It includes the *closed-left-oriented* condition [6, Definition 62]. Now we are going to see that the intersection points $p \in P_{\langle W_1 \rangle}$ and $\varphi_{\mathrm{int}}(p) \in P_{\langle W_2 \rangle}$ can be adjusted to a common position by a sequence of modified H-moves; see Figure 42. The techniques developed in [6, Section 7.8] can be directly applied to our situation without any essential modification, since the situation around a crossing shared route is exactly the same as in the bounded case, and the sets $P_{\langle W_\nu \rangle}$ are finite. Then we get:

Lemma 6.16 (cf [6, Lemma 66]) *There are sequences of modified H-moves applicable to the webs W_1 and W_2 respectively, after which the bijection φ_{int} satisfies the property that for each intersection point p in $\langle W_1 \rangle$, the two points p and $\varphi_{\mathrm{int}}(p)$ lie in the same shared-route-biangle* [6, Definition 65].

Apply the sequence of modified H-moves to W_1 and W_2 prescribed above. We claim that the two signed webs W_1 and W_2 are now isotopic.

In the same way as in the proof of [6, Lemma 67], we see that the finite sequences of oriented strands on each edge of the split triangulation $\widehat{\triangle}$ are the same for $\langle W_1 \rangle$ and $\langle W_2 \rangle$. We have a correspondence (6-2) that relates the travelers in $\langle W_1 \rangle$ and $\langle W_2 \rangle$, in particular the ends incident to punctures and their signs.

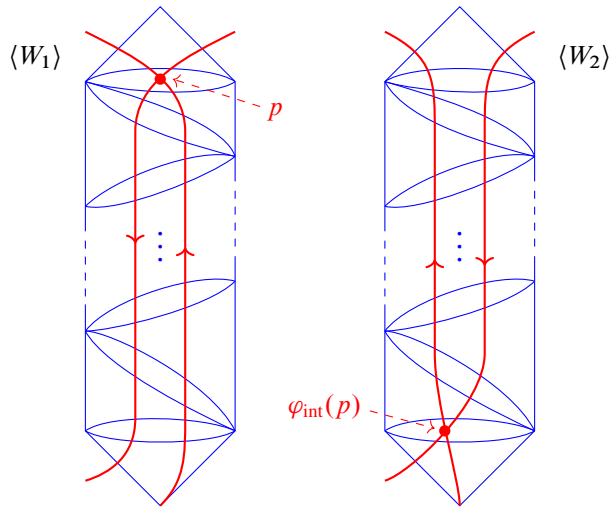

Figure 42: Adjustment of intersection points. Here only the difference from the situation in [6] is that some of the travelers can end at a puncture.

The travelers can intersect with each other inside biangles, whose pattern is uniquely determined by the sequence of oriented strands on the side edges. Thus $\langle W_1 \rangle$ and $\langle W_2 \rangle$ restricts to the same collection of oriented curves (with signed ends at punctures) in each triangle and biangle in $\widehat{\triangle}$. Since we can uniquely recover the honeycombs from these diagrams, we get $W_1 = W_2$ up to isotopy. Thus Proposition 6.8 is proved.

Proof of Theorem 3.19 Let us consider an integral unbounded $\mathfrak{sl}_3$-lamination, which is represented by a signed nonelliptic web W_1. Let $W_2 := \xi_\triangle \circ \mathrm{x}^{\mathrm{uf}}_\triangle(W_1)$ be the signed nonelliptic web obtained from the reconstruction. By Proposition 3.18, we have $\mathrm{x}^{\mathrm{uf}}_\triangle(W_1) = \mathrm{x}^{\mathrm{uf}}_\triangle(W_2)$. Then Proposition 6.8 tells us that W_1 and W_2 determine an equivalent $\mathfrak{sl}_3$-lamination. Combining with the $\mathbb{Q}_{>0}$-equivariance, we get the desired assertion. □

Appendix Cluster varieties associated with the pair $(\mathfrak{sl}_3, \Sigma)$

Here we briefly recall the general theory of cluster varieties [13], and the construction of the seed pattern $\boldsymbol{s}(\mathfrak{sl}_3, \Sigma)$ that encodes the cluster structures of the spaces of $\mathfrak{sl}_3$-laminations in consideration.

A.1 Seeds, mutations and the labeled exchange graph

Fix a finite set $I = \{1, \dots, N\}$ of indices, and let $\mathcal{F}_A$ and $\mathcal{F}_X$ be fields both isomorphic to the field $\mathbb{Q}(z_1, \dots, z_N)$ of rational functions on N variables. We also fix a subset $I_{\mathrm{uf}} \subset I$ ("unfrozen") and let $I_{\mathrm{f}} := I \setminus I_{\mathrm{uf}}$ ("frozen"). A (*labeled*, *skew-symmetric*) *seed* in $(\mathcal{F}_A, \mathcal{F}_X)$ is a triple $(\varepsilon, \boldsymbol{A}, \boldsymbol{X})$, where

- $\varepsilon = (\varepsilon_{ij})_{i,j \in I}$ is a skew-symmetric matrix (*exchange matrix*) with values in $\frac{1}{2}\mathbb{Z}$ such that $\varepsilon_{ij} \in \mathbb{Z}$ unless $(i, j) \in I_{\mathrm{f}} \times I_{\mathrm{f}}$;

- $\boldsymbol{A} = (A_i)_{i\in I}$ and $\boldsymbol{X} = (X_i)_{i\in I}$ are tuples of algebraically independent elements (*cluster $\mathcal{A}$- and $\mathcal{X}$-variables*) in $\mathcal{F}_A$ and $\mathcal{F}_X$, respectively.

The exchange matrix ε can be encoded in a quiver with vertices parametrized by the set I and $|\varepsilon_{ij}|$ arrows from i to j (resp. j to i) if $\varepsilon_{ij} > 0$ (resp. $\varepsilon_{ji} > 0$). In figures, we draw n dashed arrows from i to j if $\varepsilon_{ij} = n/2$ for $n \in \mathbb{Z}$, where a pair of dashed arrows is replaced with a solid arrow.

For an unfrozen index $k \in I_{\mathrm{uf}}$, the *mutation* directed to k produces a new seed $(\varepsilon', \boldsymbol{A}', \boldsymbol{X}') = \mu_k(\varepsilon, \boldsymbol{A}, \boldsymbol{X})$ according to an explicit formula [17]. See, for instance, [23, (2.1), (2.3) and (2.4)] for a formula which fits in with our convention. A permutation $\sigma \in \mathfrak{S}_{I_{\mathrm{uf}}} \times \mathfrak{S}_{I_{\mathrm{f}}}$ induces a transformation $\sigma : (\varepsilon, \boldsymbol{A}, \boldsymbol{X}) \to (\varepsilon', \boldsymbol{A}', \boldsymbol{X}')$ by the rule

$$\varepsilon'_{ij} := \varepsilon_{\sigma^{-1}(i),\sigma^{-1}(j)}, \quad A'_i := A_{\sigma^{-1}(i)}, \quad X'_i := X_{\sigma^{-1}(i)}. \tag{A-1}$$

We say that two seeds in $(\mathcal{F}_A, \mathcal{F}_X)$ are *mutation-equivalent* if they are transformed to each other by a finite sequence of mutations and permutations. The equivalence class is usually called a *mutation class*.

The relations among the seeds in a given mutation class s can be encoded in the (*labeled*) *exchange graph* $\mathbb{E}\mathrm{xch}_{\mathsf{s}}$. It is a graph with vertices v corresponding to the seeds $\mathsf{s}^{(v)}$ in s, together with labeled edges of the following two types:

- edges of the form $v \overset{k}{\text{---}} v'$ whenever the seeds $\mathsf{s}^{(v)}$ and $\mathsf{s}^{(v')}$ are related by the mutation μ_k for $k \in I_{\mathrm{uf}}$;
- edges of the form $v \overset{\sigma}{\text{---}} v'$ whenever the seeds $\mathsf{s}^{(v)}$ and $\mathsf{s}^{(v')}$ are related by the transposition $\sigma = (j\ k)$ for $(j,k) \in I_{\mathrm{uf}} \times I_{\mathrm{uf}}$ or $I_{\mathrm{f}} \times I_{\mathrm{f}}$.

When no confusion can occur, we simply denote a vertex of the labeled exchange graph by $v \in \mathbb{E}\mathrm{xch}_{\mathsf{s}}$ instead of $v \in V(\mathbb{E}\mathrm{xch}_{\mathsf{s}})$. When we write $\mathsf{s}^{(v)} = (\varepsilon^{(v)}, \boldsymbol{A}^{(v)}, \boldsymbol{X}^{(v)})$, it is known that $(\varepsilon^{(v)}, \boldsymbol{A}^{(v)}) = (\varepsilon^{(v')}, \boldsymbol{A}^{(v')})$ if and only if $(\varepsilon^{(v)}, \boldsymbol{X}^{(v)}) = (\varepsilon^{(v')}, \boldsymbol{X}^{(v')})$ for two vertices v and v' (the *synchronicity phenomenon* [38]). We call $(\varepsilon^{(v)}, \boldsymbol{A}^{(v)})$ and $(\varepsilon^{(v)}, \boldsymbol{X}^{(v)})$ an *$\mathcal{A}$-seed* and an *$\mathcal{X}$-seed*, respectively. We also remark that the labeled exchange graph depends only on the mutation class of the underlying exchange matrices. Indeed, it is unchanged if we transform the cluster variables simultaneously by an automorphism of the ambient field.

Remark A.1 In geometric applications, $\mathcal{A}$- and $\mathcal{X}$-seeds are constructed in the field of rational functions on a space of interest. For $\mathcal{Z} \in \{\mathcal{A}, \mathcal{X}\}$, a *cluster $\mathcal{Z}$-atlas* on a variety (scheme, stack) V is a collection of $\mathcal{Z}$-seeds in the field $\mathcal{K}(V)$ of rational functions which are mutation-equivalent to each other. A cluster atlas can be uniquely extended to a *cluster $\mathcal{Z}$-structure*, which is a maximal collection of $\mathcal{Z}$-seeds in $\mathcal{K}(V)$, thus forming a mutation class s. See Remark A.3 below.

A.2 Cluster varieties

The cluster varieties associated with a mutation class s are constructed by patching algebraic tori parametrized by the vertices of the labeled exchange graph.

Notation A.2 A multiplicative algebraic group is denoted by $\mathbb{G}_m = \operatorname{Spec} \mathbb{Z}[u, u^{-1}]$. For a lattice Λ (ie a free abelian group of finite rank), let $\mathbb{T}_\Lambda := \operatorname{Hom}(\Lambda, \mathbb{G}_m)$ denote the associated algebraic torus. For a (split) algebraic torus $T \cong (\mathbb{G}_m)^N$, let

$$X^*(T) := \operatorname{Hom}(T, \mathbb{G}_m) \quad \text{and} \quad X_*(T) := \operatorname{Hom}(\mathbb{G}_m, T)$$

denote the lattices of characters and cocharacters, respectively. These lattices are dual to each other by via the canonical pairing $X_*(T) \otimes X^*(T) \to \operatorname{Hom}(\mathbb{G}_m, \mathbb{G}_m) \cong \mathbb{Z}$. The contravariant functors $\mathbb{T}_\bullet \colon \Lambda \mapsto \mathbb{T}_\Lambda$ and $X^* \colon T \mapsto X^*(T)$ are inverses to each other: $\Lambda = X^*(\mathbb{T}_\Lambda)$, $T = \mathbb{T}_{X^*(T)}$. A vector $\lambda \in \Lambda$ gives rise to a character $\chi_\lambda \colon \mathbb{T}_\Lambda \to \mathbb{G}_m$.

For $v \in \mathbb{E}\mathrm{xch}_\mathrm{s}$, consider a lattice $N^{(v)} = \bigoplus_{i \in I} \mathbb{Z} e_i^{(v)}$ with a fixed basis and its dual $M^{(v)} = \bigoplus_{i \in I} \mathbb{Z} f_i^{(v)}$. Let $\mathcal{X}_{(v)} := \mathbb{T}_{N^{(v)}}$ and $\mathcal{A}_{(v)} := \mathbb{T}_{M^{(v)}}$ denote the associated algebraic tori of dimension $|I|$. The characters $X_i^{(v)} := \chi_{e_i^{(v)}} \colon \mathcal{X}_{(v)} \to \mathbb{G}_m$ and $A_i^{(v)} := \chi_{f_i^{(v)}} \colon \mathcal{A}_{(v)} \to \mathbb{G}_m$ are called the *cluster coordinates*. The exchange matrix $\varepsilon^{(v)}$ defines a $\frac{1}{2}\mathbb{Z}$-valued bilinear form on $N^{(v)}$ by $(e_i^{(v)}, e_j^{(v)}) := \varepsilon_{ij}^{(v)}$, which induces Poisson and K_2-structures on $\mathcal{X}_{(v)}$ and $\mathcal{A}_{(v)}$, respectively. The mutation rule turns into birational maps $\mu_k^x \colon \mathcal{X}_{(v)} \to \mathcal{X}_{(v')}$ and $\mu_k^a \colon \mathcal{A}_{(v)} \to \mathcal{A}_{(v')}$, called the *cluster transformations* [13, (13) and (14)]. Then the *cluster $\mathcal{X}$- and $\mathcal{A}$-varieties* are the schemes defined as

$$\mathcal{X}_\mathrm{s} := \bigcup_{v \in \mathbb{E}\mathrm{xch}_\mathrm{s}} \mathcal{X}_{(v)}, \quad \mathcal{A}_\mathrm{s} := \bigcup_{v \in \mathbb{E}\mathrm{xch}_\mathrm{s}} \mathcal{A}_{(v)}.$$

Here for $(z, \mathbb{Z}) \in \{(a, \mathcal{A}), (x, \mathcal{X})\}$, (open subsets of) tori $\mathcal{Z}_{(v)}$ and $\mathcal{Z}_{(v')}$ are identified via the cluster transformation μ_k^z if there is an edge of the form $v \overset{k}{\text{---}} v'$, or via the coordinate permutation (A-1) if there is an edge of the form $v \overset{\sigma}{\text{---}} v'$. As a slight variant, let $\mathcal{X}_{(v)}^{\mathrm{uf}} := \mathbb{T}_{N_{\mathrm{uf}}^{(v)}}$, and $\mathcal{X}_\mathrm{s}^{\mathrm{uf}} := \bigcup_{v \in \mathbb{E}\mathrm{xch}_\mathrm{s}} \mathcal{X}_{(v)}^{\mathrm{uf}}$ the cluster $\mathcal{X}$-variety without frozen coordinates. Since the cluster transformation of unfrozen $\mathcal{X}$-coordinates does not refer the frozen ones, we have a natural projection $\mathcal{X}_\mathrm{s} \to \mathcal{X}_\mathrm{s}^{\mathrm{uf}}$. We remark that the cluster varieties are constructed only from the mutation class of the underlying exchange matrices.

For $(Z, \mathcal{Z}) \in \{(A, \mathcal{A}), (X, \mathcal{X})\}$, each pair $(\varepsilon^{(v)}, (Z_i^{(v)})_{i \in I})$ of the exchange matrix and the cluster $\mathcal{Z}$-coordinates defines a $\mathcal{Z}$-seed in the field $\mathcal{F}_Z := \mathcal{K}(\mathcal{Z}_\mathrm{s})$ of rational functions in the sense of the previous section. The rings $\mathcal{O}(\mathcal{A}_\mathrm{s}) \subset \mathcal{F}_A$ and $\mathcal{O}(\mathcal{X}_\mathrm{s}) \subset \mathcal{F}_X$ of regular functions are called the *upper cluster algebra* and the *cluster Poisson algebra*, respectively. The *cluster algebra* [16] is the subring $\mathscr{A}_\mathrm{s} \subset \mathcal{O}(\mathcal{A}_\mathrm{s})$ generated by all the cluster coordinates $A_i^{(v)}$, $i \in I$, $v \in \mathbb{E}\mathrm{xch}_\mathrm{s}$.

Ensemble maps and their extensions The cluster varieties $\mathcal{X}_\mathrm{s}$ and $\mathcal{A}_\mathrm{s}$ are coupled as a *cluster ensemble*. For $v \in \mathbb{E}\mathrm{xch}_\mathrm{s}$, let $N_{\mathrm{uf}}^{(v)} \subset N^{(v)}$ denote the sublattice spanned by $e_i^{(v)}$ for $i \in I_{\mathrm{uf}}$. Then by the assumption on the exchange matrix, we have the linear map

$$p_{(v)}^* \colon N_{\mathrm{uf}}^{(v)} \to M^{(v)}, \quad e_i^{(v)} \mapsto \sum_{j \in I} \varepsilon_{ij}^{(v)} f_j^{(v)}. \tag{A-2}$$

Moreover, it can be verified that the maps between tori induced by (A-2) commute with cluster transformations, and combine to give a morphism $p \colon \mathcal{A}_\mathrm{s} \to \mathcal{X}_\mathrm{s}^{\mathrm{uf}}$. We call this map the *ensemble map*,

and the triple $(\mathcal{A}_{\mathsf{s}}, \mathcal{X}_{\mathsf{s}}, p)$ the *cluster ensemble* associated with s. If we pick up a suitable extension $\tilde{p}^*_{(v)}\colon N^{(v)} \to M^{(v)}$ of the map (A-2) (see [22, (A.2)] for the required condition), then it still commutes with cluster transformations and hence we get an *extended ensemble map* $\tilde{p}\colon \mathcal{A}_{\mathsf{s}} \to \mathcal{X}_{\mathsf{s}}$. It is shown in [21, Section 13.3] that such a choice exactly corresponds to a choice of compatibility pairs [3] defining a quantum cluster algebra.

Tropicalizations The positive structures on the cluster varieties allow us to consider their semifield-valued points. For $\mathbb{A} = \mathbb{Z}$, $\mathbb{Q}$ or $\mathbb{R}$, let $\mathbb{A}^T := (\mathbb{A}, \max, +)$ denote the corresponding *tropical semifield* (or the *max-plus semifield*). For an algebraic torus H, let $H(\mathbb{A}^T) := X_*(H) \otimes_{\mathbb{Z}} (\mathbb{A}, +)$. A positive rational map $f\colon H \to H'$ between algebraic tori naturally induces a piecewise-linear (PL for short) map $f^T\colon H(\mathbb{A}^T) \to H'(\mathbb{A}^T)$. We call f^T the *tropicalized map*. In particular we have the tropicalized cluster transformations $\mu_k^T\colon \mathcal{Z}_{(v)}(\mathbb{A}^T) \to \mathcal{Z}_{(v')}(\mathbb{A}^T)$ for $(\mathsf{z}, \mathcal{Z}) \in \{(\mathsf{a}, \mathcal{A}), (\mathsf{x}, \mathcal{X})\}$, explicitly given as

$$(\mu_k^T)^*\mathsf{x}_i^{(v')} = \begin{cases} -\mathsf{x}_k^{(v)} & \text{if } i = k, \\ \mathsf{x}_i^{(v)} - \varepsilon_{ik}^{(v)}[-\operatorname{sgn}(\varepsilon_{ik}^{(v)})\mathsf{x}_k^{(v)}]_+ & \text{if } i \neq k, \end{cases} \tag{A-3}$$

$$(\mu_k^T)^*\mathsf{a}_i^{(v')} = \begin{cases} -\mathsf{a}_k^{(v)} + \max\{\sum_{j\in I}[\varepsilon_{kj}^{(v)}]_+\mathsf{a}_j^{(v)}, \sum_{j\in I}[-\varepsilon_{kj}^{(v)}]_+\mathsf{a}_j^{(v)}\} & \text{if } i = k, \\ \mathsf{a}_i^{(v)} & \text{if } i \neq k. \end{cases} \tag{A-4}$$

Here $\mathsf{x}_i^{(v)}$ and $\mathsf{a}_i^{(v)}$ are the coordinate functions induced by the basis vectors $e_i^{(v)}$ and $f_i^{(v)}$ respectively, and $[u]_+ := \max\{0, u\}$ for $u \in \mathbb{A}$. We can use them to define the *tropical cluster varieties*

$$\mathcal{X}_{\mathsf{s}}(\mathbb{A}^T) := \bigcup_{v\in\mathbb{E}\mathrm{xch}_{\mathsf{s}}} \mathcal{X}_{(v)}(\mathbb{A}^T), \quad \mathcal{A}_{\mathsf{s}}(\mathbb{A}^T) := \bigcup_{v\in\mathbb{E}\mathrm{xch}_{\mathsf{s}}} \mathcal{A}_{(v)}(\mathbb{A}^T),$$

which are naturally equipped with canonical PL structures. Since the PL maps are equivariant for the scaling action of $\mathbb{A}_{>0}$, the tropical cluster varieties inherit this $\mathbb{A}_{>0}$-action. We also consider the tropical $\mathcal{X}$-varieties $\mathcal{X}_{\mathsf{s}}^{\mathrm{uf}}(\mathbb{A}^T)$ without frozen coordinates. In the body of this paper, the main objects of study are the spaces $\mathcal{X}_{\mathsf{s}}^{\mathrm{uf}}(\mathbb{Q}^T)$ and $\mathcal{X}_{\mathsf{s}}(\mathbb{Q}^T)$ associated with a particular mutation class s.

Cluster modular group The cluster ensemble is naturally equipped with a discrete symmetry group. Let $\mathrm{Mat}_{\mathsf{s}}$ denote the mutation class of exchange matrices underlying the mutation class s. Then we have a map

$$\varepsilon^\bullet\colon V(\mathbb{E}\mathrm{xch}_{\mathsf{s}}) \to \mathrm{Mat}_{\mathsf{s}}, \quad v \mapsto \varepsilon^{(v)}.$$

Then the *cluster modular group* $\Gamma_{\mathsf{s}} \subset \mathrm{Aut}(\mathbb{E}\mathrm{xch}_{\mathsf{s}})$ consists of graph automorphism ϕ which preserves the fibers of the map $\varepsilon^\bullet$ and the labels on the edges. An element of the cluster modular group is called a *mutation loop*. The cluster modular group acts on the cluster varieties $\mathcal{A}_{\mathsf{s}}$ and $\mathcal{X}_{\mathsf{s}}$ so that $\phi^* Z_i^{(v)} = Z_i^{(\phi^{-1}(v))}$ for all $\phi \in \Gamma_{\boldsymbol{s}}$, $v \in \mathbb{E}\mathrm{xch}_{\boldsymbol{s}}$ and $i \in I$, where $(Z, \mathcal{Z}) \in \{(A, \mathcal{A}), (X, \mathcal{X})\}$. These actions commute with the ensemble map.

Since the actions are by positive rational maps, they induce actions of Γ_{s} on $\mathcal{A}_{\mathsf{s}}(\mathbb{A}^T)$ and $\mathcal{X}_{\mathsf{s}}(\mathbb{A}^T)$ by PL automorphisms, which commute with the (extended) ensemble map. Moreover, these actions commute with the rescaling action of $\mathbb{A}_{>0}$.

A.3 The cluster ensemble associated with the pair $(\mathfrak{sl}_3, \Sigma)$

Here we quickly recall the cluster structures on the moduli spaces $\mathcal{A}_{\mathrm{SL}_3,\Sigma}$, $\mathcal{X}_{\mathrm{PGL}_3,\Sigma}$ and $P_{\mathrm{PGL}_3,\Sigma}$ constructed in [10; 21]. We are going to recall the *Fock–Goncharov atlas* associated with ideal triangulations of Σ and their mutation-equivalences, since it is typical difficult to describe the entire cluster structure.

Let $\triangle$ be an ideal triangulation of Σ. Then we construct a quiver $Q_\triangle$ with the vertex set $I(\triangle)$ by drawing the quiver

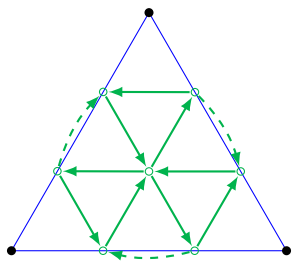

on each triangle, and glue them by the *amalgamation* construction [9]. In our case, this just means that we glue the quivers on adjacent triangles by identifying the two vertices on the shared edge and eliminate the pair of opposite dashed arrows. The vertices on the boundary intervals of Σ are declared to be frozen, forming the subset $I_{\mathrm{f}}(\triangle) \subset I(\triangle)$ as in Section 2.1. Let $\varepsilon^\triangle = (\varepsilon^\triangle_{ij})_{i,j\in I(\triangle)}$ be the corresponding exchange matrix.

These quivers $Q^\triangle$ (or the exchange matrices $\varepsilon^\triangle$) associated with ideal triangulations of Σ are mutation-equivalent to each other. Indeed, the quivers $Q^\triangle$ and $Q^{\triangle'}$ associated with two triangulations $\triangle$ and $\triangle'$ connected by a single flip $f_E : \triangle \to \triangle'$ are transformed to each other via one of the mutation sequences shown in Figure 43. Then the assertion follows from the classical fact that any two ideal triangulations of the same marked surface can be transformed to each other by a finite sequence of flips.

Remark A.3 For each ideal triangulation $\triangle$, we can associate an $\mathcal{A}$-seed $(\varepsilon^\triangle, \boldsymbol{A}^\triangle)$ (resp. $\mathcal{X}$-seed $(\varepsilon^\triangle, \boldsymbol{X}^\triangle)$) in the field of rational functions on the moduli space $\mathcal{A}_{\mathrm{SL}_3,\Sigma}$ (resp. $\mathcal{P}_{\mathrm{PGL}_3,\Sigma}$). Forgetting the frozen part in the latter, we get an $\mathcal{X}$-seed for the moduli space $\mathcal{X}_{\mathrm{PGL}_3,\Sigma}$. See [10, Section 9] or [21, Section 3] for construction. These birational coordinate systems define cluster atlases on these moduli spaces in the sense of Remark A.1.

Then there exists a unique mutation class $\mathfrak{s}(\mathfrak{sl}_3, \Sigma)$ containing the seeds associated with any ideal triangulations $\triangle$. More precisely, a *labeled* $\mathfrak{sl}_3$*-triangulation* $(\triangle, \ell)$, namely an ideal triangulation $\triangle$ together with a bijection $\ell\colon I(\triangle) \to \{1, \dots, N\}$, give rise to vertices of the labeled exchange graph $\mathbb{E}\mathrm{xch}_{\mathfrak{s}(\mathfrak{sl}_3,\Sigma)}$. Figure 43 describes a subgraph containing $(\triangle, \ell)$ and $(\triangle', \ell')$, where the labels ℓ and ℓ' are consistently chosen. Let us simply denote the objects related to $\mathfrak{s}(\mathfrak{sl}_3, \Sigma)$ by

$$\mathcal{A}_{\mathfrak{sl}_3,\Sigma} := \mathcal{A}_{\mathfrak{s}(\mathfrak{sl}_3,\Sigma)}, \quad \mathcal{X}_{\mathfrak{sl}_3,\Sigma} := \mathcal{X}_{\mathfrak{s}(\mathfrak{sl}_3,\Sigma)}, \quad \mathbb{E}\mathrm{xch}_{\mathfrak{sl}_3,\Sigma} := \mathbb{E}\mathrm{xch}_{\mathfrak{s}(\mathfrak{sl}_3,\Sigma)}, \quad \Gamma_{\mathfrak{sl}_3,\Sigma} := \Gamma_{\mathfrak{s}(\mathfrak{sl}_3,\Sigma)},$$

and so on.

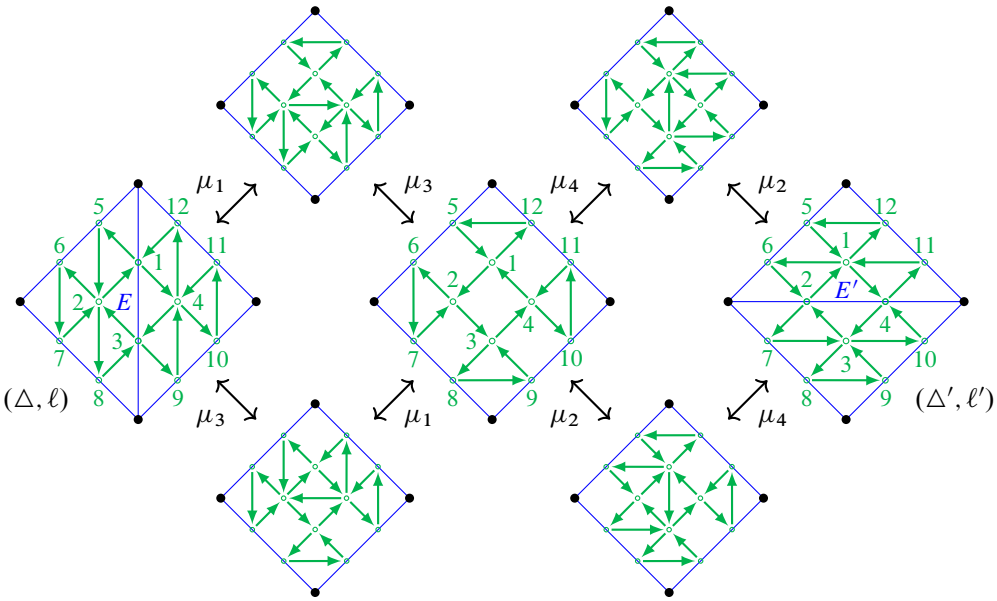

Figure 43: Some of the sequences of mutations that realize the flip $f_E\colon \triangle \to \triangle'$. Here we partially fix labelings ℓ and ℓ' of vertices in $I(\triangle)$ and $I(\triangle')$, respectively.

The following can be verified from (A-3) by a direct computation:

Lemma A.4 *For two labeled $\mathfrak{sl}_3$-triangulations $v = (\triangle, \ell), v' = (\triangle', \ell') \in \mathbb{E}\mathrm{xch}_{\mathfrak{sl}_3,\Sigma}$ as in Figure 43, the (max-plus) tropical coordinates $x_i := x_i^{(v)}$ and $x'_i := x_i^{(v')}$ for $i \in \{1, \dots, 12\}$ are related as follows:*

$$\begin{aligned}
x'_1 &= x_2 + [x_3, x_4, x_1]_+ - [x_1, x_2, x_3]_+, & x'_2 &= -x_1 - x_2 + [x_1]_+ - [x_3]_+,\\
x'_3 &= x_4 + [x_1, x_2, x_3]_+ - [x_3, x_4, x_1]_+, & x'_4 &= -x_3 - x_4 + [x_3]_+ - [x_1]_+,\\
x'_5 &= x_5 + [x_1]_+, & x'_6 &= x_6 + [x_1, x_2, x_3]_+ - [x_1]_+,\\
x'_7 &= x_7 + x_1 + x_2 + [x_3]_+ - [x_1, x_2, x_3]_+, & x'_8 &= x_8 - [-x_3]_+,\\
x'_9 &= x_9 + [x_3]_+, & x'_{10} &= x_{10} + [x_3, x_4, x_1]_+ - [x_3]_+,\\
x'_{11} &= x_{11} + x_3 + x_4 + [x_1]_+ - [x_3, x_4, x_1]_+, & x'_{12} &= x_{12} - [-x_1]_+.
\end{aligned}$$

Here $[x]_+ := \max\{0, x\}$ and $[x, y, z]_+ := \max\{0, x, x + y, x + y + z\}$.

Goncharov–Shen extension of the ensemble map Following [21], we choose the following extension of the ensemble map. Let

$$C(\mathfrak{sl}_3) = (C_{st})_{s,t\in\{1,2\}} = \begin{pmatrix} 2 & -1 \\ -1 & 2 \end{pmatrix}$$

denote the Cartan matrix of the Lie algebra $\mathfrak{sl}_3$. For an ideal triangulation $\triangle$, let $\tilde{\varepsilon}^{\triangle} = (\tilde{\varepsilon}^{\triangle}_{ij})_{i,j\in I(\triangle)}$ be the matrix given by $\tilde{\varepsilon}^{\triangle}_{ij} := \varepsilon^{\triangle}_{ij} + m_{ij}$, where

$$m_{ij} := \begin{cases} -\frac{1}{2}C_{st} & \text{if } i = i^s(E) \text{ and } j = i^t(E) \text{ lie on a common boundary interval } E \in \mathbb{B},\\ 0 & \text{otherwise.} \end{cases} \tag{A-5}$$

Then we define $\tilde{p}^*_\Delta : N^\Delta \to M^\Delta$ by $e_i^\Delta \mapsto \sum_{i,j\in I(\triangle)} \tilde{\varepsilon}_{ij}^\Delta f_j^\Delta$ inducing a morphism

$$\tilde{p}_{\mathrm{GS}} : \mathcal{A}_{\mathfrak{sl}_3,\Sigma} \to \mathcal{X}_{\mathfrak{sl}_3,\Sigma}, \tag{A-6}$$

which we call the *Goncharov–Shen extension of the ensemble map*. This choice naturally comes from the geometry of the moduli spaces of local systems on Σ, so $\tilde{p}_{\mathrm{GS}}$ agrees with the map $p : \mathcal{A}^{\times}_{\mathrm{SL}_3,\Sigma} \to \mathcal{P}_{\mathrm{PGL}_3,\Sigma}$ [21, Proposition 9.4].

Cluster modular group Although the entire structure of the cluster modular group $\Gamma_{\mathfrak{sl}_3,\Sigma}$ is yet unknown, it is known to include the subgroup $(\mathrm{MC}(\Sigma) \times \mathrm{Out}(\mathrm{SL}_3)) \ltimes W(\mathfrak{sl}_3)^{\mathbb{M}_\circ} \subset \Gamma_{\mathfrak{sl}_3,\Sigma}$ [20]. Here $\mathrm{MC}(\Sigma)$ denotes the mapping class group of the marked surface Σ, $\mathrm{Out}(\mathrm{SL}_3)) = \mathrm{Aut}(\mathrm{SL}_3)/\mathrm{Inn}(\mathrm{SL}_3)$ is the outer automorphism group of SL_3, and $W(\mathfrak{sl}_3)$ is the Weyl group of the Lie algebra $\mathfrak{sl}_3$. The group $\mathrm{Out}(\mathrm{SL}_3)$ has order 2, and generated by the *Dynkin involution* $*: G \to G$, $g \mapsto (g^{-1})^{\mathsf{T}}$. For each element ϕ in this subgroup, let us call the induced PL action $\phi : \mathcal{Z}_{\mathfrak{sl}_3,\Sigma}(\mathbb{Q}^T) \to \mathcal{Z}_{\mathfrak{sl}_3,\Sigma}(\mathbb{Q}^T)$ the *cluster action*, in comparison to the geometric action we introduce in the body of this paper in terms of signed $\mathfrak{sl}_3$-webs.

References

[1] **D G L Allegretti**, *Quantization of canonical bases and the quantum symplectic double*, Manuscripta Math. 167 (2022) 613–651 MR Zbl

[2] **D G L Allegretti**, **H K Kim**, *A duality map for quantum cluster varieties from surfaces*, Adv. Math. 306 (2017) 1164–1208 MR Zbl

[3] **A Berenstein**, **A Zelevinsky**, *Quantum cluster algebras*, Adv. Math. 195 (2005) 405–455 MR Zbl

[4] **S Y Cho**, **H Kim**, **H K Kim**, **D Oh**, *Laurent positivity of quantized canonical bases for quantum cluster varieties from surfaces*, Comm. Math. Phys. 373 (2020) 655–705 MR Zbl

[5] **B Davison**, **T Mandel**, *Strong positivity for quantum theta bases of quantum cluster algebras*, Invent. Math. 226 (2021) 725–843 MR Zbl

[6] **D C Douglas**, **Z Sun**, *Tropical Fock–Goncharov coordinates for SL_3–webs on surfaces, I: Construction*, Forum Math. Sigma 12 (2024) art. id. e5 MR Zbl

[7] **D C Douglas**, **Z Sun**, *Tropical Fock–Goncharov coordinates for SL_3-webs on surfaces, II: Naturality*, Algebr. Comb. 8 (2025) 101–156 MR Zbl

[8] **V V Fock**, **L O Chekhov**, *Quantum Teichmüller spaces*, Teoret. Mat. Fiz. 120 (1999) 511–528 MR Zbl In Russian; translated in Theoret. Math. Phys. 120 (1999) 1245–1259

[9] **V V Fock**, **A B Goncharov**, *Cluster $\mathcal{X}$-varieties, amalgamation, and Poisson–Lie groups*, from "Algebraic geometry and number theory", Progr. Math. 253, Birkhäuser, Boston, MA (2006) 27–68 MR Zbl

[10] **V Fock**, **A Goncharov**, *Moduli spaces of local systems and higher Teichmüller theory*, Publ. Math. Inst. Hautes Études Sci. 103 (2006) 1–211 MR Zbl

[11] **V V Fock**, **A B Goncharov**, *Dual Teichmüller and lamination spaces*, from "Handbook of Teichmüller theory, I", IRMA Lect. Math. Theor. Phys. 11, Eur. Math. Soc., Zürich (2007) 647–684 MR Zbl

[12] **V V Fock**, **A B Goncharov**, *Moduli spaces of convex projective structures on surfaces*, Adv. Math. 208 (2007) 249–273 MR Zbl

[13] **V V Fock**, **A B Goncharov**, *Cluster ensembles, quantization and the dilogarithm*, Ann. Sci. École Norm. Sup. 42 (2009) 865–930 MR Zbl

[14] **V V Fock**, **A B Goncharov**, *Cluster Poisson varieties at infinity*, Selecta Math. 22 (2016) 2569–2589 MR Zbl

[15] **S Fomin**, **M Shapiro**, **D Thurston**, *Cluster algebras and triangulated surfaces, I: Cluster complexes*, Acta Math. 201 (2008) 83–146 MR Zbl

[16] **S Fomin**, **A Zelevinsky**, *Cluster algebras, I: Foundations*, J. Amer. Math. Soc. 15 (2002) 497–529 MR Zbl

[17] **S Fomin**, **A Zelevinsky**, *Cluster algebras, IV: Coefficients*, Compos. Math. 143 (2007) 112–164 MR Zbl

[18] **B Fontaine**, **J Kamnitzer**, **G Kuperberg**, *Buildings, spiders, and geometric Satake*, Compos. Math. 149 (2013) 1871–1912 MR Zbl

[19] **C Frohman**, **A S Sikora**, *$SU(3)$-skein algebras and webs on surfaces*, Math. Z. 300 (2022) 33–56 MR Zbl

[20] **A Goncharov**, **L Shen**, *Donaldson–Thomas transformations of moduli spaces of G-local systems*, Adv. Math. 327 (2018) 225–348 MR Zbl

[21] **A Goncharov**, **L Shen**, *Quantum geometry of moduli spaces of local systems and representation theory*, preprint (2019) arXiv 1904.10491

[22] **M Gross**, **P Hacking**, **S Keel**, **M Kontsevich**, *Canonical bases for cluster algebras*, J. Amer. Math. Soc. 31 (2018) 497–608 MR Zbl

[23] **R Inoue**, **T Ishibashi**, **H Oya**, *Cluster realizations of Weyl groups and higher Teichmüller theory*, Selecta Math. 27 (2021) art. id. 37 MR Zbl

[24] **T Ishibashi**, *On a Nielsen–Thurston classification theory for cluster modular groups*, Ann. Inst. Fourier (Grenoble) 69 (2019) 515–560 MR Zbl

[25] **T Ishibashi**, **S Kano**, *Sign stability of mapping classes on marked surfaces, I: Empty boundary case*, preprint (2020) arXiv 2010.05214

[26] **T Ishibashi**, **S Kano**, *Sign stability of mapping classes on marked surfaces, II: General case via reductions*, preprint (2020) arXiv 2011.14320

[27] **T Ishibashi**, **S Kano**, *Algebraic entropy of sign-stable mutation loops*, Geom. Dedicata 214 (2021) 79–118 MR Zbl

[28] **T Ishibashi**, **S Kano**, *Unbounded $\mathfrak{sl}_3$-laminations around punctures*, preprint (2024) arXiv 2404.18236

[29] **T Ishibashi**, **H Oya**, **L Shen**, *$\mathcal{A} = \mathcal{U}$ for cluster algebras from moduli spaces of G–local systems*, Adv. Math. 431 (2023) art. id. 109256 MR Zbl

[30] **T Ishibashi**, **W Yuasa**, *Skein and cluster algebras of unpunctured surfaces for $\mathfrak{sl}_3$*, Math. Z. 303 (2023) art. id. 72 MR Zbl

[31] **S Kano**, *Train track combinatorics and cluster algebras*, preprint (2023) arXiv 2303.03190

[32] **H K Kim**, *SL_3-laminations as bases for PGL_3 cluster varieties for surfaces* (2020) arXiv 2011.14765 To appear in Mem. Amer. Math. Soc.

[33] **G Kuperberg**, *Spiders for rank 2 Lie algebras*, Comm. Math. Phys. 180 (1996) 109–151 MR Zbl

[34] **I Le**, *Higher laminations and affine buildings*, Geom. Topol. 20 (2016) 1673–1735 MR Zbl

[35] **I Le**, *Cluster structures on higher Teichmüller spaces for classical groups*, Forum Math. Sigma 7 (2019) art. id. e13 MR Zbl

[36] **T T Q Lê**, **T Yu**, *Quantum traces and embeddings of stated skein algebras into quantum tori*, Selecta Math. 28 (2022) art. id. 66 MR Zbl

[37] **T Mandel**, **F Qin**, *Bracelets bases are theta bases*, preprint (2023) arXiv 2301.11101

[38] **T Nakanishi**, *Synchronicity phenomenon in cluster patterns*, J. Lond. Math. Soc. 103 (2021) 1120–1152 MR Zbl

[39] **A Papadopoulos**, **R C Penner**, *The Weil–Petersson symplectic structure at Thurston's boundary*, Trans. Amer. Math. Soc. 335 (1993) 891–904 MR Zbl

[40] **R C Penner**, *Decorated Teichmüller theory*, Eur. Math. Soc., Zürich (2012) MR Zbl

[41] **F Qin**, *Cluster algebras and their bases*, from "Representations of algebras and related structures", Eur. Math. Soc., Berlin (2023) 335–369 MR Zbl

[42] **D P Thurston**, *Positive basis for surface skein algebras*, Proc. Natl. Acad. Sci. USA 111 (2014) 9725–9732 MR Zbl

[43] **W P Thurston**, *On the geometry and dynamics of diffeomorphisms of surfaces*, Bull. Amer. Math. Soc. 19 (1988) 417–431 MR Zbl

[44] **T Yurikusa**, *Acyclic cluster algebras with dense g-vector fans*, from "McKay correspondence, mutation and related topics", Adv. Stud. Pure Math. 88, Math. Soc. Japan, Tokyo (2023) 437–459 MR Zbl

Mathematical Institute, Tohoku University
Sendai, Japan

Mathematical Science Center for Co-creative Society, Tohoku University
Sendai, Japan

tsukasa.ishibashi.a6@tohoku.ac.jp, s.kano@tohoku.ac.jp

Received: 24 September 2022 Revised: 24 January 2024

ALGEBRAIC & GEOMETRIC TOPOLOGY

msp.org/agt

See inside back cover or msp.org/agt for submission instructions.

The subscription price for 2025 is US $760/year for the electronic version, and $1110/year (+$75, if shipping outside the US) for print and electronic. Subscriptions, requests for back issues and changes of subscriber address should be sent to MSP. Algebraic & Geometric Topology is indexed by Mathematical Reviews, Zentralblatt MATH, Current Mathematical Publications and the Science Citation Index.

Algebraic & Geometric Topology (ISSN 1472-2747 printed, 1472-2739 electronic) is published 9 times per year and continuously online, by Mathematical Sciences Publishers, c/o Department of Mathematics, University of California, 798 Evans Hall #3840, Berkeley, CA 94720-3840. Periodical rate postage paid at Oakland, CA 94615-9651, and additional mailing offices. POSTMASTER: send address changes to Mathematical Sciences Publishers, c/o Department of Mathematics, University of California, 798 Evans Hall #3840, Berkeley, CA 94720-3840.

AGT peer review and production are managed by EditFlow® from MSP.

PUBLISHED BY

mathematical sciences publishers

nonprofit scientific publishing

https://msp.org/

ALGEBRAIC & GEOMETRIC TOPOLOGY

Volume 25 Issue 3 (pages 1265–1915) 2025